The Role of the Myotubularin Pseudophosphatase MTMR13 in Myelination and Disease

by

Danielle C. Robinson

A DISSERTATION

Presented to the Neuroscience Graduate Program

at the Oregon Health & Science University School of Medicine

in partial fulfillment of the requirements

for the degree of

Doctor of Philosophy

December 5, 2016

Oregon Health & Science University

CERTIFICATE OF APPROVAL

This is to certify that the Ph.D. dissertation of

DANIELLE C. ROBINSON

has been approved on December 5, 2016

Advisor, Fred Robinson, Ph.D

Member and Chair, Philip Stork, M.D

Member, Gary Westbrook, M.D.

Member, Ben Emery, Ph.D.

Member, Mary Logan, Ph.D

The role of MTMR13 in myelination and disease

Table of Contents

Tables, Figures, and Abbreviations

List of Abbreviations

AKT	Serine/threonine-specific protein kinase, protein kinase B (PKB)
CA	constitutively active
cAMP	cyclic adenosine monophosphate
CMT	Charcot-Marie-Tooth
CNS	central nervous system
DAPI	4',6-diamidino-2-phenylindole
DIV	days in vitro
DLG1	discs large 1
DRG	dorsal root ganglia
EEA1	early endosomal antigen 1
EGFP	enhanced green fluorescent protein
EM	electron microscopy
FBS	fetal bovine serum
FYVE	Fab1/YOTB/Vac1/
GEF	guanine (nucleotide) exchange factor
GRAM	PH-glucosyltransferase, Rab-like GTPase activator and myotubularins
KO	knockout
LAMP1	lysosomal associated membrane protein1
Lv	lentivirus
MAG	myelin associated glycoprotien
MAPK	mitogen-activated protein kinase
MBP	myelin basic protein
MTMR	myotubularin related
mTOR	mechanistic target of rapamycin
NCV	nerve conduction velocity
NDRG1	N-myc downstream-regulated gene-1

NFH	neurofilament, heavy chain
NGF	nerve growth factor
NgR1	Nogo receptor
NRG1	neuregulin 1
Omgp	oligodendrocyte myelin glycoprotein
P0	myelin protein zero
P2	myelin protein 2
Pals1	Protein Associated with Lin Seven 1
PBS	phosphate buffered saline
PFA	paraformaldehyde
PH	Pleckstrin homology
PI	Phosphoinositide
$PI(3,4,5)P_2$	Phosphatidylinositol 3,4,5-triphosphate
$PI(3,5)P_2$	Phosphatidylinositol 3,5-diphosphate
PI3P	Phosphatidylinositol 3-phosphate
PI4P	Phosphatidylinositol 4-phosphate
PLP	Proteolipid protein
PMP22	peripheral myelin protein 22
PNS	peripheral nervous system
SEM	standard error of the mean
SC	Schwann cell
SCP	Schwann cell precursor
Sox10	SRY related HMG box 10
WT	wild type

Nomenclature

Mtmr13	Mouse protein
Mtmr13	Mouse gene
MTMR13	Human protein
MTMR13	Human gene

Acknowledgments
Thank you to my mentor Fred Robinson and my lab mates (past and present) Anna Mammel, Andrea Chin, Alec Condon, and Annie Logan.

Thank you to the members of my Dissertation Advisory Committee, Philip Stork, Gary Westbrook, Ben Emery, and Mary Logan. With particular appreciation for Phil and Gary, who have helped me through challenging transitions and always given great advice. And of course thanks to Liz Lawson-Weber for all your help and support over the last 5.5 years.

Thank you to the Advanced Light Microscopy Core, Stefanie Kaech Petrie and Aurelie Snyder, as well as the electron microscopy facility, Bob Kayton, Sue Aicher, Maria Boriskova, Lisa Vecarelli.

Deep appreciation and thanks to:

The entering class of 2011: Lilly Winfree, Paul Kramer, Chris Vaaga, Marie Xun Wang, Ben Murphy-Baum. Truly, the best class.

Jackie Wirz, Robin Champieux, and Allison Fryer for professional support and mentorship way above and beyond the call of duty.

Mark and Ellen Richardson for friendship and support. I will always remember Mark's unique approach to leadership and mentorship and carry it with me on my professional journey. The Portland chapter of ARCS for financial support 2011-2013, introducing me to so many fantastic people, and for bringing Ellen into my life.

Mozilla & the Mozilla Science Lab: Stephanie Wright, Aurelia Moser, Kaitlin Thaney, and my fellow fellows Teon, Kirstie, and Bruno for good conversations and for believing in me.

My friends and colleagues Biliana Rotse, Jeannie Hunnicutt, Delia Chiu, Daniela Thorson, Maria Purice, Danielle Jorgens, Molly Marra, and Everyone on the 4th floor of the BRB from 2014-2016. My friends, Dr. Autumn Polidor, Jamie Matson, Krystina Lankone, Doug Reitmeyer, Holly Hawk, Jen Batchelor, Katie Powell, Hanna Neuschwander, John Mayer for saving my sanity.
Stumptown Coffee and Water Ave Coffee for coffee, friendly faces, music, and tables with outlets.

Leo's daycare center, Atlas Hawthorne, and his babysitters Laura Griffin and Anu Naeole, without their support none of this would be possible.

Academic Mamas! and FugeeLand for support, community, and useful distractions.

And, of course, thank you to my very supportive partner Andy Pressman and son Leo, as well as my family Kathy and Tony Robinson, Annie and Brian Rehill, Patrick and Megan Robinson, Steve and Myra Pressman, Elise, Dave, Charlie and Elliot Schwarz.

Abstract (500 words)

The phosphoinositide (PI) content of an internal membrane is a key regulator of intracellular trafficking. PIs recruit effector proteins to the membrane surface to coordinate signaling and trafficking inside the cell, this is particularly critical in the endosomal/lysosomal pathway where endosomes are sorted for recycling or degradation. The interchange of PI species is regulated by PI kinases and phosphatases, which add or remove phosphate groups to the 3, 4, or 5 position of the *myo*-inositol ring to regulate the PI identity of membrane. Coordination of PIs is critical for membrane trafficking through the endosomal/lysosomal system. Human disease causing mutations impact PI regulation in the endosomal/lysosomal pathway and primarily affect Schwann cells (SCs), leading to demyelinating forms of Charcot-Marie-Tooth (CMT) inherited peripheral neuropathy. These conditions underscore the critical nature of PI regulation and the endosomal/lysosomal pathway in normal SC function and myelination. Myotubularin (MTMR) phosphatases are a family of PI 3-phosphatases that dephosphorylate phosphotidylinositide 3-phosphate (PI3P) and 3,5-diphosphate ($PI(3,5)P_2$). CMT4B2 is caused by the loss of MTMR13, a catalytically inactive myotubularin pseudophosphatase. Though the genetic cause of this disease is known, the mechanism by which loss of MTMR13 causes dysfunction and pathology in SCs remains unclear. The work presented here translates a mouse model of CMT4B2, *Mtmt13*$^{-/-}$, into a robust *in vitro* system where lentivirus mediated expression of exogenous proteins can be used to better understand the roots of CMT4B2 myelin pathology. Using this system, both the active phosphatase MTMR2 and a consitituvely active Rab21 mutant were shown to impact *Mtmt13*$^{-/-}$ myelin abnormalities. These promising findings support the use of the *in vitro* CMT4B2 disease model and provide new evidence that MTMR13 may act through multiple pathways during myelination. Currently, there is no treatment or cure for any form

of CMT. Through studying the role of PI phosphatases and pseuodphosphatases and the endosomal/lysosomal pathway in myelination, the role of MTMR13 in the SC will be better understood, potentially leading to avenues for future CMT therapies.

Chapter 1 — Introduction to the Mechanisms of Schwann Cell Myelination and Inherited Peripheral Neuropathy

Forward

All cells depend on efficient protein synthesis, appropriate trafficking, and effective degradation machinery to maintain cellular homeostasis. Many specialized cell types are polarized, or have unique asymmetrical structure with specialized internal compartments (Masaki, 2012). All polarized cells must establish and maintain compartments and asymmetrical specializations in order to perform their functions (Trapp et al., 1995; Masaki, 2012; Pereira et al., 2012). Polarized cell types depend on tightly regulated intracellular protein trafficking to avoid mistargeting of new proteins, and efficient degradation pathways to prevent accumulation of proteins in specialized cellular compartments (Trapp et al., 1995; Mellman and Nelson, 2008; Masaki, 2012; Pereira et al., 2012). Polarized cell types maintain multiple specialized regions, and this specialization is maintained via internal compartmentalization (Masaki, 2012). A myelinating Schwann cell (SC) relies on spatial and temporal compartmentalization of signaling machinery to develop and maintain its characteristic myelin sheath (Poliak et al., 2002; Ozçelik et al., 2010; Simons et al., 2012; Heller et al., 2014). Disruptions in internal protein localization can dramatically affect the function of polarized cell types. Genetic conditions that only affect certain cell types, despite the ubiquitous loss of the protein, help further the understanding of the basic biology of specialized cells. This work explores disrupted phosphoinositide lipid signaling caused by the loss of a myotubularin pseudophosphatase. The loss of this myotubularin phosphatase has major impacts specifically on myelinating Schwann cells. I have advanced an *in vitro* system to study effects of the loss of this phosphatase in Schwann cells, as well as a lentivirus

mediated method to manipulate gene expression in this system. By studying endosomal signaling in the context of myelination and an inherited peripheral neuropathy that specifically impacts myelinating Schwann cells, I hope to add to the understanding of basic Schwann cell biology that may one day yield therapies for patients.

1.1 — Introduction to the Peripheral Nervous System (PNS)

The human nervous system is divided into the central nervous system (CNS) and the peripheral nervous system (PNS). The CNS includes the brain and spinal cord, and the PNS encompasses the neurons and non-neuronal cells that exist outside the brain and spinal column (Hildebrand et al., 1994; Jessen and Mirsky, 2005; Kidd et al., 2013; Puelles, 2013). The PNS feeds our CNS information on the world outside — it allows us to sense our environment and respond with movement. Sensory neurons, with their cell bodies in the peripheral dorsal root ganglion facilitate our experience of touch, temperature, and vibration, while motor neurons enable complex motor responses to movement (Jessen and Mirsky, 2005; Ashwell and Waite, 2012; Kidd et al., 2013). Axons in the PNS can be extremely long, for example motor neurons with a cell body in the lumbar spinal cord send axons to innervate distal limbs (Hildebrand et al., 1994; Nave, 2010a; Puelles, 2013). Axons communicate via electrical action potentials that travel from the sodium channel rich axon hillock to the nerve terminal to release, in the example of a motor neuron, acetylcholine neurotransmitter to muscles (Salzer, 2003; Kaplan et al., 2009). Because axons are so long, passive electrical conduction is not fast or efficient enough to move signals down the axon (Lillie, 1925; Huxley and Stämpeli, 1949; Salzer, 2003). In the PNS, myelinating SCs line up to insulate the axon, clustering sodium channels between then and enabling salutatory conduction, wherein an axon potential jumps between nodes without losing strength (Lillie,

1925; Tasaki, 1939; Huxley and Stämpeli, 1949; Waxman, 1980; Rosenbluth, 1999; Salzer, 2003). SCs are critical to sensory perception and motor responses. Without the support of glia like SCs, long axons could not efficiently transmit electrical signals or keep themselves healthy. Indeed, SCs are critical to human biology, and loss of SC function leads to debilitating disease.

1.1.1 —Schwann Cell Myelin

Myelin was first described in 1719 by van Leeuwenhoek, whose early artistic descriptions of myelin were enabled by his technical skills at creating lenses (Rosenbluth, 1999; Boullerne, 2016). In the mid-1800s, myelin was described by scientists with names that are familiar to today's researchers: Remak, Schwann, Charcot, Ranvier, Schmidt and Lanterman (Rosenbluth, 1999; Kidd et al., 2013; Boullerne, 2016). Myelin was named by Virchow, based on the Greek word for bone marrow, who was also the first to suggest that myelin acted as an insulator in 1858 (Rosenbluth, 1999; Baumann and Pham-Dinh, 2001; Kidd et al., 2013; Boullerne, 2016). This theory was expanded on by Ranvier in 1878, but evidence for the idea salutatory conduction would not come until early in the 20th century (Lillie, 1925; Tasaki, 1939; Huxley and Stämpeli, 1949). Only in the last 50 years has the study of genetics, cell biology, and myelin disease research sufficiently advanced to enable a nuanced understanding of myelin development, normal function, and genetic causes of disease. Now, the focus is on the molecular mechanisms that enable the formation of healthy myelin, and how these are dysregulated in disease.

1.1.2 — Schwann Cell Differentiation and Development

SCs reside in the PNS, where they are the primary glial cell. During development, the neural crest cells that will become the PNS neurons, SCs, and other PNS cell types migrate

throughout the embryo (Woodhoo and Sommer, 2008; Snaidero and Simons, 2014; Monk et al., 2015). These neural crest cells differentiate as they migrate to form PNS structures, as well as non-neural cell types such as melanocytes, smooth muscle, connective tissue, and bone (Woodhoo and Sommer, 2008; Monk et al., 2015). Schwann cells, DRG neurons, and other PNS cell types exit the neural crest by moving along the ventral pathway (Kidd et al., 2013; Monk et al., 2015). Migratory neural crest cells differentiate into Schwann cell precursors (SCPs). This transition from neural crest cell to SCP requires expression of the transcription factor SRY related HMG box 10 (Sox10) (Britsch et al., 2001; Svaren and Meijer, 2008). The activation of Sox10, in turn, begins a cascade towards the eventual transition to mature SCs (Suter and Scherer, 2003; Jessen and Mirsky, 2010; Pereira et al., 2012). SCPs migrate along developing axons and continue to proliferate. As they transition into immature SCs, SCPs halt their migration along axons within the developing nerve, begin generate basal lamina, and are no longer dependent on the axonal cues that guide migration (Jessen, 2004; Jessen and Mirsky, 2005; 2010; Monk et al., 2015).

A Schwann cell's relationship to axons begins early in development as Schwann cell precursors (SCPs) migrate to axon bundles and send out processes that interdigitate and eventually encircle the axon bundle (Nave, 2010b; Kidd et al., 2013; Salzer, 2015). In the developing nerve, immature SCs corral and organize axons. Immature SCs encircle multiple axons of various sizes, and these axons are sorted by the immature SC in a process known as radial sorting (Yang et al., 2005; Jessen and Mirsky, 2010; Monk et al., 2015; Feltri et al., 2016; Taveggia, 2016). This process separates out larger caliber axons (≥1 μm in diameter) for 1 axon : 1 SC relationships for eventual myelination. Radial sorting in the PNS was recently shown to depend on Protein Associated with Lin Seven 1 (Pals1), a protein critical for establishing polarity in other cell types (Ozçelik et al., 2010; Zollinger et al., 2015). While

Pals1 was shown to be nonessential for normal CNS myelination, loss of Pals1 (via a conditional knockout strategy) impaired radial sorting and delayed myelination in the PNS (Zollinger et al., 2015), pointing to SC-specific myelination mechanisms that rely on the establishment of polarity in the SC.

During radial sorting, individual axons are segregated out for 1:1 relationships. The immature SCs continue to proliferate (and differentiate into myelinating SCs) in order to create enough SCs to fully myelinate the larger caliper axons in a bundle (Snaidero and Simons, 2014; Feltri et al., 2016). SC proliferation and differentiation are regulated by gene expression as well as signaling including Jun activation domain-binding protein 1 (Jab1; which coordinates laminin211 signaling in SCs to regulate cell cycle, proliferation, and differentiation) and the cyclin-dependent kinase inhibitor p27 (a positive regulator of myelination required for differentiation to pro-myelinating SC) (Li et al., 2011; Feltri et al., 2016) (Porrello et al., 2014). As radial sorting progresses, smaller axons are retained in bundles, and will eventually be encircled by non-myelinating SCs in mature Remak bundles (Feltri et al., 2016). Eventually, mature axon bundles contains only small caliber axons, these small fibers include nociceptive C-fibers (see (Feltri et al., 2016) for an excellent review of SC axon sorting). SCs that enter into 1:1 relationships with axons are termed pro-myelinating SCs, while SCs that encircle multiple smaller axons are termed non-myelinating SCs (Monk et al., 2015).

1.1.3 —Regulation of Myelination

Tight gene regulation, as well as controlled production and targeting of myelin proteins is critical to SC differentiation and myelination. Transcriptional control of myelination relies on a network of transcription factors, whose expression enables the developing SC to

transition from a migrating neural crest cell to a mature SC (Jessen and Mirsky, 2010; Stolt and Wegner, 2016). As mentioned above, Sox10 is a critical transcriptional regulator of SCPs. Sox10 activation of the Oct6 SC enhancer (SCE), upregulates the transcription factor Oct6, which in turn acts with Sox10 to drive transcription myelin transcription factor Krox20 (Jagalur et al., 2011; Pereira et al., 2012; Stolt and Wegner, 2016). In order to initiate a myelin sheath, timely transcription of the transcription factor Krox20 is essential for SC myelination (Murphy et al., 1996; Parkinson et al., 2004; Jessen and Mirsky, 2010; Monk et al., 2015). Activation of Krox20 triggers the synthesis of proteins critical for the structure of the myelin sheath, including myelin basic protein (MBP) and myelin protein zero (P0) (Murphy et al., 1996; Parkinson et al., 2004; Jessen and Mirsky, 2010; Stolt and Wegner, 2016).

Axonal neuregulin-1 type III (NRG1-III) regulates multiple stages of SC development and via SC ErbB receptors. NRG1-ErbB2/3 signaling controls differentiation, and drives MAPK (Shp2, Mek, Erk1/2) and PI 3-kinase pathways to initiate myelination (Nave and Salzer, 2006; Sheean et al., 2014; Lee et al., 2016). Production of critical myelin proteins (MBP, P0, PMP22) and NRG1-ErbB2/3 signaling is significantly downregulated as SCs mature and require less myelin protein synthesis to as myelin sheath formation is completed (Garratt et al., 2000; Sheean et al., 2014). Interestingly, sustaining MAPK activation at this critical time of maturation can lead to sustained myelin overgrowth. MAPK activation overwhelms the normal response to a maturing SCs reduction in NRG1-ErbB2/3 signaling (Sheean et al., 2014). These studies illustrates one pathway that can be dysregulated to a more immature state to induce protein expression and myelin over-production in SCs.

1.1.4 — Endosomal Trafficking is Critical to Schwann Cell Polarization and Myelination

Once in a 1:1 relationship with an axon, a Schwann cell transitions from a pro-myelinating to a mature, myelinating SC. As Kidd et al. eloquently describe in their 2013 review, one human Schwann cell can produce 20 mm^2 of specialized myelin membrane. This is several orders of magnitude greater than the membrane area produced by other cell types. In terms of area alone, myelin production places unique and extreme demands on a Schwann cell (Kidd et al., 2013; Snaidero and Simons, 2014). Myelinating SCs must tightly regulate gene expression, cellular polarity, and intracellular trafficking in order to successfully create and maintain a myelin sheath (Scherer and Wrabetz, 2008; Masaki, 2012).

Shen and colleagues recently showed that normal SC polarity at the point of contact between the SC and the axon is required for normal myelination and axon conduction velocity. They showed that liver kinase B1 (LKB1/Par4) was asymmetrically localized to the area of the SC in contact with the axon, and that protein kinase A phosphorylation of LKB1/Par4 critical to its polarized localization and to myelination (Shen et al., 2014). Loss of LKB1/Par4 leads to reduced myelination and impaired axon conduction velocity. Disruption in the phosphorylation of LKB1/Par4 (or loss of the protein) appeared to interfere with the process of SC maturation. SCs without LKB1/Par4 showed elevated Oct-6 transcription factor levels, indicating that they remain immature (Jagalur et al., 2011; Shen et al., 2014; Stolt and Wegner, 2016). This work provides a framework for understanding polarity in SCs. In this case, interfering with phosphorylation of LKB1/Par4 disrupts its polarized localization to the axon interface. Loss of this polarized localization is sufficient to arrest the development of the SC and attenuate myelination, underscoring the importance of cell polarization in SCs.

The myelin sheath has many functions. It serves to electrically insulate the axon it wraps, clustering the axon's ion channels between Schwann cells at the nodes of Ranvier and thereby promoting salutatory conduction (Elmer et al., 1990) (Girault and Peles, 2002; Occhi et al., 2005; Sherman and Brophy, 2005). It also physically protects and provides tropic support to the axons (Nave, 2010b). To establish a mature myelin sheath, SCs turn on the genes needed to synthesize, traffic, target the relevant proteins and lipids to the developing sheath. The SC wraps the axon multiple times and compacts the new layers of myelin (Monk et al., 2015; Salzer, 2015). The thickness of the myelin sheath is critical to maintain nerve conduction velocity (NCV) (Waxman, 1980; Cotter et al., 2010). Thick myelin sheaths have been shown to be toxic to axons, and myelin sheaths that are too thin are also unhealthy for axons (Cotter et al., 2010). The wrapping of the myelin sheath is tightly regulated. Discs large 1 (Dlg1) and phosphatase and tensin homolog deleted on chromosome 10 (PTEN) interact to negatively regulate myelination (positively regulated by axonal axonal NRG1/Erb2/3 signaling) via by reducing activation of AKT, and thereby inhibiting myelination (Cotter et al., 2010). Without this critical interaction, in models with reduced Dlg1, hypermyelination, abnormal redundant loops of myelin (myelin outfoldings), and demyelination ensued (Cotter et al., 2010).

Within a myelinating SC, new proteins are synthesized in the cytoplasm near the nucleus as well as in other regions on non-compact myelin, including witin cytoplasmic channels (Gould and Mattingly, 1990; Salzer, 2015). Myelin microdomains, or lipid rafts, contain lipids, cholesterol, and myelin proteins like myelin basic protein (MBP; destined for compact myelin) or 2',3'-cyclic nucleotide 3'-phosphodiesterase (CNP; destined for noncompact myelin) (Taylor et al., 2002; DeBruin et al., 2005). The creation and shipping these, and other signaling and myelin components, to the correct internal compartment is critical to

myelin formation (Taylor et al., 2002; DeBruin et al., 2005; Simons and Trotter, 2007). The early endosome is a sorting station critical to protein trafficking, endocytosis, and protein degradation (Di Paolo and De Camilli, 2006; Zoncu et al., 2009; Marko Jovic, 2010). Plasma membrane containing myelin components are assembled with the help of MPB, endocytosed, and trafficked to the endosome. (Taylor et al., 2002; Simons and Trotter, 2007). As myelin assembly progresses, myelin microdomain containing endosomes are trafficked and exocytosed.

Beyond myelin components, Rabs, PIs, and other membrane associated singling molecules traffick via the endosomal/lysosomal system(Jean and Kiger, 2012). Dysfunction in the cellular systems of protein sorting and trafficking can have disastrous effects for cells, leading to the accumulation or impaired targeting of proteins. For example, the loss of *Fig4* leads to impaired endosomal/lysosomal trafficking and impairs normal autophagic processes, by interrupting the fusion of the lysosome and autophagosome (to form the autophagolysosome (Ferguson et al., 2009; Vaccari et al., 2015). Diseases that impair protein trafficking do not always impact all cell types. For example, many forms of the CMT family of inherited peripheral neuropathies only impact the PNS (Timmerman et al., 2014). Despite the functional similarity between CNS and PNS myelinating cells, most demyelinating peripheral neuropathies do not affect CNS oligodendrocytes (Saporta and Shy, 2013). Inherited peripheral neuropathies that disrupt PNS function by impacting endosomal trafficking are reviewed in detail later in this chapter. By studying a genetic condition that preferentially impacts SC myelination in the PNS, we can better understand the the specialized biology of SCs and basic membrane biology of all cells.

1.1.5 — PNS Myelin Sheath Assembly Requires Key Lipids and Proteins

Unique mechanisms enable myelin sheath assembly and compaction in SCs. While aspects of the sheath are common between SCs and their CNS counterparts, key proteins and lipids are unique to PNS myelin. It is known that myelin basic protein (MBP), myelin protein zero (P0), peripheral myelin protein 22 (PMP22), and peripheral myelin protein 2 (P2) are involved in compaction and compact SC myelin stabilization, while the larger proteins 2',3'-Cyclic-nucleotide 3'-phosphodiesterase (CNP) and myelin associated glycoprotein (MAG) are found in specialized non-compact regions. MBP and P2 each facilitate stacking of lipid bilayers, and their ability to stack increases when together (Suresh et al., 2010; Aggarwal et al., 2011; 2013). Stable CNS myelin compaction is dependent on proteolipid proteins PLP and DM20, where PLP is thought to self-associate when myelin compacts, forming a zipper that stabilizes compact myelin (Klugmann et al., 1997; Bakhti et al., 2014). In the PNS, once MPB reaches a critical mass, its self-association drives a zipper-like action that excludes both cytoplasm and large proteins like MAG and CNP from SC myelin (Aggarwal et al., 2011; Zuchero and Barres, 2011; Bakhti et al., 2014).

The understanding of myelin compaction at a molecular level has recently grown due to the work of Mikael Simons' group. MPB makes up five percent of PNS myelin protein (Kidd et al., 2013). It is described as a small (15 — 25 kDa) unstructured protein with multiple size and charge isomers and size isoforms (Boggs, 2006; Kidd et al., 2013; Steshenko et al., 2016). MBP thought to be involved in myelin layer adhesion and is found at the cytoplasmic membrane where it binds negatively charged lipids and associates with a number of other structural and signaling proteins (Boggs, 2006; Aggarwal et al., 2013). Simons' group studied the mechanisms by which MBP proteins assemble and exclude large membrane proteins. They found the MBP molecules undergo a phase transition as they aggregate into a linked network, largely mediated by hydrophobic phenylalanine residues

(Aggarwal et al., 2011; 2013). This phase transition is facilitated by the MBP's self association via hydrophobic interactions. In this way, MBP polarizes the developing myelin membrane by excluding large proteins in order to enable membrane compaction (Aggarwal et al., 2011; Zuchero and Barres, 2011; Aggarwal et al., 2013). The experiments informing this model were done in oligodendryocytes, but MBP is abundant in Schwann cell myelin as well. Beyond it's role as a myelin adhesion molecule or scaffold, recent work has shown an active role for MBP in cerebellar neurons. Lutz et al. elegantly showed that it is expressed by cerebellar neurons and this MBP cleaves the adhesion molecule L1 in its extracellular domain. Cleaved L1 stimulates neurite outgrowth and pays a role in neuroprotection (Lutz et al., 2014). Any similar role of MBP in the PNS has yet to be determined, however this work illustrates an active role that MPB can play.

Other key players in SC compact myelin include P0, PMP22, and P2 (Kidd et al., 2013; Salzer, 2015). P0 and PMP22 are two small proteins found in compact myelin that are critical for normal myelination. Mutations in both cause CMT (Hayasaka et al., 1993; Suter and Scherer, 2003; Nave et al., 2007)3. P0 (m.w. 30 kD) is a immunoglobulin-family glycoprotein with a transmembrane domain and a cytoplasmic c-terminus with an extracellular domain (Liu et al., 2012). P0 is located throughout the compact region of the myelin sheath, and its structure is thought to be critical for homophilic interactions that stabilize PNS compact myelin (Filbin and Tennekoon, 1993; Liu et al., 2012; Kidd et al., 2013). CMT type 1B is caused by mutations to the gene that codes for P0 on chromosome 1 (Hayasaka et al., 1993; Corrado et al., 2016). Approximately 50-70% of PNS myelin protein is P0, and it is critical for adhesion of myelin layers in the compact regions of the sheath (Greenfield et al., 1973; Kidd et al., 2013). PMP22 (m.w. 22 kD) is a protein with four transmembrane domains thought to be critical in early myelin sheath formation (Amici et al., 2006; Kidd et al., 2013).

PMP22, like P0, is located throughout the compact regions of the myelin sheath. PMP22 knockout mice show delayed myelination, aberrant basal lamina deposition, and markedly reduced expression of beta-4 integrin (Amici et al., 2006), indicating a role for PMP22 in extracellular matrix adhesion with alpha-6 beta-4 laminin-integrin complex. Mutations to the gene that codes for PMP22 cause CMT type 1A. Duplication of a *PMP22* allele as the most common form of CMT overall, however a deletion of *PMP22* also causes disease (Suter and Scherer, 2003).

Not every myelin protein is critical for myelination. Peripheral myelin protein 2 (P2 or Pmp2) is another small (14.5kD) protein found in peripheral myelin, however unlike P0 and PMP22, its loss does not derail myelination. A fatty acid binding family member, it was thought to function similarly to MBP. However is 2014 the work of Zenker et al. showed that a Pmp2 knockout mouse, $Pmp2^{-/-}$, can construct largely normal myelin sheaths with little effect on motor nerve conduction (Zenker et al., 2014). This is markedly different form $MBP^{-/-}$ or "Shiverer" mice which do not myelinate normally. $Pmp2^{-/-}$ mice do, however, show alterations to their lipid profiles at P10, indicating altered fatty acid composition. Pmp2 is able to bind fatty acids and transport them to membranes, and the loss of this function disrupts the lipid homeostasis of myelin (Zenker et al., 2014). This underscores that cellular compensation for genetic mutations can occur in SCs.

Beyond the compact areas of myelin, maintenance of non-compact regions in the myelin sheath are critical to SC health. The non-compact myelin regions such as Schmidt-Lanterman incisures and paranodal loops serve as reservoirs of Schwann cell cytoplasm that house a collection of proteins distinct from compact regions, including signaling complexes, junctional proteins, and adhesion complexes (Kidd et al., 2013). Gap and tight junctions are found in non-compact regions, where they form an efficient pathway between cytoplasm in

non-compact regions and the rest of the myelin sheath internode (Salzer, 2015). Several larger proteins, MAG and CNP, are excluded from compact myelin and found in the non-compact regions of the myelin sheath. MAG (100kD) is a relatively large protein found in non-compact areas of Schwann cell myelin, such as Schmidt-Lanterman incisures and paranodal loops (Quarles, 2007; Kidd et al., 2013). MAG knockout mice provided an early example of myelin disruption impacting axon function (Yin et al., 1998). MAG and oligodendrocyte myelin glycoprotein (Omgp) have been shown to bind Nogo receptor (NgR1) to restrict axon growth after injury and play a role in CNS plasticity myelin (Liu et al., 2002; Quarles, 2007). CNP is an enzyme present in non-compact regions of the myelin sheath (Myllykoski et al., 2016). It is more abundant in oligodendrocyte CNS myelin than in Schwann cell PNS. Recent work questions the enzymatic activity of CNP in all cell types and posits a structural role instead in myelinating cells wherein CNP would stabilize interactions between the cytoskeleton and membranes (Myllykoski et al., 2013; 2016).

A SC's mature myelin sheath is maintained, likely though cytoplasmic channels (as posited by Nave et al., described in 1.1.6) and Schmidt-Lanterman incisures (Snaidero and Simons, 2014; Snaidero et al., 2014a; Salzer, 2015). Gillespie et al. developed a mouse lacking L- and S-periaxin, PDZ-domain containing proteins involved in myelin stability. This *Prx* $^{-/-}$ knockout mouse myelinated abnormally, showing evidence of hypermyeination, followed by demyelination and remyelination (Gillespie et al., 2000). In addition to abnormal myelination *Prx* $^{-/-}$ also exhibited a loss of Schmidt-Lanterman incisures (Gillespie et al., 2000). This may indicate the critical nature of these structures in myelin sheath establishment, health, and maintenance (Gillespie et al., 2000; Salzer, 2015). Taken together, studies of the proteins present in non-compact myelin and its structural role in the sheath

illustrate the critical nature of non-compact myelin as a site for signaling, stabilization, and cytoplasmic exchange via gap junctions in the SC myelin sheath.

1.1.6 — Myelin Sheath Wrapping Requires Phosphoinositide Membrane Lipids and Trafficking Via Non-Compact Regions

Though the structure of the completed myelin sheath is well described, the precise method by which the myelin sheath is established via membrane wrapping in SCs and oligodendrocytes is still a subject of debate (BUNGE et al., 1989; Simons and Trotter, 2007; Sobottka et al., 2011; Snaidero and Simons, 2014; Snaidero et al., 2014a). The origins of pathological redundant loops of myelin termed outfoldings, a hallmark of CMT, are also unclear (Mathis et al., 2015). The temporal regulation of the wrapping process itself may hold clues to how myelin outfoldings form. Mechanisms and structural processes behind myelin wrapping in the CNS have been recently explored via high pressure freeze electron microscopy. Such work has lead to a new model of oligodendrocyte myelination (Snaidero and Simons, 2014; Snaidero et al., 2014a). Several theories have been put forth to describe how a myelinating cell might wrap spirally while extending all or part of its processes along the full length of the internode. Models include "the carpet crawler" wherein a myelinating SC extends the length of the node before the adaxonal inner tongue spirals around the axon to wrap, like a carpet being rolled up (BUNGE et al., 1989). Alternately, the "liquid croissant" model of CNS myelination posits a spiraling action that does not require full node coverage before wrapping begins (Sobottka et al., 2011).

New methods have allowed high resolution examination of myelin structure, and support a pattern of development wherein the inner tongue of a myelinating oligodendrocyte process encircles an axon and then continues to wrap from the inside, i.e. with the inner

tongue as the leading edge of myelination (Snaidero et al., 2014a; Nawaz et al., 2015). This group, led by Nave, found that myelin compaction occurs from the outside layers in. Specifically, they propose a of model of myelination wherein myelin basic protein (MBP) is made in the inner region of the Schwann cell, close to the axon, and as the inner tongue continues to push forward and wrap the axon, the MBP diffuses back and is compacted. As this is occurring, the inner tongue region is rich in CNP which prevents myelin compaction (Kidd et al., 2013; Myllykoski et al., 2016). Trafficking was observed oriented towards the inner tongue region of the developing myelin sheath, pointing polarization and growth at the inner tongue.

This process was shown to be regulated by the availability of membrane lipid phosphatidylinositol (3,4,5) tri-phosphate (PI $(3,4,5)P_3$) (Vanhaesebroeck et al., 2012). Specifically, when more PI $(3,4,5)P_3$ was available to oligodendrocytes *in vitro*, the oligodendrocyte outer rim — a proxy for the inner tongue of an oligodendrocyte *in vivo* — myelin was larger (Snaidero et al., 2014a). Similarly, when PI $(3,4,5)P_3$ was available via open cytoplasmic channels, myelin thickness increased (Snaidero et al., 2014a). The group also showed cytoplasmic channels critical for myelin biogenesis, and described the relative frequency cytoplasmic channels as tracking closely with that of myelin abnormalities resembling outfoldings in wild-type oligodendrocyte myelin sheaths (in the optic nerve) during development (≤7% at P10, reducing to nearly between 0 and 1% by P60) (Snaidero and Simons, 2014; Snaidero et al., 2014a). This work presents a model wherein cytoplasmic channels critical for protein trafficking transiently form during development in response to the availability of membrane lipids like $PI(3,4,5)P_3$ to enable myelin growth in the inner tongue as the outer layers of myelin compact. The authors also posit that because the frequency of outfoldings in genetically normal cells tracks with the frequency of cytoplasmic

channels during development, diseases that manifest with myelin outfolding phenotypes may include dysfunction in the regulation of cytoplasmic channels (Snaidero and Simons, 2014; Snaidero et al., 2014a). While this model is specific for oligodendrocytes, it contains ideas such as dependence on availability of specific membrane lipids, use of cytoplasmic channels to traffic material, and relationship between those channels and outfoldings that may apply to SCs as well.

1.1.7 — Basal Lamina Enable Schwann Cells to Interact with Their Enviornment

Studies of the basal lamina have clarified novel mechanisms by which SCs regulate and interact with their environment. SCs deposit a characteristic basal lamina of extracellular matrix proteins at their abaxonal (outer) membrane. Basal lamina deposition begins in immature SCs and the lamina matures as the SC matures (Monk et al., 2015; Feltri et al., 2016). Components of the basal lamina differ depending on the Schwann cell's stage in development and duties (Occhi et al., 2005; Court et al., 2006). The basal lamina consists of a collagen-rich outer layer and a laminin rich Lamina Lucida close to the abaxonal Schwann cell membrane (Court et al., 2006). Laminin has three subunits (α, β, and γ) that combine to form a trimeric glycoprotein. The specific type of integrin receptors expressed by the Schwann cell vary according to the Schwann cell's role. For example, it has been shown that specific laminin-binding subunits of the β-1 integrin receptor are critical for radial sorting (Pellegatta et al., 2013). It has also been shown that laminin composition of the basal lamina is heterogeneous even within a cell and that specialized regions of laminin at the nodes of Ranvier, for example, play a role in normal node organization and sodium channel clustering (Elmer et al., 1990; Girault and Peles, 2002; Feltri and Wrabetz, 2005; Occhi et al., 2005; Sherman and Brophy, 2005; Court et al., 2006). Recent work from Kelly Monk's group has

indicated the critical role that adhesion-class g-protein coupled receptor 126 (Gpr126) plays in radial sorting and peripheral myelination. Gpr126 undergoes autoproteolytic cleavage resulting in a laminin-binding N-terminus fragment. When the N-terminus fragment binds lamnin, it stabilizes the C-terminus transmembrane fragment in an inactive conformation, inhibiting G_s signaling, which limits cyclic adenosine monophosphate (cAMP) levels and signaling to keep the SC in an immature state (Petersen et al., 2015). Ligands for Gpr126 include extracellular matrix proteins like specific collagens and laminins that are known components of the basal lamina (Occhi et al., 2005; Court et al., 2006). This work adds to our understanding of how SCs regulate the environment of the developing axon through their basal lamina and signaling interactions with the extracellular matrix.

1.1.8 — Schwann Cells and Axons Engage in Bidirectional Signaling and Support

Myelin sheaths are the electrical insulators of the nervous system. These dense lipid-rich membranes increase electrical resistance and physically cluster ion channels at the nodes of Ranvier to speed electrical signaling via salutatory conduction (Occhi et al., 2005; Sherman and Brophy, 2005; Nave, 2010b; Salzer, 2015). SCs in contact with axons inhibit ankyrin G mediated clustering of axonal sodium channels, this restricts sodium channels to the axon initial segment and Nodes of Ranvier, which facilitates salutatory conduction (Ching et al., 1999; Voas et al., 2009). SCs and the axon engage in bidirectional signaling and trophic support. Both myelinating and nonmyelinating SCs are critical to the axons they ensheath or bundle. Beyond electrical insulation, communication between axon and Schwann cell via multiple signaling pathways has shown bidirectional influence, with both the axons and SC retaining ability to influence to other (Nave, 2010a). Downregulation of SC myelin genes can impact axon growth. For example, mice lacking either the peripheral myelin protein 22 gene

(trembler mice, *Pmp22*$^{-/-}$) or the myelin basic protein gene (shiverer mice, *MBP*$^{-/-}$) have smaller axons, indicating that axons are influenced by SC dysfunction early in development (de Waegh et al., 1992; Brady et al., 1999). A classic part of SC function is to provide trophic support to axons, so the impact of impaired SCs on axons is not surprising. However, axons also provide instruction to SCs during development. Developing SCs respond to axonally expressed neuregulin-1 type III (NRG1-III), and threshold levels of NRG1-III signaling to SC ErbB receptors, as well as threshold axonal diameter, are needed to initiate myelination (Nave and Salzer, 2006; Lee et al., 2016). In nonmyelinating SCs, which bundle axons in so-called Remak bundles, the SCs remain critical to axonal survival. Work by Beirowski et al. showed that LKB1 kinase activity in nonmyelinating SCs is necessary for survival of Remak bundle axons (Beirowski et al., 2014). Meanwhile, axons in relationships with myelinating SCs were less affected by the loss of LKB1. Another group recently showed that abnormal lipid metabolism by SCs can cause the release of toxic compounds that directly damage adjacent axons (Viader et al., 2013). These reports underscore the importance of SC health from the perspective of local axons, and illustrate some of the signaling pathways that SCs and axons use to communicate (Monk et al., 2015).

1.2 — Myelin Dysfunction and Disease

Myelinating and non-myelinaitng SCs have complex and specific metabolic needs. Diseases that impair myelination have heterogeneous causative mechanisms. Clinical literature, now informed by next generation sequencing, has illustrated the consequences of SC dysfunction in the PNS. Myelin diseases were historically diagnosed in a way that did not separate them from other types of neuropathies, for example identified thorough functional examination of a patient in the clinic. Diseases that affect CNS or PNS myelination can be

inherited, due to sporadic genetic mutation, immune-mediated, acquired through chemotherapy or idiopathic (Shubin and Weiner, 1989; Waldman and Banwell, 2011; Gajofatto et al., 2013; Sylvester et al., 2014; Presas-Rodríguez et al., 2016). Multiple Sclerosis (MS) is a common CNS demyelinating disease, impacting 1 in 400 people worldwide (Compston and Coles, 2002; Giovannetti et al., 2017). MS may be idiopathic or acquired and the disease manifests with an initial demyelinating event (IDE) that may be accompanies by sudden disability (Compston and Coles, 2002; Gajofatto et al., 2013; Giovannetti et al., 2017). Inherited demyelinating neuropathies, on the other hand, are more likely to be known to a family (Brooks and Emery, 1982; Klein et al., 2013; Saporta and Shy, 2013). These include some forms of familial amyotrophic lateral sclerosis (ALS), the Charcot-Marie-Tooth (CMT) family of neuropathies (discussed in detail in the next section), as well as Hereditary Neuropathy with Liability to Pressure Palsies (HNPP), Dejerine-Sottas syndrome (DSS), and congenital hypomyelinating neuropathy (CHN) (Suter and Scherer, 2003; Mathis et al., 2015). In the last twenty years, advances in genetic tools have clarified the genetic roots of myelin disease (Timmerman et al., 2014). Only in the last five years has the rescue of CMT myelin disease phenotypes been demonstrated in model systems (Bolis et al., 2009; Vaccari et al., 2015; Kagiava et al., 2016). Though therapeutic strategies have advanced to clinical trials for some forms of CMT, none have yet succeed to make meaningful impact on patient outcomes (Gess et al., 2015). As the pace of discovery continues to accelerate in cell biology, I am optimistic that better understanding of disease mechanisms will lead to therapies for patients.

1.2.1 — Introduction to Charcot-Marie-Tooth Peripheral Neuropathy

Charcot-Marie-Tooth (CMT) neuropathies are a group of hereditary neuropathies classified originally by three physicians in the 1880's, J.M. Charcot, P. Marie, and H.H. Tooth (Brooks and Emery, 1982; Saporta and Shy, 2013). It is classically described as a progressive inherited neuromuscular disease preferentially affecting long axons (Saporta and Shy, 2013). CMT patients are heterogeneous, the disease can be caused by multiple genetic mutations, and even two patients with similar genetic profiles can have different levels of functional disability and different paces of disease progression (Cornett et al., 2016).

CMT neuropathies are the most common type of inherited peripheral neuropathy, affecting 1:2500 people (ninds.nih.gov, charcot-marie-tooth.org), with heterogeneous genetic cause and clinical presentation. Over 80 genes are known to be involved in CMT peripheral neuropathy (Saporta and Shy, 2013; Timmerman et al., 2014). There are two types of CMT, demyelinating CMT (types 1, 3, and 4) and axonal CMT (type 2) (Suter and Scherer, 2003; Nave et al., 2007; Saporta and Shy, 2013). Demyelinating forms of CMT are often Schwann cell autonomous, meaning they affect SCs first, which leads to secondary axonal loss of function and axon death. Demyelinating forms of CMT are characterized in the clinic by reduced nerve conduction velocities (NCVs) (Suter and Scherer, 2003). Axonal CMT affects the neuron itself, leading to a loss of axons and loss of motor function with no reduced NCV (Suter and Scherer, 2003). Forms of CMT can be autosomal dominant recessive, x-linked, intermediate dominant, or recessive (Szigeti et al., 2006; Saporta and Shy, 2013). CMT can present in the clinic as sporadic, but may be the result of previously undescribed genetic mutations (Nakhro et al., 2013). Inheritance patterns of CMT, genes involved in CMT, and distinctions between subtypes of CMT are not always straightforward (Claramunt et al., 2005; Berciano et al., 2012; Timmerman et al., 2014). For example, both autosomal dominant and recessive inheritance patterns have been reported with CMT-causing

mutations in the PMP22 (CMT1A) and GDAP1 (CMT4A) genes, though CMT1 is classically defined as autosomal dominant and CMT4 is classically defined as recessive (Claramunt et al., 2005). Similarly, mutations in the P0 gene have been reported to cause demyelinating and axonal CMT in different cases (Hayasaka et al., 1993; Marrosu et al., 1998; de Jonghe et al., 1999). Despite this heterogeneity, clinical characteristics and genetic profiles group patients with CMT in major categories, described in more detail below.

1.2.2 — Diagnosis of CMT

Today, CMT is diagnosed through a combination of functional and genetic testing in the clinic. Most patients present at the clinic in childhood or young adulthood, though some forms of CMT remain subclinical and do not seriously interfere with motor function until adulthood (Suter and Scherer, 2003; Claramunt et al., 2005; van Paassen et al., 2014). CMT is classically characterized by progressive distal muscle weakness and wasting, and may also involve distal sensory loss, foot deformities, pain, and loss of tendon reflexes(Reilly, 2016) (Mathis et al., 2015). The Charcot-Marie-Tooth disease (CMT) neuropathy score (CMTNS) was developed in 2005 by Michael Shy, Mary Reilly, and colleagues as a more specific CMT neuropathy measure

(Shy et al., 2005; Mannil et al., 2014). This assessment emphasizes motor function in order to more accurately capture information on the patient's history and disease progression (Shy et al., 2005). At the time this scoring system was developed, there was disagreement in the field on the efficacy of the CMTNS (Padua et al., 2006). However, in the intervening years, the CMTNS has become a common method for scoring CMT disability. It is often reported along with other methods, like the Overall Neuropathy Limitations Scale (ONTS). The goal of measurement of function and quality of life in CMT research is to

improve researcher's ability to detect changes over time and measure impact of therapy in clinical trials (Pagliano et al., 2011; Mannil et al., 2014).

Over the years, as the understanding of the genetic causes of inherited peripheral neuropathy have improved, the number of genes involved in CMT has ballooned. Although the cost of genetic testing and next generation sequencing is falling, it can still be a long road for patients to get a precise diagnosis (Berciano et al., 2012; Li et al., 2016; Reilly, 2016). Mary Reilly, in a 2016 editorial, eloquently makes the case that all patients should have access to genetic testing to understand their specific disease subtype (Reilly, 2016). She argues that knowing the genetic cause of a patient's disease can help the patient come to terms with their condition, enables the patient to participate in clinical trials, and - importantly - provides the information a clinician needs to give an accurate prognosis and to help the patient understand inheritance pattern of their specific condition (Reilly, 2016). Saporta and Shy's 2013 review illustrates the clinical decision tree for genetic testing based on nerve conduction velocity testing. Most patients are initially tested for forms of CMT1. These account for about 70% of the CMT patients in North America and about 40-50% globally (Saporta and Shy, 2013; Fridman et al., 2015; Rossor et al., 2016). Less common forms, such as CMT4B2, require more specialized testing that is becoming more widely available and affordable (Saporta and Shy, 2013; Rossor et al., 2016). As next generation sequencing becomes less expensive, new genetic causes for inherited peripheral neuropathies are being discovered, and more complex genetic causes are being clarified (Lupski et al., 2010; Nakhro et al., 2013; Timmerman et al., 2014; Mathis et al., 2015). For example, the deeper understanding of CMT enabled by more complete sequencing clarified that a family where half the siblings had demyelinating CMT was the result of distinct subclinical heterozygous mutations in *SH3TC2* in both parents, and the clinical result for the compound

heterozygous children is CMT4C (Lupski et al., 2010). While the number of known genetic causes continues to grow, the patient experience of CMT can also improve through next generation sequencing enabled improvements in diagnoses.

For informative tables detailing the forms of CMT and other hereditary peripheral neuropathies, I refer the reader to the following reviews (Suter and Scherer, 2003; Saporta and Shy, 2013; Rossor et al., 2016).

1.2.3 — The CMT Family of Inherited Peripheral Neuropathies

Generally, patients with inherited autosomal dominant, demyelinating peripheral neuropathy are classified as CMT1. CMT1A is the most common form of CMT (Saporta and Shy, 2013). CMT1A accounts for 40-50% of CMT patients worldwide and is often the first genetic test offered to patients presenting unexplained muscle weakness, atrophy, and reduced NCVs (Szigeti et al., 2006). CMT1A patients also experience pain, caused by the abnormalities in unmyelinatied bundles of C and A- δ fibers (Laurá et al., 2014; Nolano et al., 2015). The mechanism of disease of CMT1A was one of the first CMT mechanisms to be explained. It is caused by duplication of the PMP22 gene, leading to a hyperproduction and accumulation of the peripheral myelin protein 22 (PMP22) (Suter and Scherer, 2003). Deletion of *PMP22* is also linked to disease, causing hereditary neuropathy with liability to pressure palsies (HNPP). Mutations in *PMP22* also cause disease, though the duplication and deletion are more common (Szigeti et al., 2006). The molecular causes of CMT1A and HNPP underscore the importance of tight regulation of myelin components in Schwann cells (Suter and Scherer, 2003). There are also reports of x-linked and recessive *MPZ* mutations (CMT1B), underscoring the hererogeneity of CMT (Sanmaneechai et al., 2015; Corrado et al., 2016).

Of special interest, the myelin phoentype of a mouse model of CMT1X was recently partially rescued via intrathacal injection of lentivirus to the lumbar spinal column. CMT1X is caused by caused by mutations to the gap junction protein beta 1 gene (*GJB1*); the gene that codes for Connexin 32 (Cx32) (Kagiava et al., 2016). This form of x-linked CMT was paritally ameliorated in a *Gjb1*$^{-/-}$ mouse model of CMT1X via sub-arachnoid spinal delivery of lentivirus vector containing human *GJB1*, illustrating the potential of lentivirus-mediated gene manipulation to address PNS-specific loss of function genetic conditions (Kagiava et al., 2016).

CMT2 patients have autosomal dominant, axonal forms of inherited peripheral neuropathy. Distinct from demyelinating forms of CMT, forms of CMT2 impairs axon function. It is typically characterized by loss of myelinated axons often no associated change to NCV (Suter and Scherer, 2003; Saporta and Shy, 2013). As an interesting point of historical perspective, it took more than ten years to correctly identify the gene responsible for most forms of CMT2A. In 2001, it was reported that *KIF1B* was the gene (Zhao et al., 2001). Recently it was discovered that mutations in the critical mitochondrial gene *mitofusin 2* (*MFN2*) cause about 20% of CMT2 patients, making it the common from of axonal CMT now termed CMT2A2 (Feely et al., 2011; Scherer, 2011). Mutations in the genes that code for cytoskeletal protein KIF1B do cause axonal CMT, but this form is rare (CMT1A1) (Zhao et al., 2001; Berciano et al., 2012). Mutations in another cytoskeletal element, *NEFL*, are responsible for CMT2E (Jordanova et al., 2003; Agrawal et al., 2014). CMT2B is caused by mutations in *RAB7* (Verhoeven et al., 2003). Interestingly, both CMT1B and CMT2I/J are caused by *MPZ* mutations, with patients who exhibit near normal NCVs and late onset CMT classified as CMT2I/J (Nelis et al., 1996; Sanmaneechai et al., 2015).

There are twelve distinct genes classified as involved in CMT4 (Timmerman et al., 2014; Rossor et al., 2016). All are autosomal recessive, and most are early onset, Schwann cell autonomous, demyelinating forms of CMT (Rossor et al., 2016). Patients present in the clinic with distal leg weakness, abnormal gait, loss of sensation, foot deformities (for example, hammertoe), and in some cases glaucoma (Suter and Scherer, 2003; Hirano et al., 2004; Chen et al., 2014; Negrão et al., 2014). Patients become symptomatic within the first decade of life, and most are significantly mobility-impaired by the age of thirty (Suter and Scherer, 2003; Negrão et al., 2014). CMT4B types 1, 2, and 3 all arise from mutations that affect myotubularin phosphatase family proteins, though the progression of CMT4B1 appears to be more rapid than that of CMT4B2 (Houlden et al., 2001; Azzedine et al., 2003; Senderek et al., 2003; Conforti et al., 2004a; Nakhro et al., 2013).

CMT4B2 is an autosomal recessive condition that causes early-onset demyelination with focally folded myelin outfoldings and secondary axonal death in the peripheral nervous system (Previtali et al., 2007). Both sensory and motor axons are affected. CMT4B2 is caused by mutations in the gene *SBF2/MTMR13* that codes for the myotubularin pesudophosphatase MTMR13 (Azzedine et al., 2003; Senderek et al., 2003; Conforti et al., 2004a). Eight forms of CMT4, including CMT4B2, specifically affect genes involved in the endosomal sorting and signaling pathway. These genes include endosomal PI 3-phosphatases (*MTMR2*, CMT4B1; *SBF2/MTMR13,* CMT4B2; *SBF1/MTMTR5,* CMT4B3; *FIG4,* CMT4J), regulators of endocytosis (*FGD4*/Frabin, CMT4H), endosomal sorting associated proteins (*LITAF/SIMPLE*, CMT4C), and recycling endosome proteins (*NDRG1,* CMT4D; *SH3TC2*, CMT4C) (Kachhap et al., 2007; Robinson et al., 2008; Arnaud et al., 2009; Vaccari et al., 2011; Horn et al., 2012; Qin et al., 2016; Vijay et al., 2016) - to be discussed in more detail later in this chapter.

1.2.4 — CMT Patient Outcomes and CMT Therapies in Development

There are no cures or therapies to slow the progression of CMT. Without a way to halt the disease progression, CMT patients rely on physical and occupational therapy, as well as orthopedic surgery in some cases, to retain some measure of mobility and comfort (Saporta and Shy, 2013). Saporta and Shy describe generalized treatment courses that involve physical therapy (PT) to support muscle tone and balance, occupational therapy (OT) to develop strategies to cope with ambulation and limb/hand weakness, orthotic support braces to assist ambulation, and in some cases surgical intervention to lengthen tendons (Saporta and Shy, 2013; Bensoussan et al., 2016). Recent research (published by Mary Reilly's group) has shown that although people with CMT use proximal muscles to compensate for distal weakness, there is little quantifiable benefit to strength training of proximal muscles for patients with CMT (Ramdharry et al., 2014). However, with improvements to the study design, the authors remained optimistic about the general benefits of exercise for CMT patients (Ramdharry et al., 2014). Further work published by Reilly's group investigated CMT patient mobility and behavior patterns to design better physical therapy programs and research studies metrics to improve the assessment of the impact of exercise and strength training in this population (Ramdharry et al., 2016). While the field continues work to better understand this disease, most patients rely on PT, OT, and supportive caregivers to stay as mobile as possible.

Ongoing clinical trials address both therapy via molecular drug-based approaches and characterization of patient motor/sensory function to improve measurement of the impact of physical therapy on patient outcomes. Over 50 active clinical trials addressing CMT are currently listed on clinicaltrials.gov. Many of these are characterization studies, which are designed to better understand forms of the disease, understand patient priorities,

and develop meaningful quantitative measurements of patient outcomes. For example, clinical trial ID# NCT02429947 is a study to measure what impacts quality of life from the patient's perspective, while NCT01193075 and NCT01203085 are designed to test pediatric CMT assessment scales on specific CMT subtypes. At the same time, preclinical work and metaanalyses continue to advance the understanding of disease roots and heterogeneous patient populations (as an example, see recent diagnostic baseline established for CMT1B (Sanmaneechai et al., 2015), and see (Cornett et al., 2016; Rudnik-Schöneborn et al., 2016) for plots showing high variability across types of CMT and within patient subgroups). This underscores how nascent the available therapies are for forms of CMT.

One clinical trial tested coenzyme Q10 as a treatment for CMT, however while this study was completed in 2013 the results have not been published (ID# NCT00541164). Coenzyme Q10 is an antioxidant though to support mitochondrial function. Indeed, mitochondrial dysfunction has been linked to peripheral neuropathy and SC function (Viader et al., 2013; Ino and Iino, 2016). A coenzyme Q10 analog called Idebenone was reported to be successful at improving respiratory function in patients with Duchenne muscular dystrophy (DMD) who suffer from weakness of respiratory muscles that can be fatal (Buyse et al., 2015) . However, pathomechanisms of DMD and CMT are quite different. Another recnet clinical trial investigating the neuroprotective potential of coenzyme Q10 in Parkinson's patients failed to find any benefit (Parkinson Study Group QE3 Investigators et al., 2014). This result, taken together with the lack of a publication from the CMT clinical trial after three years, is probably a negative indicator for the potential of coenzyme Q10 in CMT.

Despite advances *in vitro* and with animal models, only the most common form of CMT, CMT1A, has been approached with drug-bases therapies with solid pre-clinical

backing. CMT1A, caused by a duplication of *PMP22* allele that leads to an overproduction of PMP22, is the only form of CMT for which drugs designed to halt the disease progression have advanced to clinical trials (Suter and Scherer, 2003). Ascorbic acid treatment of genetic knockout model animals of CMT1A was shown to reduce pathological overexpression of pmp22 via reducing cAMP levels. cAMP reduction was shown to negatively regulate *PMP22* expression, promote myelination, and improve behavioral measures of rodent coordination (Kaya et al., 2007). However, no effect of ascorbic acid treatment has been observed in human patients, across several clinical trials (Lewis et al., 2013; Gess et al., 2015).

A new study of low doses of a three drug cocktail of baclofen, naltrexone and sorbitol, termed PXT3003, has recently moved to Phase III clinical trials as a treatment for CMT1A (clinicaltrials.gov identifier: NCT02579759). The preceding Phase II trial indicated that this cocktail was safe and found a small improvement (approximately 5%, based on 2016 published erratum correction (Attarian et al., 2016)) in several measures of clinical outcome at the highest dose high dose (6 mg baclofen, 0.7 mg naltrexone and 210 mg sorbitol)(Attarian et al., 2014). This cocktail is believed to affect CMT1A phenotype by through multiple mechanisms to reduce PMP22 expression (via impacting cAMP levels) and support axon function (Chumakov et al., 2014). Baclofen is a γ-aminobutyric acid [GABA]-B receptor agonist. GABA-B receptors are metabotropic seven-transmembrane g-protein coupled receptors that activate adenylate cyclase and are known to be present on SC membranes (Procacci et al., 2013; Faroni et al., 2014). In the context of CMT1A, baclofen is anticipated to agonize the GABA-B receptor, activating adenylate cyclase, reducing the levels of SC intracellular cAMP, and therefore reducing transcription of PMP22 . Naltrexone, an opioid receptor antagonist, at low doses has been shown to potentiate opioid receptor and g-alpha inhibitory ($G_{\alpha i}$) signaling and reduce cAMP levels (Chumakov et al., 2014). D-sorbitol

is the third drug in the cocktail. It binds muscarinic acetylcholine receptors to impact cAMP levels (Chumakov et al., 2014).

Architects of this approach posit that a multi-drug strategy is more likely to have a functional impact on patient motor/sensory outcomes (Attarian et al., 2014; Chumakov et al., 2014) The next step in the process, a Phase III clinical trial, is currently enrolling participants (clinicaltrials.gov identifier: NCT02579759). As CMT loss of function begins early in life for most patients, it will remain challenging to measure functional improvement in adults who have more advanced disease progression (Mannil et al., 2014). Ultimately any successful therapy will likely need to assessed in children for the best chance at efficacy (Pagliano et al., 2011; Cornett et al., 2016). If successful, a combinatorial drug approach may conceptually inform approaches to treat rarer forms of CMT.

1.3 — Endosomal/Lysosomal Signaling in Demyelinating Forms of CMT

Though many genes are involved in CMT, a distinct group of genes critical to the endosomal/lysosomal pathway are implicated. Of the 80 known CMT genes, 16 are linked to demyelinating forms of CMT (Rossor et al., 2016), see Figure 1.1. Of these, a subset of nine are linked to genes involved in endosomal/lysosomal signaling and pathway (Timmerman et al., 2014; Rossor et al., 2016). These genes code for endosomal phospholipid phosphatases (*MTMR2*, CMT4B1; *SBF2/MTMR13,* CMT4B2; *SBF1/MTMTR5,* CMT4B3; *FIG4,* CMT4J), regulators of endocytosis (*FGD4*/Frabin, CMT4H), proteins involved in endosomal-multivesicular body sorting (*LITAF/SIMPLE*, CMT4C), proteins present at recycling endosomes (*NDRG1,* CMT4D; *SH3TC2*, CMT4C), and proteins critical for endocytosis and vesicle trafficking (*DNM2*, CMTDIB/CMT2M; *ARHGEF10*, SNCV/CMT1 (Rossor et al., 2016) (Bolino et al., 2000; Kachhap et al., 2007; Robinson et

al., 2008; Arnaud et al., 2009; Bitoun et al., 2009; Vaccari et al., 2011; Horn et al., 2012; Qin et al., 2016; Shibata et al., 2016; Vijay et al., 2016). Of special interest to this work are the mutations in three myotubularin family members, the active phosphatidylinositol-3-phosphatase MTMR2, as well as two catalytically inactive myotubularin family members, MTMR5 and MTMR13. Loss of function mutations in all three lead to CMT4B peripheral neuropathy. All of these forms of CMT4B are demyelinating, though their severity and precise phenotype vary. This cluster of CMT genes that when mutated lead to demyelinating neuropathy are key evidence for the critical role of the endosomal/lysosomal pathway in myelination, see Figure 1.1.

Phosphoinositides (PIs) are fundamental regulators of the endosomal/lysosomal trafficking system. Genes that encode PI phosphatases cause CMT4 when mutated (CMT types 4B1, 4B2, 4B3, as well as CMT4J). These proteins, MTMR2, MTMR13, MTMR5, and FIG4, respectively, belong to proteins families of PI phosphatases and pseudophosphatases (Laporte et al., 1996; Blondeau et al., 2000; Taylor et al., 2000; Duex et al., 2006; Chow et al., 2007). Specifically, MTMR2, MTMR13, and MTMR5 are myotubularin-family phosphatidylinositol 3-phosphate (PI3P) 3-phosphatases, though MTMR13 and MTMR5 are both inactive pseudophosphatases (Firestein et al., 2002; Kim et al., 2003; Dang et al., 2004; Robinson and Dixon, 2006). While FIG4 both stimulates the PI 3-kinase PIKfyve and is a PI 3,5-biphosphate ($PI(3,5)P_2$) 5-phosphatase (Duex et al., 2006; Chow et al., 2007; Vaccari et al., 2011). Reported mutations in CMT4B types 1, 2, 3, and CMT4J confer a loss of function, or in some cases a truncated protein (Hirano et al., 2004; Conforti et al., 2004a; Murakami et al., 2013; Nakhro et al., 2013; Guimarães-Costa et al., 2015). In these forms of CMT loss of the active or inactive phosphatase in SCs is pathological; despite ubiquitous expression of these proteins, SCs are affected while other cells in the body are largely

unaffected. These phosphatases are expressed ubiquitously, and disease causing loss of the phosphatases occurs in all cell types. The genetic causes of SC dysfunction have strongly suggested a critical role for PI phosphatases in myelination. However, in most cases, the role of the protein in the cell and the mechanistic connection between myelin abnormalities and the genetic cause of disease remain unclear.

1.3.1 — Phosphoinositides are Critical to Intracellular Membrane Trafficking

Phosphoinositides (PIs) are membrane lipids that represent a relatively small fraction (<1%) of all cellular lipids, yet play a critical role in intracellular membrane trafficking and signaling (Amoasii et al., 2012; Jean and Kiger, 2012; Maffucci, 2012; Balla, 2013). Phosphoinositides consist of a hydrophilic, polar *myo*-inositol ring joined to two hydrophobic, non-polar fatty acid chain tails (Balla, 2013). The *myo*-inositol ring has three locations, the 3, 4, and 5 positions, where it can be reversibly phosphorylated (Falkenburger et al., 2010; Balla, 2013). This enables the creation of seven distinct phosphoinositides, which serve as the cell's internal membrane identity regulation system, see Figure 1.2. Each PI is able to recruit and bind different effectors at the membrane (Cantley, 2002; Di Paolo and De Camilli, 2006; Maffucci, 2012). Phosphoinositide-binding effectors include proteins that specific domains with affinity for one or more PI(Kutateladze, 2010). Of interest here are Fab1/YOTB/Vac1/EEA1 (FYVE) domains, which specifically bind PI3P (Cantley, 2002; Kutateladze, 2010; Maffucci, 2012). Plextrin homology (PH) domains bind multiples PIs with weak specificity (Salim et al., 1996; Lemmon, 2008; Leonard and Hurley, 2011; Maffucci, 2012). Pleckstrin homology-glucosyltransferase, Rab-like GTPase activator and myotubularins (PH-GRAM) domains, reported to bind PI(3,5)P_2 and PI4P (Berger et al., 2003; Maffucci, 2012). Though PIs are make up a small fraction of total cellular lipids,

specific PIs are enriched on specific membranes (Falkenburger et al., 2010; Balla, 2013). PI(4,5)P_2 and PI4P are reported to be the most abundant PIs, found on the cytoplasmic side of the plasma membrane and the golgi apparatus (Stahelin et al., 2014). PI3P, PI(3,5)P_2 and PI(3,4,5)P_3 are less abundant, but enriched on the early endosome, late endosome/lysosome, and plasma membrane, respectively (Marko Jovic, 2010; Stahelin et al., 2014). Enrichment of specific PIs on creates a flexible and reversible system of membrane tagging that is tightly regulated by PI kinases and PI phosphatases. Through regulated spatiotemporal alterations of the phosphate groups in the 3, 4, and 5 positions, PI phosphatases and PI kinases contribute to regulating the identity of intracellular membranes and thus, in cooperation with Rabs, direct trafficking of these membranes inside the cell.

1.3.2 — Phosphoinositide Regulation by Kinases and Phosphatases

Membrane identity is controlled by PI composition, which is in turn regulated by PI kinases and PI phosphatases, recruited to the PI-containing membranes by the kinase or phosphatase's intrinsic PI-binding regions (FYVE, PH-GRAM, etc) or relationships with other PI-binding effector proteins (Stahelin et al., 2014). This creates a coincidence detection system, wherein a PI3P rich membrane will recruit both PI kinases/phosphatases and other signaling proteins with FYVE domains together at the subcellular compartment (Stahelin et al., 2014). Cells have dramatic responses to altered PI identity, for example overexpression of an inactive version of PI 5-kinase PIKfyve results in enlarged endosomes and vacuoles, indicating accumulation of incorrectly tagged membrane quickly interferes with cellular function (Ikonomov et al., 2001). PI regulation by kinases and phosphatases is critical in all cells, but SCs appear to be uniquely susceptible to disruptions in endosomal PI regulation, perhaps due to the sheer volume of membrane that a myelinating SC need to maintain.

Class II PI 3-kinases (PI3K) C2α, C2β, C2γ and the class III PI 3-kinase Vps34 phosphorylate the 3 position of phosphatidylinositol, and to have diverse downstream effects on the cell (Vanhaesebroeck et al., 2012). PI3K-C2α and VPS34 were shown to work in concert to create $PI(3,5)P_2$, which regulate the activation of mTOR (Bridges et al., 2012). Vps34 is known to be critical for β2-adrenergic receptor (β2-AR) recycling. When Vps34 is inhibited, β2-ARs are trafficked incorrectly, accumulating in the cell rather than trafficking back to the membrane or the the early endosome for sorting (Awwad et al., 2007). Recent work confirmed this with more specific inhibitors and showed that inhibition of Vps34 limited activated β2-AR's ability to elicit a cAMP response in the cell (Uchida et al., 2016). This work highlights the broad impact that PI kinases and phosphatases have in the cell.

Class I PI 3-kinases are involved in acute AKT-mTOR signaling at the SC abaxonal and adaxonal membranes (Salzer, 2015). Salzer's group recently identified PI 3-kinases (that generate $PI(3,4)P_2$ and triphosphate $PI(3,4,5)P_3$) as key players in multiple pathways in SC, influencing both the developing SC at the abaxonal membrane and mature SC at the adaxonal membrane (Heller et al., 2014). PI 3-kinases can support myelination in promyelinating SCs, where axonal NRG1 III interacts with SC ErbB signaling, via PI 3-kinases to activate AKT and mTOR. In myelinating SCs, on the other hand, laminin-α6β4 signaling mediated by PI 3-kinases downregulates myelination. Laminin-α6β4 / PI 3-kinase signaling activates the Sgk1 kinase which phosphorylates NDRG1, inhibiting myelination(Heller et al., 2014; Salzer, 2015). Normally, NDRG1 is upregulated at myelin initiation and expressed throughout the SC, but phosphorylated only in the abaxonal compartment (Heller et al., 2014). This work illustrates the different roles PI 3-kinases can take on depending on their subcellular localization and temporal regulation.

PI phosphatases act to dephosphorylate the 3, 4, or 5 position on the PI *myo*-inositol ring (Amoasii et al., 2012; Balla, 2013). The human CMT disease relevant PI 3-phosphatases MTMR2 MTMR13, MTMR5, and FIG4 will be discussed in detail in sections 1.3.5 — 1.3.7. Phosphatases too have demonstrated interactions with signaling pathways beyond PIs. For example, Bolino's group showed that MTMR2, a critical early endosomal PI 3-phosphatase, also interacts with the membrane scaffold and polarization protein Discs large 1 (Dlg1) to influence membrane formation (Bolino et al., 2004; Bolis et al., 2005; 2009). In the context of PI regulation, the importance of PI kinases and PI phosphatases is clear - PI membrane identity is critical for intracellular membrane trafficking. However, the work of Salzer, Bolino, and others illustrates that PI kinases and phosphatases may play multiple roles, some of which may be non-catalytic.

1.3.3 — Regulation of the Early Endosome is Critical to Cell

The early endosome is an intermediate sorting stop for vesicles endocytoced in from the plasma membrane (Di Paolo and De Camilli, 2006; Marko Jovic, 2010). Receptors and other membrane proteins are endocytosed and these vesicles fuse with the early endosome (Marko Jovic, 2010). From the early endosome, membrane can be recycled back to the plasma membrane, sent on to the lysosome for degradation, or trafficked back to the *trans*-Golgi (Bonifacino and Rojas, 2006; Luzio et al., 2010; Marko Jovic, 2010). The Golgi is rich in PI4P, while endocytoced vesicles and early endosome are rich in both PI3P and Rabs, including Rab5, Rab21, and Rab35 (Jean and Kiger, 2012). Recycling endosomes require Rab11 and PI4P, whereas late endosomes and lysosomes are richer in Rab7 and PI(3,5)P_2 (Sönnichsen et al., 2000; Stenmark, 2009; Jean and Kiger, 2012; 2014; Stahelin et al., 2014; Ketel et al., 2016). Rab activity is also required for the transition from early endosome to late

endosome (Stenmark, 2009). Specifically blocking Rab35, or its activation by DENN1a, results in enlarged early endosomes and a failure of cells to initiate recycling (Allaire et al., 2010). Regulation of endosomal PI identity and Rab activation have emerged as key to the flow of trafficking and sorting intracellular endosomes (Stenmark, 2009).

Of the genes linked to the endosomal/lysosomal system that are associated with forms of CMT, a distinct group are directly associated with endocytosis and endosomal trafficking. These genes include endosomal PI 3-phosphatases (*MTMR2*, CMT4B1; *MTMR13,* CMT4B2; *MTMTR5,* CMT4B3; *FIG4,* CMT4J), endocytosis regulator (*FGD4*/Frabin, CMT4H), endosomal sorting (*LITAF/SIMPLE*, CMT4C)*,* recycling endosome proteins (*NDRG1,* CMT4D; *SH3TC2*, CMT4C), and proteins critical for clathrin-mediated endocytosis and vesicle trafficking (*DNM2*, CMTDIB/CMT2M; *ARHGEF10*, SNCV/CMT1 (Rossor et al., 2016) (Bolino et al., 2000; Kachhap et al., 2007; Robinson et al., 2008; Arnaud et al., 2009; Bitoun et al., 2009; Vaccari et al., 2011; Horn et al., 2012; Qin et al., 2016; Shibata et al., 2016; Vijay et al., 2016). See Figure 1.1 and 1.2 for illustrations of specific early endosomal genes linked to CMT and more detail on the role of myotubularins in the endosomal/lysosomal pathway.

While this cluster of endosome-related mutations causes demyelinating CMT, the mechanisms of action for individual proteins are quite different, and some remain unclear. Disrupted endocytosis, endosomal sorting, and intracellular vesicle trafficking all appear to have major impacts on myelination SCs. Disrupting any part of this pathway apparently results in SC dysfunction. CMT4H, for example, is a form of autosomal recessive demyelinating CMT caused by disruptions to *FGD4* gene. FGD4 is a Cdc42 guanine nucleotide exchange factor (GEF), which acts to catalyze the activity of the Rho-GTPase Cdc42 (Horn et al., 2012). *Fgd4*$^{-/-}$ mice exhibit myelin abnormalities similar to those seen in

patients, as well as a reduction in active Cdc42-GTP and reduced endocytosis (as assessed by fluorescent cell sorting for the transferrin receptor *in vitro*) (Horn et al., 2012). Disruption of FGD4's Cdc42 GEF activity has a significant impact on Schwann cell myelination, though its cellular impact appears to be restricted to endocytosis-related pathways, in patients and rodent models. DNM2 is critical to clathrin mediated endocytosis, and mutations that affect *DMN2* lead to centornuclear myopathy (CNM), intermediate CMTDIB, and axonal CMT2M (Bitoun et al., 2009). DMN2 mutants were shown to have impaired endocytosis in both cell lines and experiments done with CMN patient fibroblasts (Bitoun et al., 2009). Further signaling defects were found in cell lines, where DMN2 mutants disrupted MEK-ERK signaling, pointing to a possible mechanism for the gross myelin abnormalities seen in patients (Bitoun et al., 2009).

1.3.4 — Regulation of Autophagic Can Impact Schwann Cell Myelination

Several groups have manipulated *Atg7*, a gene critical for autophagy, and seen effects on SC myelin. Gomez-Sanchez et al. knocked out *Atg7* and saw no changes to mature myelin sheaths, but did observe a significantly impaired response to injury in SCs (Gomez-Sanchez et al., 2015). They coined the term "myelinophagy" to describe the specific JNK/c-Jun signaling mediated autophagy used by SCs in response to injury (Thumm and Simons, 2015; Jessen and Mirsky, 2016). Another group, on the other hand, did see a SC myelin phenotype. Jang et al. knocked out *Atg7* in SCs and reported abnormally large SC cytoplasm. Atg7 is an essential component of macroautophagy. Loss of Atg7 resulted in SCs with abnormally large cytoplasm, increased numbers of ribosomes, and large ER structures. Modest hypermyelination of small axons was also observed. Jang et al. posit that normally SCs reduce cytoplasm via Atg7-dependent autophagy during myelin development and

maturation, and that this autophagy may be one part of SC regulation of myelination and myelin sheath maturity (Jang et al., 2015).

The *Drosophila* homologue of MTMR13, Sbf, was recently shown to be critical for autophagosome fusion with the lysosome via its Rab21 GEF activity (Jean et al., 2015). Though this work did not address myelination, if Schwann cell maturation does require autophagy and MTMR13 is a key player part of in that pathway, then MTMR13 and Rab21 mediated autophagy pathway could present a mechanism for the myelin dysfunction seen in CMT4B2.

1.3.5 — The Myotubularin Phosphatase Family's Role in Disease

Myotubularin phosphatases are family of protein tyrosine phosphatases (PTP) that act as specific PI 3-phosphatases and pseudophosphatases (Taylor et al., 2000; Raess et al., 2016). These proteins are evolutionarily conserved in eukaryotes - found in humans as well as lower organisms like worms, flies, and yeast (Laporte et al., 1998; Taylor et al., 2000; Robinson and Dixon, 2006; Amoasii et al., 2012; Jean and Kiger, 2012; Raess et al., 2016). There are fourteen member proteins in this family, however only eight of them are active phosphatases (Robinson and Dixon, 2006; Hnia et al., 2012; Jean and Kiger, 2012; Raess et al., 2016). Phosphatase activity depends on an amino acid motif of Cys-X_5-Arg (Denu et al., 1995; Denu and Dixon, 1998). During PI 3-phosphatase activity, the Cys associates a with phosphoinositide PO_3, disassociating from the PI to form a phosphocysteine that is stabilized by the arginine, until the phosphate group is released to a water molecule, and finally an neighboring aspartic acid group stabilizes an oxygen on the phosphatase group (Guan and Dixon, 1991; Robinson and Dixon, 2006). The other six myotubularins are inactive phosphatases. Most are structurally similar to the active myotubularins, but their

PTP domains contain mutations at the Cys and Arg positions of the Cys-X_5-Arg motif and are therefore not catalytically active. These inactive substitutions are conserved across species (Robinson and Dixon, 2006). Mutations that lead to loss of function of three myotubularin family members lead to peripheral neuropathy. These are active phosphatases MTMR2, as well as two inactive myotubularin family members, MTMR5 and MTMR13. MTMR5 and MTMR13 are larger and more complex than the other family members (Robinson and Dixon, 2006). As we gain insight into their role in the basic biology of cell, we can better understand how the loss of MTMRs contributes to SC-specific disease.

Mutations in the active MTMR MTM1 lead to the muscle disorder X-linked centronuclear myopathy (XLCNM). While not a condition affecting SCs, the work on XLCNM is of interest as a mouse knockdown model has shown that the loss of MTM1 impaired exocytosis from endosomes (Ketel et al., 2016) (Amoasii et al., 2012). The same group used cells from XLCNM patients to establish a direct link between PI hydrolysis at endosome and patients XLCNM, observing a buildup of β1-integrin (Ketel et al., 2016). This work lead to a model in which the transition from sorting early endosome to recycling endosome is dependent on both MTM1 and the conversion of PI3P (sorting early endosome) to PI4P (recycling endosome)(Ketel et al., 2016). This model illustrates how myotubularins may impact trafficking, and how endosomal dysfunction can have broad effects. Dysregulation of recycling endosomal trafficking also alters cellular β1-integrin signaling and exocytosis, leading to debilitating effects in patients (Amoasii et al., 2012; Ketel et al., 2016).

Mutations in MTMR2, an active myotubularin family PI 3-phosphatase, cause CMT4B1 (Bolino et al., 2000). CMT4B1 is characterized in humans as a recessive demyelinating

inherited neuropathy featuring myelin outfoldings (Houlden et al., 2001; Suter and Scherer, 2003; Berger et al., 2006). *Mtmr2*$^{-/-}$ mice exhibit myelin abnormalities similar to human patients, including the characteristic myelin outfoldings (Bolino et al., 2004). These outfoldings in *Mtmr2*$^{-/-}$ mouse SCs have now been ameliorated in multiple way *in vitro*. Re-introduction of MTMR2, inhibition of Sec8, and inhibition of PIKfyve have all reduced *Mtmr2*$^{-/-}$ myelin outfoldings (Bolis et al., 2009; Vaccari et al., 2011). These approaches will be discussed in more detail in section 1.3.7. These studies support the concept that recovering the levels of PI3P, that are disrupted when MTMR2 phosphatase activity is lost, can recover SC myelin dysfunction.

The active myotubularin phosphatase MTM1, MTMR2 are critical to cell function. Loss of either results in human disease (Buj-Bello et al., 1999; Houlden et al., 2001). However, inactive pseudophosphatase family members are also linked to disease (Azzedine et al., 2003; Nakhro et al., 2013). Mounting evidence points to a role for myotubularin pseudophosphatases in localization, stabilization, and enhancement of catalytic activity in active counterparts (Robinson and Dixon, 2005; Zou et al., 2009; Jean et al., 2012; Zou et al., 2012; Ng et al., 2013). For example, Zou et al. showed that the inactive pseudophosphatase MTMR9 has been reported to complex with the active phosphatases MTMR6, MTMR7, and MTMR8 where it influences which PIs they prefer to dephosphoryate and increases their activity (Zou et al., 2009; 2012). Recent work in the Robinson lab has shown that pseudophosphatases MTMR13 acts to stabilize levels of the active phosphatase MTMR2 (Ng et al., 2013). The critical role of both the active and pseudophosphatases has been underscored by the consequences of protein loss in both human patients mouse models. Mutations in the genes for the active myotubularin phosphatases MTMR2 (CMT4B1) and MTM1 (X-linked centronuclear myopathy, XLCNM) lead to SC autonomous demyelinating

CMT and congenital myopathy, respectively (Buj-Bello et al., 1999; Houlden et al., 2001). However, mutations in the genetic code for inactive phosphatases MTMR5 (CMT4B3) and MTMR13 (CMT4B2) also lead to demyelinating peripheral neuropathy (Azzedine et al., 2003; Senderek et al., 2003; Nakhro et al., 2013; Negrão et al., 2014). Understanding the role of these inactive phosphatases is critical to helping patients who currently have limited treatment options.

1.3.6 — MTMR13 Structure and Function

MTMR13 is a large, multidomain protein that is associated with early endosomal membranes and is critical to SC myelination. While it does not act as a phosphatase, it is known to stabilize the active PI 3-phosphatase MTMR2 at the early endosome (Ng et al., 2013). Literature describing patient outcomes and rodent models with the loss or mutation of MTMR13's multidomain architecture points to a critical role in SCs. Patients with frame-shifts, large deletions, and likely truncated proteins have been reported (Azzedine et al., 2003; Senderek et al., 2003; Conforti et al., 2004a; Chen et al., 2014; Negrão et al., 2014). Figure 1.3, adapted from several sources (Robinson and Dixon, 2006; Amoasii et al., 2012; Raess et al., 2016), illustrates a general cartoon of the structure of myotubularin family members, including MTMR13.

MTMR13 and MTMR5 are unique among the myotubularin family due to their size and structure, which could confer distinctive function in the cell. MTMR13 (1849 amino acids) and MTMR5 (1867 amino acids) are significantly larger than other family members, and include distinct functional domains not found in any of the active phosphatases (Raess et al., 2016). A review of their domain architecture presents multiple locations that are candidates for critical associations and signaling relationships. MTMR13's domains include a

coil-coil domain that is likely important for complexing with other myotubularin family members (MTMR2, MTMR5) (Robinson and Dixon, 2005; Ng et al., 2013). A pleckstrin homology glucosyltransferase, Rab-like GTPase activator and myotubularins (PH-GRAM) domain is a common element to all myotubularin family members, thought to be involved in associations with other myotubularins and membrane association via $PI(3,5)P_2$ binding (Maffucci, 2012; Raess et al., 2016). In addition to this, MTMR13 and MTMR5 have a second c-terminus pleckstrin homology (PH) domain, also thought to at aid in membrane association (Amoasii et al., 2012). MTMR13's DENN domain is at the N-terminus of the protein, and in model systems the DENN domain has been shown to act as a Rab-GEF (Jean and Kiger, 2012; Jean et al., 2012; 2015). This multidomain architecture hints that MTMR13 may function as a scaffold, capable of bringing the active myotubularin phosphatase MTMR2 and Rabs together on the PI3P, $PI(3,5)P_2$—rich membrane of the early endosome to facilitate signaling and appropriate endosomal trafficking. Understanding which of MTMR13 and MTMR5's domains are critical for myelination presents a technical challenge and an important key to understanding the disease mechanisms of CMT4B2 and CMT4B3.

MTMR13's DENN domain or its downstream partners may eventually be a therapeutic target, if indeed it is the loss of this domain that is critical for SC function. DENN domains can bind PIs, hinting at a role for MTMR13's DENN domain in localization and stability at the membrane (Allaire et al., 2010). DENN domains have been shown to act as Rab-GEFs in several systems, for example the DENN1A domain is a GEF for Rab35 (Allaire et al., 2010; Yoshimura et al., 2010). Perhaps more relevant for its role in SCs, the MTMR13 homologue in *Drosophila* (Sbf), has been shown to interact with both PI 3P-phosphatases and kinases as well as Rabs, coordinating PI regulation and Rab signaling at

the early endosome to control cellular processes (Jean et al., 2012). More specifically, Jean et al. showed that the Sbf and Mtm form a complex, homologous to human MTMR13 and MTMR2, which is necessary for both regulation of PI3P turnover and actin-related membrane dynamics(Jean et al., 2012). In addition, this group showed that both Rab21 and Rab11 interact with Sbf. Rab21 was shown to colocalize with Sbf at the early endosome, while Rab11 is a well characterized recycling endosome-associated Rab. However, only Rab21 appeared to act as a guanine exchange factor (GEF) for the DENN domain of Sbf, indicating that Sbf-DENN can activate Rab21 (Jean et al., 2012). Rab GEFs are essential for appropriate Rab recruitment to membranes. Recent work in human cell lines suggests that the MTMR13 activation of Rab21 is specifically required for autophagosome-lysosome fusion in starvation conditions (Jean et al., 2015). If the DENN domain of human MTMR13 or MTMR5 acts as a Rab GEF, even if this only happens in stressed cellular conditions, it would help to explain the CMT4B2 and 3 phenotypes and provide a new avenue of approach for therapeutic intervention (Jean and Kiger, 2012; Jean et al., 2012; Blümer et al., 2013).

1.3.7 — The Balance of Phosphoinositides, PI Kinases, and PI Phosphatases at the Early Endosome

Phosphoinositide dysregulation has been implicated as the cause of multiple conditions. Figure 1.1 details the eight forms of peripheral neuropathy that are specifically linked to the early endosome (Rossor et al., 2016). Of interest here, several forms of CMT are caused by mutations that affect PI kinases and PI phosphatases known to be important in maintaining the PI internal membrane identity code (Robinson and Dixon, 2006; Falkenburger et al., 2010).

Mutations in *MTMR2* (CMT4B1), *SBF2/MTMR13* (CMT4B2); *SBF1/MTMTR5,* (CMT4B3) and *FIG4* (CMT4J) cause forms of demyelinating CMT (Houlden et al., 2001; Azzedine et al., 2003; Chow et al., 2007; Nakhro et al., 2013). Rodent models of these diseases have advanced the understanding of disease mechanisms. A mouse model of CMT4B1 was developed by Alessandra Bolino's group who have approached rescuing the myelin outfolding phenotype via rebalancing the PI phosphatase/kinase system (Bolino et al., 2000; 2004; Bolis et al., 2009). CMT4B1 is caused by loss of the myotubularin family PI3P phosphatase MTMR2 (Bolino et al., 2000; 2004). Cultured DRG Schwann cell and neurons have been used to rescue the knockout phenotype and learn more about the mechanisms behind the CMT4B1 outfoldings. *Mtmr2*$^{-/-}$ mice display myelin outfoldings in the peripheral nerve similar to those seen in patients (Bolino et al., 2000; 2004; Bolis et al., 2005; 2009). These outfoldings can be partially rescued *in vitro* with lentivirus mediated re-introduction of MTMR2 (and reduced by altering exocytosis machinery via inhibition of Sec8) (Bolis et al., 2009). Inhibition of PIKfyve with shRNA or the YM201636 PIKfyve inhibitor also reduced *Mtmr2*$^{-/-}$ myelin outfoldings (Vaccari et al., 2011). This model has provided insight not only into CMT4B1, but also into MTMR2's mechanistic interactions with Fig4, Sec8, and DLG1 (Bolis et al., 2009; Vaccari et al., 2011)

Bolino's group also created a double knockout mutant mouse lacking both PI 3-phosphatase Mtmr2 and CMT-relevant 5-phosphatase Fig4 (*Mtmr2*$^{-/-}$ *Fig4*$^{-/-}$), as well as a Fig4 heterozygote and Mtmr2 null (*Mtmr2*$^{-/-}$ *Fig*$^{+/-}$) mouse (Vaccari et al., 2011). CMT4J is caused by mutations in *FIG4*, an early endosomal PI 5-phosphatase that dephosphorylates PI(3,5)P_2 at the 5 position. FIG4 also activates Fab1, a 5-kinsase that phosphorylates PI3P to create PI(3,5)P_2, thus FIG4 acts both to inhibit formation of PI (3,5)P_2 by Fab1 and to reduce the amount of PI (3,5)P_2 at the membrane through direct dephosphorylation (Chow et al., 2007;

Vaccari et al., 2011; 2015). The *Fig4*$^{-/-}$ (or *plt* "pale tremor") mouse is a model of CMT4J wherein *FIG4* is mutated, resulting in disrupted PI (3,5)P_2 5-phosphatase activity and severe demyelination and axonal dysfunction (Chow et al., 2007). This mouse exhibited exacerbated neurodegeneration, including evidence of hypermyelination in the sciatic nerve (Chow et al., 2007; Vaccari et al., 2011). In neuron and SC co-cultures, there is an increased number of neurons with vacuoles and a decreased number of myelin segments. Even in fibroblasts, enlarged late endosomes were observed (Vaccari et al., 2011). Interestingly, *Fig4*$^{+/-}$ combined with *Mtmr2*$^{-/-}$ rescued the number of myelin outfoldings relative to *Mtmr2*$^{-/-}$, pointing to the PI balance as the cause of these outfoldings (Vaccari et al., 2011).

To bring this idea to a system with reduced complexity and faster outcomes, Vaccari et al. moved to *in vitro* co-cultures of DRG neurons and SCs. They compared the fraction of segments containing outfoldings *in vitro* in *Mtmr2*$^{-/-}$ *Fig4*$^{+/+}$ cultures to *Mtmr2*$^{-/-}$ *Fig4*$^{+/-}$ cultures. Indeed, even *in vitro, Mtmr2*$^{-/-}$ *Fig4*$^{+/-}$ co-cultures showed a 40% reduction in the fraction of segments containing outfoldings relative to *Mtmr2*$^{-/-}$ *Fig4*$^{+/+}$(Vaccari et al., 2011). The *Mtmr2*$^{-/-}$ *Fig4*$^{+/-}$ genotype have an absence Mtmr2 of PI3P phosphatase as well as a reduction in Fig4 activity. Reduced Fig4 phosphatase activity could both disinhibit Fab1, a 5-kinase that produces PI(3,5)P_2 from PI3P, and reduce direct 5-dephosphorylation of PI(3,5)P_2 by Fig4, both resulting in increased PI(3,5)P_2. Potentially this *Mtmr2*$^{-/-}$ *Fig4*$^{+/-}$ genotype could enhance the levels of both PI3P and PI(3,5)P_2 and rebalance PI3P phosphatase activity lost in *Mtmr2*$^{-/-}$. In their hands, adjusting the phosphatase-kinase balance with shRNA against PI 5-kinsae PIKfyve or a PIKFyve inhibitor drug also reduced the outfoldings in *Mtmr2*$^{-/-}$ cultures (Vaccari et al., 2011). Taken together, this work presents an intriguing idea — that myelin pathology can be reduced or prevented by tweaking the levels of PI kinases and phosphatases.

Vaccari et al. developed a model of CMT4J in which the loss of Fig4 was specific to Schwann cells or neurons (Vaccari et al., 2015). They found that the loss of Fig4 in either cell type resulted in a distinct disease phenotype. Both motor neurons and Schwann cells are sensitive to loss (or partial loss) of Fig4, underscoring the different and specific role Fig4 plays in each cell type (Vaccari et al., 2015). Loss of Fig4 in motor neurons (via HB9-Cre) caused neuron/axon degeneration, while loss of Fig4 in SCs (P0-Cre) caused issues with myelin development, maintenance, and repair after injury.

Myotubularin related proteins MTMR2 and MTMR13 are both implicated in CMT4B, types 1 and 2 respectively (Robinson and Dixon, 2006). MTMR13 and MTMR2 associate though coiled-coil interactions (Robinson and Dixon, 2005; Robinson et al., 2008) MTMR13 is known to associate with membrane, shown via fractionation and MTMR2 is present in both membrane and cytosolic fractions (Robinson and Dixon, 2005; Ng et al., 2013). MTMR13's pseudophospahatse domain is associated with endomembrane fractions and is thought to be sufficient for membrane targeting (Robinson and Dixon, 2005). The Robinson lab has developed a knockout mouse model of CMT4B2, where Mtmr13 is lost from all tissues and human disease phenotype of myelin outfoldings is recapitulated (Robinson et al., 2008). These mice form myelin sheaths, but abnormal myelin loops form early and (postnatal day 14), and the percentage of myelin sheaths with outfoldings and the complex nature of these outfoldings increases as the animal ages (Robinson et al., 2008). Similar to human patients, these mice exhibit no behavioral abnormalities, and the defects in their peripheral nervous system appear limited to myelin abnormalities. Just as in the human patients, loss of Mtmr13 in mice results in myelin outfolding production. Ng et al. explored the interactions between MTMR2 and MTMR13, clarifying that not only do these myotubularins interact but they levels of each will fall in the absence of the other (Ng et al.,

2013). Because Mtmr2 protein levels fall in *Mtm13*$^{-/-}$ mice, it is possible that the myelin outfolding phenotype may be in part due to this loss of Mtmr2.

1.4 — Summary and Major Questions in the Field

Therapies for only the most common forms of CMT have advanced to clinical trials, and to date, none of these trials have yielded treatments (Gess et al., 2015). A new clinical trial (clinicaltrials.gov identifier: NCT02579759) combines three drugs to reduce cAMP, which is reported to inhibit overproduction of Pmp22, and potentially improve CMT1A patient outcomes (Chumakov et al., 2014). This multi-drug approach may prove a more effective route than pervious trials that focused on one mechanism of action (Lewis et al., 2013). To approach rare forms of CMT, a more robust understanding of their individual causative mechanisms and basic biology is needed. Some evidence suggests that causative CMT mutations resulting in the loss of a PI phosphatase can be balanced out by tweaking levels of other phosphatases and kinases (Vaccari et al., 2011; 2015). However, this is not effective in all cases. Further work is needed to clarify why this approach is inconsistent. In addition, forms of CMT caused by the loss of pesudophosphatases MTMR13 and MTMR5 may result in outfoldings through a mechanism other than the loss of PI 3-phosphatase activity. Their specific domain architecture hints that the loss of these proteins may impair additional signaling pathways (Raess et al., 2016). Work in homologous systems has shown a link between MTMR13 homologue *Drosophila* Sbf and Rab21 signaling, however the same link has yet to be established in cell-types that are relevant to CMT or *in vivo* (Jean and Kiger, 2012; Jean et al., 2012; 2015).

The Robinson lab is uniquely positioned to explore the role of MTMR13 in the Schwann cell. Specifically, this work seeks to better understand the role of MTMR2 in the absence of

MTMR13 and to investigate the role of MTMR13's domains in myelination and signaling. Using the mouse model of CMT4B2, I have worked to develop methods and perform experiments that get at the root of how loss of MTMR13 affects myelination. To accelerate exploration of the mechanisms behind myelin outfoldings, I have cultured Schwann cells (SC) and dorsal root ganglia (DRG) neurons from *Mtmr13*$^{-/-}$ mice. Even *in vitro,* the Schwann cells recapitulate the myelin outfolding phenotype of the disease. This allows the use the myelin outfoldings as a read-out of the disease state of the Schwann cells, creating a simpler system that is amenable to screening. I have used this cell culture system to dissect the function of MTMR13's domains *in vitro*. By culturing myelinating Schwann cells from a knockout *Mtmr13*$^{-/-}$ mouse model of CMT4B2 and manipulating protein expression in these cultures with lentivirally expressed pieces of Mtmr13 and other relevant proteins, I hope to better understand the role of MTMR13 in Schwann cell myelination.

Figure 1.1 — Endosomal proteins are critical for PNS Schwann cell myelination.

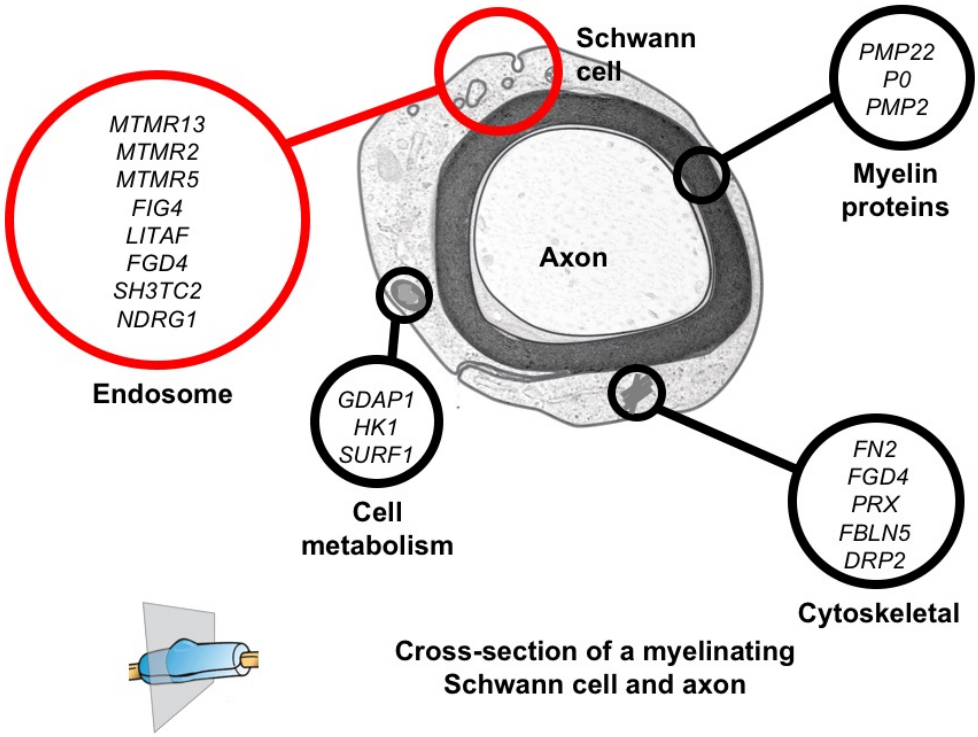

Figure 1.1 — Endosomal proteins are critical for PNS Schwann cell myelination. The largest group is of demyelinating CMT genes code for endosomal proteins. Eight forms of CMT4 are caused by mutations to genes involved in the endosomal sorting and signaling pathway. These genes are highlighted in the red circle. They include endosomal PI 3-phosphatases (MTMR2, CMT4B1; SBF2/MTMR13, CMT4B2; SBF1/MTMTR5, CMT4B3; FIG4, CMT4J), regulators of endocytosis (FGD4/Frabin, CMT4H), endosomal sorting associated proteins (LITAF/SIMPLE, CMT4C), and recycling endosome proteins (NDRG1, CMT4D; SH3TC2, CMT4C). Other forms of demyelinating CMT are caused by mutations that affect myelin, cell metabolism, and cytoskeletal proteins. Axon and Schwann cell are pictured in cross-section. Adapted from Timmerman et al. (2014) and Rossor et al. (2016).

Figure 1.2 — Phosphoinositide structure localization, and regulation.

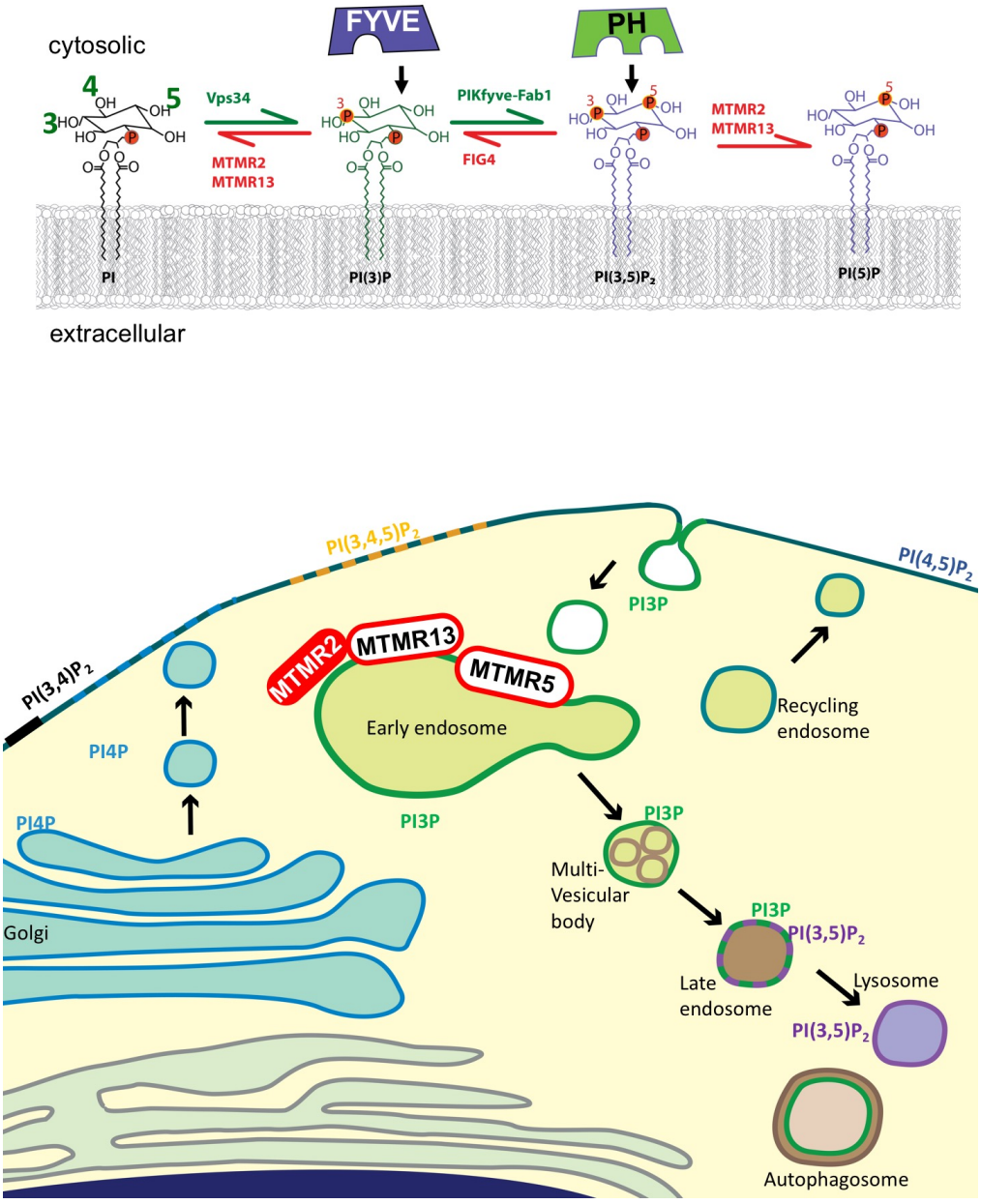

Figure 1.2 — Phosphoinositide structure, localization, and regulation. Phosphoinositides (PIs) from a network of interchangeable membrane identifiers that can be reversibly phosphorylated in the 3, 4, and 5 positions. Upper portion of figure depicts the transition between PIs. The transition between PI and PI3P, mediated by the kinase Vps34 or the active phosphatase MTMR2 stabilized by the inactive phosphatse MTMR13 is on the left. The transition between PI3P and PI(3,5)P, mediated by the kinase PIKfyve-Fab1or the phosphatse Fig4, on the right. The lower portion illustrates a cluster of genes related to endosomal function that are involved in forms of Charcot-Marie-Tooth inherited peripheral neuropathy. PIs enriched on specific internal membranes are also depicted. 3Adapted from Robinson and Dixon (2006), Jean and Kiger (2012), Stahelin et al. (2014).

Figure 1.3 — The myotubularin family of PI 3-phosphatases.

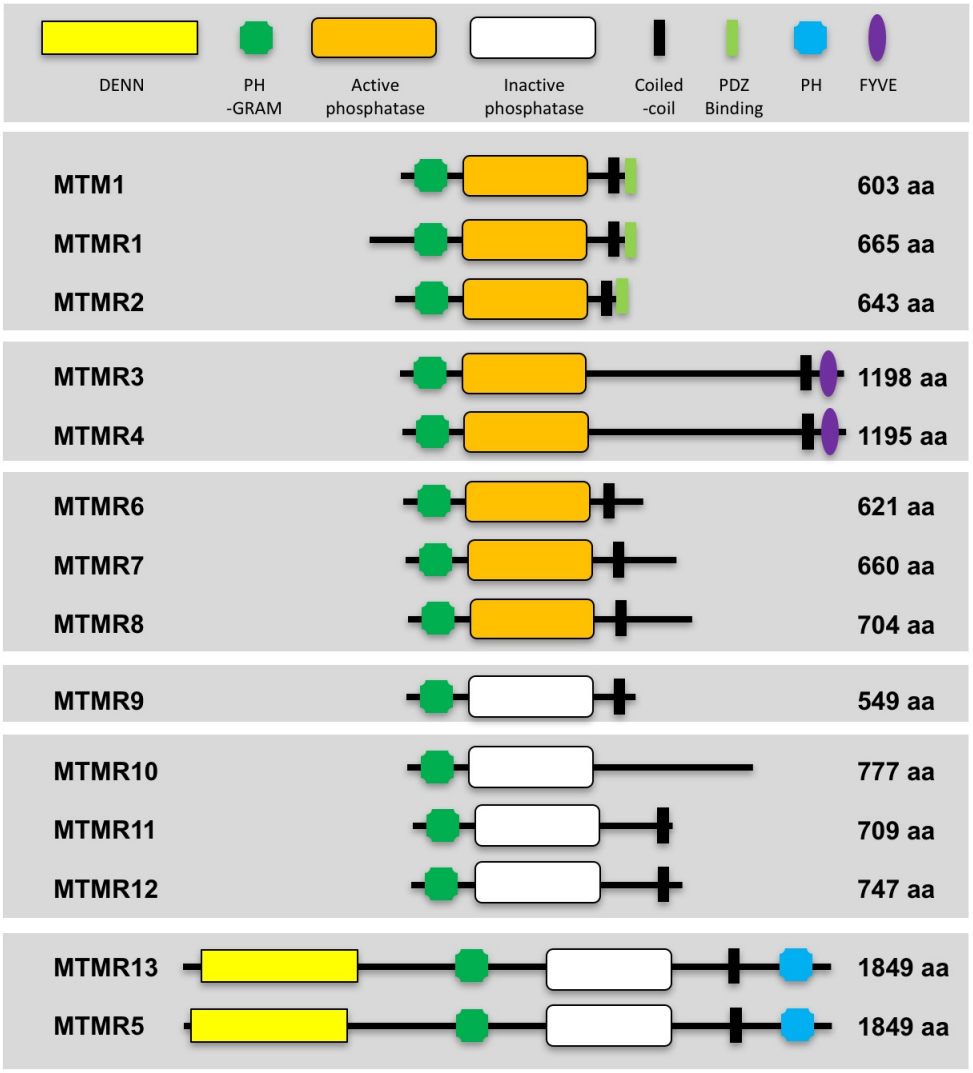

Figure 1.3 — The myotubularin family of PI 3-phosphatases. There are 14 myotubularin phosphatases, eight of which are active phosphatases (orange) and six inactive pseudophosphatase family members. This cartoon depicts the family members grouped according to phylogenetic relationship and domain organization, with important domains highlighted, and size noted on the right. Adapted from Raess et al. (2016)

Chapter 2 — An *In Vitro* Model of CMT2B2 Enables Exploration of the roles of Myotubularin Phosphatases in Myelin Disease

Forward

Fred Robinson (FLR) developed the Mtmr13$^{-/-}$ mouse (Robinson et al., 2008). Danielle Robinson (DCR) and Anna Mammel (AEM) adapted SC DRG co-culture protocol from one originally developed by Fred Robinson, Annie Logan (AL), and Aubree Ng (AN)(based on a protocol from Jonah Chan's lab). DCR developed data acquisition, sampling and analysis protocol for DRG co-cultures. AEM assisted with data collection for data shown in Figure 2.1, 2.2. DCR did data collection and analysis for other experiments. DCR cultured and fixed *in vitro* samples used for electron microscopy (EM), AL prepared *in vivo* EM. Robert Kayton microwave-processed and resin-embedded the samples for EM of cultured cells shown, this process is described in the text and detailed in Table 1. DCR ultra-thin sectioned the resin-embedded samples onto copper grids, counterstained the grids, and imaged the cultured cell samples on a Technai T12 Spirit transmission electron microscope. FLR processed and imaged the electron micrographs of sciatic nerve shown in Figure 2.3. The LVPG-EGFP vector was originally created by Gregory A. Dissen and was given to FLR as a gift. FLR and AN designed and created LVPG-EGFP-MTMR2. DCR made, concentrated and titred the lentivirues and designed co-culture experiments using these viruses. Virus concentration was done with the use of the Cohen lab ultracentrifuge, based on a protocol kindly provided by Jeffrey Huang, PhD and and Michael Cohen, PhD. Virus titring protocol is based on a protocol developed by Dr. Kim-Hien Dao, who also kindly provided training and access to the Guava Flow cytometer. DCR and AEM adapted virus

production and titring protocols, and DCR produced, concentrated, and titred all viruses used in this chapter.

Chapter 2 is a draft of a paper that will be submitted to the journal eNeuro. DCR wrote the draft with editing help from AEM. DCR and FLR made the figures.

2.1 — Introduction

Myelin is a multilayer membrane specialization produced by Schwann cells in the peripheral nervous system and oligodendrocytes in the central nervous system (Jessen and Mirsky, 2010; Kidd et al., 2013; Fields, 2014). Making and sustaining a myelin sheath requires efficient genesis and polarized trafficking of myelin components, as well as cytoskeletal coordination, and efficient endosomal trafficking. Phosphoinositide (PI) regulation is critical for a cell's internal membrane trafficking system, and multiple kinases and phosphatases regulate the identity of internal membranes by reversibly phosphorylating and dephosphorylating phosphatidylinositol at the 3, 4, or 5 position on its inositol ring (Maffucci, 2012). This system of membrane coding yields seven distinct species of PI, that can be flexibly interchanged as membrane is trafficked from one cellular compartment to another (Kutateladze, 2010; Hnia et al., 2012; Jean and Kiger, 2012). Controlling PI membrane identity regulates the movement of endosomes and cargo via tagging membrane for exocytosis, endocytosis, trafficking through the sorting early endosome, returning to the plasma membrane via recycling endosomes, or lysosomal degradation(Marko Jovic, 2010). This regulatory system may be especially critical for myelinating Schwann cells (SCs), which need to produce and maintain an order of magnitude more membrane that other cell types (Kidd et al., 2013).

SCs are particularly susceptible to disruptions in the endosomal system. Several inherited peripheral neuropathies, including forms of the Charcot-Marie-Tooth (CMT) family of disorders, are caused genetic deletion or loss of function of proteins in the endosomal/lysosomal pathway. Over 80 genes have been implicated in CMT family disorders, but the mechanism by which many of these genetic mutations cause disease is poorly understood (Timmerman et al., 2014). Of the demyelinating forms of CMT, a discrete subgroup are known to code for proteins important at the early endosome, recycling endosome, and lysosome (Raess et al., 2016; Rossor et al., 2016). These genes code for endosomal phospholipid phosphatases (*MTMR2*, CMT4B1; *SBF2/MTMR13,* CMT4B2; *SBF1/MTMTR5,* CMT4B3; *FIG4,* CMT4J), regulators of endocytosis (*FGD4*/Frabin, CMT4H), proteins involved in endosomal-multivesicular body sorting (*LITAF/SIMPLE*, CMT4C), proteins present at recycling endosomes (*NDRG1,* CMT4D; *SH3TC2*, CMT4C) (Kachhap et al., 2007; Robinson et al., 2008; Arnaud et al., 2009; Bitoun et al., 2009; Vaccari et al., 2011; Horn et al., 2012; Qin et al., 2016; Rossor et al., 2016; Shibata et al., 2016; Vijay et al., 2016), see Chapter 1, Figure 1.1. Mutations in these genes lead to demyelinating froms of CMT peripheral neuropathy (Rossor et al., 2016) (Bolino et al., 2000; Kachhap et al., 2007; Robinson et al., 2008; Arnaud et al., 2009; Bitoun et al., 2009; Vaccari et al., 2011; Horn et al., 2012; Qin et al., 2016; Shibata et al., 2016; Vijay et al., 2016).

CMT type 4B is a autosomal-recessive form of demyelinated CMT caused by mutations in myotubularin related protein MTMR2, MTMR5, or MTMR13 (Robinson and Dixon, 2006). All forms of CMT4B are characterized by loss of nerve conduction velocity, focally folded myelin sheaths (known as myelin outfoldings), and secondary axon loss leading to distal muscle weakness/atrophy and mobility impairment (Suter and Scherer, 2003; Conforti et al., 2004b; Previtali et al., 2007; Nakhro et al., 2013; Negrão et al., 2014).

Although disease-causing mutations result in the loss of these proteins throughout the body, loss of these CMT-causing MTMR function appears to primarily affect Schwann cell myelination in both patients and *in vivo* animal models (Bolino et al., 2004; Robinson and Dixon, 2006; Robinson et al., 2008). Knockout mouse models of CMT4B1 (*Mtmr2*$^{-/-}$) and CMT4B2 (*Mtmr13*$^{-/-}$) recapitulate the myelin outfoldings found in patient nerves (Bolino et al., 2004; Bolis et al., 2005; Robinson et al., 2008). CMT4B1 is caused by the loss of MTMR2, an active myotubularin PI 3-phosphatase (Bolino et al., 2004; Bolis et al., 2005; Previtali et al., 2007). Loss of MTMR2 disrupts the cells' balance of kinases and phosphatases that maintain the PI membrane identity code, and is reported to lead to an accumulation of PI3P and PI(3,5)P_2 and a reduction in available PI5P (Vaccari et al., 2011). CMT4B2 is caused by loss of MTMR13 function (Previtali et al., 2007; Saporta and Shy, 2013).

The severe phenotype of CMT4B2 in patients and rodent models shows that the loss of the inactive phosphatase MTMR13 disrupts SC myelination. However, the mechanism of disease is less clear. MTMR13 is a myotubularin-family pseudophosphatase thought to be critical for early endosomal trafficking, Rab activation, and phosphoinositide regulation(Robinson and Dixon, 2006; Jean and Kiger, 2012). Mtmr13 is known to associate with the active PI 3-phosphatase MTMR2, where it may coordinate PI hydrolysis, and possibly act as a Rab GEF (Jean and Kiger, 2012; Jean et al., 2012; Ng et al., 2013). MTMR13's domains include a coil-coil domain that is important for complexing with MTMR2, a PH-GRAM domain that may be critical for associations with other myotubularin family members and association PI(3,5)P_2 containing membrane, a separate C-terminus PH domain also though to be involved in membrane association, a DENN domain that may act as a Rab-GEF, and an inactive pseudophosphatase domain that known to associate with

endosomal membranes to localize MTMR13 at the endosomal membrane (Robinson and Dixon, 2005; Maffucci, 2012; Ng et al., 2013). This multidomain architecture hints that MTMR13 may function as a scaffold, capable of bringing the active myotubularin phosphatase MTMR2 and Rabs together on the on PI3P and/or PI(3,5)P_2—rich membrane of the early/late endosome to facilitate signaling and appropriate trafficking.

To study the role of MTMR13 in SCs, we have developed an *in vitro* system using cultured DRG and SCs from *Mtmr13*$^{-/-}$ mice (SC DRG co-cultures), which recapitulate the hallmark myelin outfolding phenotype both *in vivo*. We have developed an *in vitro* SC DRG co-culture model of CMT4B2. Using this model, we were able to manipulate gene expression using lentivirus and measure myelination and myelin outfoldings. We have used this system to ask whether exogenous expression of the active phosphatase MTMR2 can impact myelin outfoldings in *Mtmr13*$^{-/-}$ SC DRG co-cultures.

2.2 — Materials and Methods

2.2.1 — Mice

All animal work was approved by the Oregon Health & Science University Animal Care and Use Committee. *Mtmr13*$^{-/-}$mice have been described previously by the Robinson Lab (Robinson et al., 2008; Ng et al., 2013). The mice analyzed here had been backcrossed for eight generations onto a C57BL/6 background.

2.2.2 — Antibodies

Rat anti-MBP was used at 1:250 (MBP Antibody Rat, Millipore, MAB386) and Chicken anti-NFH was used at 1:10,000 (NF-H Neurofilament Chicken Abcam AB4680).

Fluorescent secondary antibodies (Jackson ImmunoResearch), Cy3 anti-Rat was used at 1:1000 (Cy3 Goat anti-Rat H+L Jackson IR 112-165-143, stock solution at 1.4mg/mL), Alexa Fluor 647-Goat Anti-Chicken IgY (Jackson IR 103-605-155, stock solution at 1.5mg/mL). Anti-MTMR2 (119-AN) antibody was affinity-purified as previously described (Ng et al., 2013) and used at 1:1000 for immunoblotting. Mouse anti-b-tubulin (E7) was obtained from the Developmental Studies Hybridoma Bank and used at 1:5000 for immunoblotting. Mouse anti-c-myc (9E10) was from Roche Applied Science. Anti-GFP (N86/8 supernatant) was obtained from Antibodies Incorporated 73-131) and used at 1:50 for immunoblotting.

2.2.3 — Myelinating Schwann Cell and Dorsal Root Ganglia Neuron Explant Cultures

We produced dorsal root ganglion neuron and Schwann cell (SC DRG) co-cultures using the following procedure. Wild type (C57BL/6) or *Mtmr13*$^{-/-}$ female mice were bred to males of their same genotype, respectively. At 13.5 days of gestation, pregnant females were deeply anesthetized with isoflurane and quickly euthanized by cervical dislocation. Embryos were removed and placed in Dulbecco's phosphate buffered saline (DPBS; Life Technologies 14040-133) on ice. To isolate E13.5 dorsal root ganglia (DRG), embryos were removed from DPBS and spinal cords were carefully dissected out in 37°C Leibovitz's L-15 medium (Life Technologies 11415-064) containing 10% fetal bovine serum (FBS) and 0.5% penicillin-streptomycin (P-S; 50 units/mL of penicillin; 50 μg/mL of streptomycin) (L-15+FBS+P-S). DRG were individually plucked off dissected spinal cords with Dumont #5 forceps (Fine Science Tools, Biology Tips/Straight/Inox/11 cm; catalog #11254-20). Great care was taken to collect only the DRG and avoid any contaminating spinal cord tissue.

DRG were then removed from the dissection dish and transferred to a 14 mL conical tube containing 7 mL of L-15+FBS+P-S where all of the DRG dissected from the embryos of a pregnant female were pooled. When the dissections were complete, the volume was adjusted to 14 mL with L-15+FBS+P-S and DRG were allowed to settle for 10-20 minutes in a 37°C. After settling, media was carefully removed and DRG were washed with 14 mL of L-15 medium lacking serum and P-S, DRG were again allowed to settle for 10 minutes in a 37°C. Then, L15 medium was replaced with 5 mL of Trypsin-EDTA (0.25%; Invitrogen; 25200-056) to help dissociate the cells and the DRG were incubated at 37°C for 45 minutes. After this incubation, five mL of L-15+FBS+P-S was added and DRG were pelleted by centrifugation for 30 seconds at 1000 rpm (170 x *g* in Model 236 rotor). DRG pellet was washed with 10 mL of 37°C L-15+FBS+P-S and centrifuged at 170 x *g* for 10 min. Media was replaced with 2-3 mL of pre-warmed (37°C) M1 medium (Modified Eagles Medium [MEM]; Life Technologies 11095-080; 4.3 g/L D-glucose; 10% FBS) containing mouse nerve growth factor (NGF 2.5S Native Mouse Protein; Life Technologies 13257-019) at 10 ng/mL. DRG were triturated by aggressively pipetting up and down, and triturated isolates were spun down and resuspended in 1 mL of M1-NGF medium. Dissociated DRG were plated on rat tail collagen coated 25 mm coverslips at density of 130,000 total cells per well in 160 μL. Cultures were incubated overnight at 37°C in 5% CO_2.

The day on which embryos were dissected was designated as Day 0. On Day 1, 1 mL of 37°C M1-NGF medium was added to each well of explant culture to flood the wells. On Day 3, media was replaced with with 2 mL of 37°C M1-NGF medium. M1 media was changed every other day until Day 8 for explants that did not receive virus.

For cultures that did receive virus, on Day 5 the media was changed again 2 mL of M1-NGF medium (pre-warmed to 37°C) containing appropriate volume of lentivirus to

achieve the desired multiplicity of infection (MOI). Based on the titre of the virus, described below, the amount of virus added was adjusted to attain the an MOI at which >90% of cells were infected. On day 6, after a 24-hour incubation with virus, virus-containing media was removed, cells were gently washed twice with C medium (10 ng/mL NGF), then 2 mL of C-medium (10 ng/mL NGF) was added to each well. On day 8, the media was exchanged for 2 mL of C-medium with ascorbic acid (10 ng/mL NGF; 50μg/mL Ascorbic Acid). Media was then changed every two days until on Day 21. On Day 21, SC DRG cultures were fixed in PFA in PBS (pH 7.4) for 15 min at room temperature on a rocking platform. Virally-mediated expression of tagged proteins in SC DRG co-culture was confirmed by assessment of the fraction of GFP positive cells bodies, as well as by immunoblotting for GFP or other protein expression.

2.2.4 — Immunofluorescence

Fixed cultures were washed three times with 1x PBS and permeabilized with ice-cold methanol for exactly 5 min on ice. After washing once with 1x PBS, cultures were blocked for 1 hour in 1x PBS containing 10% normal goat serum (NGS). Fixed cells were covered with a solution of PBS with 0.1% Tween-20 (PBST), which contained 2% NGS and appropriately diluted primary antibodies, and subsequently incubated overnight at 4°C on a rocking platform. After overnight incubation, cultures were washed three times with 1x PBST (10 min each). Fluorescent secondary antibodies diluted in 1X PBST containing 2% NGS and and cultures were incubated with secondary antibodies for 1 hour at room temperature (protected from light) on a rocking platform.

After incubation with secondary antibodies, the cultures were washed three times with 1x PBST (10 min per wash) at room temperature on the rocker. Cell nuclei were labeled

with 4',6-diamidino-2-phenylindole (DAPI), via a one minute room temperature incubation in 0.36 μM final DAPI (Molecular Probes D-21490; 14.3 mM stock in deionized water (dH2O) diluted 1:40,000 in PBST). Cultures were washed twice with 1x PBST, rinsed once by dipping in distilled deionized water, and mounted on slides ColorFrost™ Plus microscope slides (Thermo, 9951APLUS-006) with Elvanol mounting media. Slides mounted were set overnight at 4°C before imaging.

2.2.5 — Image Acquisition and Analysis

Images for quantification of myelin segments were acquired using a Nikon/Yokogawa CSU-W1 spinning disk microscope and NIS-Elements AR imaging software (Nikon, V. 4.20.01 build 982). Images were acquired using a 40x or 60x oil immersion objective (Nikon Plan Fluor, 40x, 1.3, oil immersion lens; 60x1.4 Plan Apo VC, oil immersion lens). Thirty-six 20 μm z stacks (sampled every 1 μm) were randomly selected over the center of the myelinated region of explant and programing the microscope to acquire a 6 by 6 grid of images spaced 1 mm apart. Z stack images were separated by 1 mm across the grid. Each image field of view was 416 x 351 μm (2560 x 2160 pixels), therefore each coverslip was randomly sampled across a total area of 5.26 mm^2. Using ImageJ (Fiji image processing package for ImageJ, version.2.0.0-rc-30/1.49t build b1cc40320c) (Schindelin et al., 2012), z stack images were projected into a single image view using the standard deviation of each pixel in Image J. These projected z-stacks were used for image analysis.

High resolution images in myelin outfoldings were acquired using the Applied Precision Deltavision CoreDV Widefield Deconvolution System built on an Olympus IX71 inverted microscope equipped with a Nikon Coolsnap ES2 HQ camera and a 60× 1.42 NA

PlanApo oil immersion objective. Acquisition and deconvolution were accomplished using the softWoRx software (Applied Precision). Images of entire 25mm coverslips were collected using the ZEISS ApoTome microscope with grid-based optical sectioning. Briefly, for each coverslip a 14x14 grid of images was collected in the DAPI and Cy3 (MBP) channel with the 5x objective (5x0.16 PlanApo, air lens) with 5x5 binning, 200ms exposure. These images were collected, stitched together to create an image of the whole coverslip for qualitative comparison of overall myelination.

2.2.6 — Image Quantification

Using the systematic randomly sampled images, described above, the total number of complete myelin segments was counted for each z-projected 40x or 60x image. A myelinated segment was included in the analysis only if the full myelin internode, i.e. both ends of the segment, was clearly present in the image. To quantify myelin segments per unit area and the fraction of myelin segments that contain one or more outfoldings, all complete segments in a field were counted and classified as containing one or more outfoldings, containing isolated small blebbing events that occur in normal myelination, or containing un-segmentized degenerating myelin. To quantify myelin segments per unit area, complete segments were counted and the total number of segments counted for a coverslip were divided by the area imaged. To quantify outfoldings, the percentage segments containing outfoldings for each coverslip was calculated as a fraction of the total number of complete segments.

Outfoldings were defined as large myelin abnormalities that look like bubbles, generally as wide or wider than a myelin segment. Outfoldings were observed as be large individual bubbles, groups of bubbles in a row, "lollipop" outfoldings where a bulbous area is connected to the main myelin sheath with a thin process, or a combination of these three

types, see Figure 2.2. A segment is counted as containing one or more outfoldings regardless of how many outfoldings it contains. Small blebbing events occur in normal myelination, and these blebs are always smaller than the crosssection of the myelin sheath and isolated, i.e., one or two isolated blebs on a myelin sheath, as opposed to outfoldings which tend to cluster together. A segment containing small blebs was classified as a segment not containing outfoldings.

To quantify myelin segment length, myelin segments were measured using the ImageJ segmented line tool in flattened z-stacks. Only complete segments were measured. 60-120 segments per coverslip were counted, and four coverslips per genotype were assessed, and data was averaged per coverslip. Statistical analysis to compare between groups for all measures assessed was performed using the Student t test; two tails, unpaired, unequal variance.

2.2.7 — Electron Microscopy of SC-DRG Co-Cultures

Cultures were established and maintained as described above. On Day 21, cultures were fixed with 2% PFA and 1.5% glutaraldehyde in 1x PBS (pH = 7.4) overnight at 4° C. Cultures were rinsed with 1x PBS, and a cell scraper (Fisher #08-100-241) was used to gently dislodge the culture from the coverslip and transfer it to a 1.5 mL tube containing 1mL of 6% bovine serum albumin (BSA) in 1x PBS. After an overnight incubation in 6% BSA at 4° C, cultures were pelleted via centrifugation at 1000 rpm (94 x *g*) for 5 min in a bench-top centrifuge at RT. BSA-PBS solution was removed from tube until only 500 μL remained, then 500 mL 1.5% paraformaldehyde and 1.5% glutaraldehyde in 0.1 M Cacodylate buffer (with 0.05M sucrose and 0.25% CaCl2, pH = 7.4) was added slowly to the tube to form a layer above the BSA. Samples were incubated at 4°C for at least 4 hours to allow the 6%

PSA to polymerize. Then the pelleted cultures, now surrounded in a BSA-gel were removed, divided into smaller pieces for further processing, rinsed with 0.1M Sodium cacodylate buffer, and postfixed in 1.5% paraformaldehyde and 1.5% glutaraldehyde in 0.1 M Cacodylate buffer (with 0.05M sucrose and 0.25% CaCl2, pH = 7.4). The samples were then loaded into individual wells of a Ted Pella PELCO Prep-Eze 12 or 6-well specimen holder with 0.1M Cacodylate buffer for microwave assisted post-fixation, dehydration, and embedding. The Prep-Eze 12 or 6-well specimen holder was then placed in a 50mm petri dish and loaded into the vacuum chamber within the microwave. The microwave processing took place according to the protocol outlined in Table 1. Briefly, samples were washed in 0.1 mol/L sodium cacodylate buffer, pH 7.4, postfixed in buffered osmium tetroxide at 2% in dH2O, stained en bloc with 1% uranyl acetate, dehydrated in graded ethanol solutions, and then embedded in epoxy resin (Embed 812 Kit EMS #14120). Ultrathin sections of 70 nm thicknesses were collected on 200 mesh grids, stained with uranyl acetate and lead citrate, and then were examined with a Technai T12 Spirit transmission electron microscope at 80 Kv. Digital images were acquired using a 16 megapixel Advanced Microscopy Techniques camera.

2.2.8 — Lentivirus Production and Concentration

To express exogenous tagged proteins via lentivirus, cDNA was cloned into an LVPG vector with an EGFP reporter, a gift from Gregory Dissen. To produce lentivirus, 10 x 10^6 cells 293FT cells were plated in a 150 cm^2 flask (Corning #430825) coated with 0.1mg/mL poly-l-lysine and allowed to grow overnight in 22 mL 293FT Complete Media. Experimental vectors were transfected into 293FT cells in Optimem (Gibco # 31985-062) using Lipofectamine2000 (Invitrogen #11668-019) along with lentiviral packaging plasmids

pVSVG, pREV and pMDL. After incubating the cells in Optimem containing the transfection complex for 8 hours at 37° C, the Optimem was removed and replaced with 293FT Complete Media. Cells were incubated at 37° C and virus-containing media was collected at 48 and 80 hours after the start of transfection. New 293FT Complete Media was carefully added after the 48 hour collection, and the collected virus-containing media was stored at 4° C and then pooled with the 80 hour collection. Pooled virus-containing media was spun for 5min at 1000xg to pellet cellular debris. Supernatant was filtered using a Millipore 50 mL disposable vacuum filter (SE1M 003 M00). Filtered viral supernatant was loaded into 10 mL ultracentrifuge tubes (Beckman Coulter 344059, 8/16 x 3 1/2) and concentrated by spinning for 2 hours at 22,000 rpm at 22° C in an ultracentrifuge (Beckman Coulter Optima L-90K). Supernatant was removed and each virus pellet was resuspended in 150 μL of sterile filtered 1% bovine albumin serum (BSA BP1605-100) in 1 x PBS via incubation on a rocker for 40 minutes at room temperature. Concentrated virus in sterile 1% BSA was stored at -80° C.

2.2.9 — Lentivirus Titring

All lentivirus expressing GFP-tagged constructs were titred by transducing serial dilutions of virus and analyzing the levels of GFP expression using Guava easyCyte Flow Cytometer (Millipore) and FlowJo (v10.2) to ensure similar batch-to-batch transduction efficiency. To titre virus, 293FT cells were plated in a 96-well plate at 3000 cells per well and incubated overnight. The following day, media was exchanged for serial dilutions of virus (1:250, 1:500, 1:1000, 1:2500) in 293FT Complete Media without antibiotic. Three replicate wells of each dilution were infected. Virus-containing media was incubated on cells for 24 hours, at which point it was removed and replaced with 293FT Complete Media without

antibiotic. Cells were incubated without virus for an additional 24 hours to ensure enough time for protein expression. After this incubation, media was removed and replaced with 15 μL trypsin per well. Cells were incubated for 1minute at 37° C, then cells were resuspended in a total volume of 200 μL in DPBS (Fisher #14190-144) and vigorouly triturated to ensure a single cell suspension. Flow cytometry was performed using the Guava easyCyte Flow Cytometer and output was analyzed using FlowJo software to calculate average titre for each virus based on the % GFP-positive cells identified by flow cytometry. To calculate the titre of a virus, for each set of dilution replicates the following was calculated. TU = transducing units.

$$\text{Titre} = \text{TU}/\ (\text{mL virus}) =$$

$$(-\ln (1-\%\text{GFPpositive}) * \#\text{cells per well}) / \text{Volume of virus added (mL)}$$

For each virus, titre values from all dilutions were averaged to calculate an average titre for the virus.

$$(\text{mL virus}) = \text{TU}/\text{Titre}$$

Based on the average titre of the virus, the amount of virus added to SC DRG co-culture was adjusted to attain the desired multiplicity of infection, or MOI, to infect >90% of cells. For SC DRG cultures, plated at 130,000 cells per well, the desired TU is 1.95x10^6 for an MOI of 15. To transduce SC DRG co-cultures, virus was diluted in appropriate cell culture media and incubated with cells for 24 hours, as described above.

2.2.10 — Immunoblotting

To assess protein expression western blot analysis of protein expression in SC DRG cell lysates was performed. Protein lysates from cultures were prepared by the following method. On Day 21 cells were rinsed with 1x PBS and lysed in 200 μL ice cold lysis buffer

(120 mM NaCl/50 mM Tris, pH 8.0/0.5% Triton X-100/100 mM sodium fluoride/1 mM sodium orthovanadate, 2 mM sodium EDTA, supplemented with cOmplete Roche Applied Science EDTA-free Protease Inhibitor Cocktail Tablets at a concentration of one tablet per 10 ml of buffer). Cells were removed from coverslips with a cell scraper and moved to a chilled 1.7 ml tube along with lysis buffer. Cells were homogenized using a drill press with tube homogenizer attachment. After homogenization, cells were vortexed for 10 seconds and then spun down 15,000xg for 15 minutes at 4 C. All available supernatant (~190 μL) was then transferred fresh, chilled 1.7ml tube. Cleared lysates were immediately assayed for protein concentration using a Bradford assay. Briefly, 20 μL of each of seven BSA protein standards was added to 1 mL of diluted Biorad protein dye and protein concentration was measured to create a standard curve. To measure protein concentration of samples, 5 μL of DRG samples was added to 1 mL of protein dye, and samples were measured and resulted multiplied by 4.

After measuring protein concentration, lysates were diluted in NuPAGE LDS sample buffer (Invitrogen) containing 1 mM DTT, boiled for 5 minutes at 85° C, mixed via vortex for 10 seconds, and spun down. 20 μg protein per lane were run in 4 — 12% NuPAGE Bis — Tris gels (Invitrogen) in MOPS buffer, transferred to polyvinylidene difluoride (PVDF) membrane. A total protein stain was done with MemCode Reversible Protein Stain Kit — for PVDF membranes after protein transfer to assess protein across lanes. Protein expression was then analyzed by immunoblotting. SuperSignal West Chemiluminescent Substrate (Thermo Scientific) was used for detection, and quantitation was with a G:BOX Chemi imaging system using the GeneSys software (Syngene). Protein levels are presented in arbitrary units, and data as mean and standard error of the mean. Statistical significance was evaluated using unpaired Student's t-tests.

2.3 — Results

2.3.1 — Mtmr13 $^{-/-}$ Schwann Cell and Neuron Co-culture as an In Vitro Model of CMT4B2

In order to meaningfully model CMT4B2 *in vitro*, we first needed to assess the viability of SC DRG cultures from *Mtmr13*$^{-/-}$ mice. *Mtmr13*$^{-/-}$ SC DRG co-cultures must myelinate comparably to wild type cultures. In human CMT4B2 patients and in our *Mtmr13*$^{-/-}$ mouse model, the hallmark phenotype is abnormal, redundant myelin loops, known as myelin outfoldings (Szigeti et al., 2006; Robinson et al., 2008; Chen et al., 2014; Negrão et al., 2014). We assessed DRG Schwann cell cultures for myelin density to capture any difference in overall myelination as well as for the fraction of myelin segments that contain outfoldings. Reduced myelination in *Mtmr13*$^{-/-}$ SC DRG co-cultures would compromise the *in vitro* system's utility. SC DRG co-cultures from wild type and *Mtmr13*$^{-/-}$ mice showed no significant difference in myelination. *Mtmr13*$^{-/-}$ myelinate robustly, and quantitative analysis revealed no difference in the density of myelin segments per unit area (mm^2), see Figure 2.1. Figure 2.1A and B show images of wild type and *Mtmr13*$^{-/-}$ SC DRG co-cultures on 25 mm coverslips, similar coverslip area is covered by both genotypes. Figure 2.1C illustrates the automated random unbiased sampling. Figure 2.1D quantifies the number of segments per unit area in each genotype. Figure 2.1F-I show examples of wild type (2.1F, G) and *Mtmr13*$^{-/-}$ (2.1H, I) images of SC DRG collected with this method. Though variability exists in the size, shape, and orientation of the myelinated region of a given co-culture, this automated sampling method provides an accurate and unbiased representation of the myelin. Our results confirm that *Mtmr13*$^{-/-}$ and wild type SC DRG co-cultures myelinate comparably, and provide an accurate *in vitro* model of CMT4B2.

To quantify the fraction of segments that contain outfoldings, we classified segments as not containing outfoldings or containing one or more outfoldings. Myelin abnormalities were counted if they met one or more the following criteria; single or multiple bubble-like structure at least half the width of the segment, small multiple bubble-like structures clustered together or in a row, filipodium-like structures extending from the myelin sheath, lollypop-type structures that include a small MBP-positive process with a bubble-like structure (Figure 2.2). A segment was counted as outfolding positive if it contained one or myelin abnormality classified as an outfolding. *Mtmr13*$^{-/-}$ co-cultures exhibit a significantly higher percentage of segments containing one or more myelin outfoldings, an average of 28% *Mtmr13*$^{-/-}$ segments contain outfoldings in this set. Figure 2.2C quantifies the fraction of myelin segments containing one or more outfoldings at 21 days *in vitro* (DIV), WT n=7 coverslips, *Mtmr13*$^{-/-}$ n=6 coverslips, p= 0.00030. While myelin abnormalities that fit the criteria for outfoldings are present in wildtype cultures, they are less complex and occur infrequently, in 7% of wild-type segments.

Wild type and *Mtmr13*$^{-/-}$ co-cultures were examined by electron microscopy (EM), and no myelin outfoldings were found in wild type cultures, while cross-sections of outfoldings were captured in *Mtmr13*$^{-/-}$ co-cultures (Figure 2.3A, B). At the ultrastructural level, outfoldings consisted of compact myelin that form loops, as well as loops of non compact myelin. Outfoldings observed via EM in *Mtmr13*$^{-/-}$ co-cultures were not observed in wild type cultures, and were morphologically similar to outfoldings previously observed in *Mtmr13*$^{-/-}$ mouse sciatic nerve (Figure 2.3C, D). Our results track closely with our previous work on the mouse model of the disease (Robinson et al., 2008). *In vitro* disease models allow accelerated exploration of molecular pathways that are not practical *in vivo,* and have helped develop the mechanistic understanding of related forms of CMT (Bolis et al., 2009).

2.3.2 — Exogenous MTMR2 Supresses Myelination and Partially Rescues the Mtmr13$^{-/-}$ Outfolding Phenotype In Vitro

Mtmr13$^{-/-}$ sciatic nerve has a 50% reduction in Mtmr2 levels (Ng et al., 2013). To better understand the relationship between Mtmr2 and Mtmr13, and the impact of Mtmr2 on *Mtmr13*$^{-/-}$ outfoldings, we exogenous expressed GFP-tagged MTMR2 in *Mtmr13*$^{-/-}$ co-cultures. *In vitro,* we observed a reduction in Mtmr2, similar to the reduction in Mtmr2 that observed *in vivo* (Ng et al., 2013). It is possible that the outfoldings observed in *Mtmr13*$^{-/-}$ myelin (nerves and cultures) are due in some part to this loss of Mtmr2. Viral infection of >90% of cells was confirmed with microscopy, and quantified by counting DAPI-positive cell nuclei associated with EGFP-MTMR2-postive cell bodies (Figure 2.4). Western blot of Mtmr2 protein expression confirmed exogenous MTMR2 expression was 4.5x over the Mtmr2 levels seen in *Mtmr13*$^{-/-}$ SC DRG co-cultures and above wild type Mtmr2 levels (Figure 2.4D, E). We observed robust cytosolic expression of EGFP-MTMR2 in >90% of cells *in vitro* in our SC DRG coculture. EGFP-MTMR2 was excluded from the nucleus. Viral infection with EGFP controls also exhibited robust GFP expression, however EGFP localization was distinct from EGFP-MTMR2 in that control EGFP was observed both in the cell body and in the nucleus. Therefore, genetic manipulation of SC DRG co-cultures with robust lentivirus' provides an idea model to study SC myelintion in *Mtmr13*$^{-/-}$ cells. With robust lentivirus expression of tagged proteins *in vitro*, co-cultures provide a useful, robust model to study the impact on altering the PI 3-kinase/phosphatase balance in *Mtmr13*$^{-/-}$ co-cultures.

We next examined the effect of exogenous GFP-MTMR2 effect on overall myelination as assessed by myelin segments per unit area and mean myelin segment length. Expression of the active PI 3-phospahtase MTMR2 should lead to depletion of PI3P and

$PI(3,5)P_2$, and may rebalance the endogenous Mtmr2 levels that are reduced in *Mtmr13*$^{-/-}$ (Ng et al., 2013). We examined the effect of exogenous LV-GFP-MTMR2 on overall myelination as assessed by myelin segments per unit area and mean myelin segment length. We found that LV-EGFP-MTMR2 significantly reduced both myelin segment number and segment length in *Mtmr13*$^{-/-}$ SC DRG co-cultures relative to LV-EGFP controls.

We examined the overall density and length of myelin segments in *Mtmr13*$^{-/-}$ co-cultures infected with LV-EGFP and LV-EGFP-MTMR2. Exogenous expression of LV-EGFP-MTMR2 resulted in a reduction in total segment number and reduced segment length. Figure 2.5A and B show whole coverslip qualitative views of SC DRG co-cultures, where MBP staining is markedly reduced in 2.5B. Figures 2.5C and D quantify the reduction in myelin segments per unit area (2.5C) and myelin segment length (2.5D). The number of myelin segments is reduced by 60% in *Mtmr13*$^{-/-}$ SC DRG co-cultures treated with LV-EGFP-MTMR2 (Figure 2.5C) relative to those treated with LV-EGFP. Mean segment was also reduced in *Mtmr13*$^{-/-}$ SC DRG co-cultures treated with LV-EGFP-MTMR2 (2.5D) as compared with LV-EGFP.

To assess the influence of MTMR2 on *Mtmr13*$^{-/-}$ myelin outfoldings, we assessed the fraction of segments containing outfoldings in SC DRG co-cultures. Exogenous expression of LV-EGFP-MTMR2 in *Mtmr13*$^{-/-}$ co-cultures (Figure 2.6A, B) resulted in a 25% reduction in outfoldings, shown in Figures 2.6C, D and quantified in 2.6E. While exogenous MTMR2 does not completely ameliorate the outfolding phenotype, taken together with our recent work showing reciprocal stabilization of Mtmr2 by Mtmr13, this finding points to both a critical role for MTMR2 in the CMT4B2 phenotype (Ng et al., 2013).

2.4 — Discussion

Loss of either MTMR13 or MTMR2 leads to CMT4B. We developed a *Mtmr13*$^{-/-}$ mouse model of MTMR13 that repeats the phenotype of myelin outfoldings seen in patients(Robinson et al., 2008). We have previously shown that MTMR13 and MTMR2 associate in mouse and human cells, and that each depends on the other to express at normal levels (Robinson and Dixon, 2005; Ng et al., 2013). *Mtmr13*$^{-/-}$ mouse sciatic nerve show a 50% reduction in the levels of Mtmr2 (Ng et al., 2013). This loss of Mtmr2 may be responsible for the myelin outfoldings in the *Mtmr13*$^{-/-}$ mouse and SC DRG co-culture model. In the *Mtmr13*$^{-/-}$ animal, the reduction in Mtmr2 caused by the loss of Mtmr13 could lead directly to an increase in PI3P and PI(3,5)P_2 levels. An increase in PI3P could affect myelination by altering early endosome trafficking during myelination. Because of this, the myelin outfoldings observed in *Mtmr13*$^{-/-}$ may be due in part to the loss of Mtmr2 protein. The loss of MTMR2 (CMT4B1) has been modeled *in vivo* and *in vitro*, and can be rescued *in vitro* via by expressing exogenous MTMR2 *in vitro* or by tweaking the phosphatase/kinase balance (Bolis et al., 2009; Vaccari et al., 2011). Our data suggest that exogenous expression of MTMR2, a recovery of the Mtmr2 phosphatase levels in *Mtmr13*$^{-/-}$ cells, leads to a partial reduction in the number of segments that contain outfoldings.

Further work is necessary to fully understand the role that MTMR2 plays in *Mtmr13*$^{-/-}$ cells. Specifically, measuring the PI3P and PI(3,5)P content of SC DRG co-cultures with and without exogenous MTMR2 will improve our ability to interpret whether MTMR2 mediated PI hydrolysis is responsible for the partial rescue. Working to measure the PI levels in the small SC DRG co-culture samples, as well as identifying the best time to measure those levels, are critical technical issues to be resolved. Preliminary work has shown that it is possible to measure lipids using SC DRG co-cultures, however the procedure will need to be refined and repeated to yield interpretable data. If we are able to confirm depletion of PI3P

levels by exogenous MTMR2 , this will will confirm PI hydrolyis activity and lend support to the idea that MTMR2 rescues *Mtmr13*$^{-/-}$ via restoring near normal PI levels.

Recovering the phosphatase and kinase balance in the PI system has been a successful strategy in other models of CMT4. Reintroduction of MTMR2 in *Mtmr2*$^{-/-}$ mice (a model for CMT4B1) *in vitro* results in an improvement in the *Mtmr2*$^{-/-}$ myelin outfolding phenotype (Bolis et al., 2009). Reduction of PI(3,5)P_2, via loss of the Pl 5-phosphatase Fig4 in Schwann cell specific *Fig4*$^{-/-}$ mice (a model of CMT4J), causes demyelination in the PNS. Interestingly, heterozygous *Fig4*$^{+/-}$ mice also homozygous *Mtmr2*$^{-/-}$ show a reduction in myelin outfoldings, relative to *Mtmr2*$^{-/-}$ mice. Reduced Fig4 PI 5-phosphatase levels is proposed to reduce Fig4 inhibition of Fab1, a 5-kinase. *Fig4*$^{+/-}$ mice could therefore increase PI(3,5)P_2 via increased Fab1 PI 5-kinase activity and reduced levels of Fig4 PI 5-phosphatase. The *Mtmr2*$^{-/-}$ *Fig4*$^{+/-}$ genotype may have increased PI3P and PI(3,5)P_2 levels, thereby rebalancing PI3P phosphatase activity lost in *Mtmr2*$^{-/-}$. This model provides evidence indicating that adjusting the balance of PI phosphatases and kinases is a reasonable strategy to improve myelination in CMT disease models(Vaccari et al., 2011; 2015). The data presented here support the the idea that phosphatase and kinase regulation of PI3P is critical for normal myelination, but that simply tweaking the balance of PI kinases and phosphatase is not enough to fully recover the myelin outfoldings initiated by the loss of *Mtmr13*$^{-/-}$. While the rebalancing of PI phosphatases/kinases has shown promise in some models of CMT, MTMR13 may have other roles in the cell that are not addressed by adjustment of PI 3-kinase or phosphatase levels.

Understanding whether this partial rescue is due to MTMR2 phosphatase activity or a non-catalytic role of MTMR2 is a necessary next step. Specifically, introducing a catalytically dead MTMR2 to *Mtmr13*$^{-/-}$ SC DRG co-cultures to test its effect on *Mtmr13*$^{-/-}$ myelin

outfoldings. This would address the possibility that MTMR2 may have a non catalytic role critical to SC myelination. MTMT2 is reported to interact with DLG1 and through it kif13B and Sec8 in SCs to facilitate exocyst transport and build membrane(Bolis et al., 2009). Mtmr2 PI hydrolysis activity is proposed to negatively regulate this pro-membrane building pathway. Indeed knocking down Sec8 in *Mtmr2*$^{-/-}$ SC DRG co-cultures reduces the fraction of segments containing outfoldings, adding support to the idea that membrane building is dysregulated in *Mtmr2*$^{-/-}$ (Bolis et al., 2009). MTMR2's role in recruitment of other proteins to the endosome, perhaps even unrelted to its phosphatase activity, may be also critical to myelination.

The pseudophosphatase MTMR13 has long been thought to have a scaffolding or other signaling function critical to SCs (Jean and Kiger, 2012; Raess et al., 2016). Recovering MTMR2 levels partially rescues outfoldings in this *Mtmr13*$^{-/-}$ model of CMT4B2, however this incomplete rescue lends support to the idea MTMR13 plays a role in signaling beyond PI hydrolysis. MTMR13's DENN domain has been studied as a potential Rab GEF. Recent evidence from Kiger's group has shown that the *Drosophila* homologue Sbf can act as a Rab21 GEF in critical for autohpagy in starvation conditions (Jean et al., 2012; 2015). Evidence for MTMR13's DENN domain acting as a Rab GEF in Schwann cells has not been identified. However, Schwann cells are known to rely on autophagic processes to reduce and remodel cytoplasm during myelination and during recovery from injury (Gomez-Sanchez et al., 2015; Jang et al., 2015). If SCs depend on Rab21 activation by MTMR13's DENN domain during a critical time in development, this could explain the mechanism of outfolding formation via dysregulation of cytoplasmic and membrane autophagy. Exploring the potential Rab GEF activity MTMR13's DENN domain in Schwann cells is a next critical step.

In vitro myelination systems provide useful models of peripheral myelin disorders that enable relatively quick genetic manipulation that cannot be performed *in vivo* (Bolis et al., 2009). Our exploration of *Mtmr13*$^{-/-}$ Schwann cells in myelinating SC DRG co-cultures shows that these cultures myelinate comparably to wild type, and that the phenotype of CMT4B2 outfoldings is recapitulated *in vitro*. We also present a replicable data collection and analysis method to assess SC DRG co-culture myelination myelin outfoldings. Using cells from CMT4B2 model *Mtmr13*$^{-/-}$ mice, we demonstrate that the CMT4B2 phenotype can be manipulated *in vitro* to reduce the myelin outfolding phenotype. We show that overexpression of MTMR2 affects SC myelination and partially rescues the myelin outfolding phenotype in *Mtmr13*$^{-/-}$ SC DRG coculture. This *in vitro* system will enable further study into the potential of the kinase-phosphatase balancing to recover the loss of function and myelin dysfunction in CMT models, as well as enable further study into the critical role of MTMR13 in myelination.

Figure 2.1 — Mtmr13$^{-/-}$ Schwann cell and neuron co-cultures myelinate robustly in vitro.

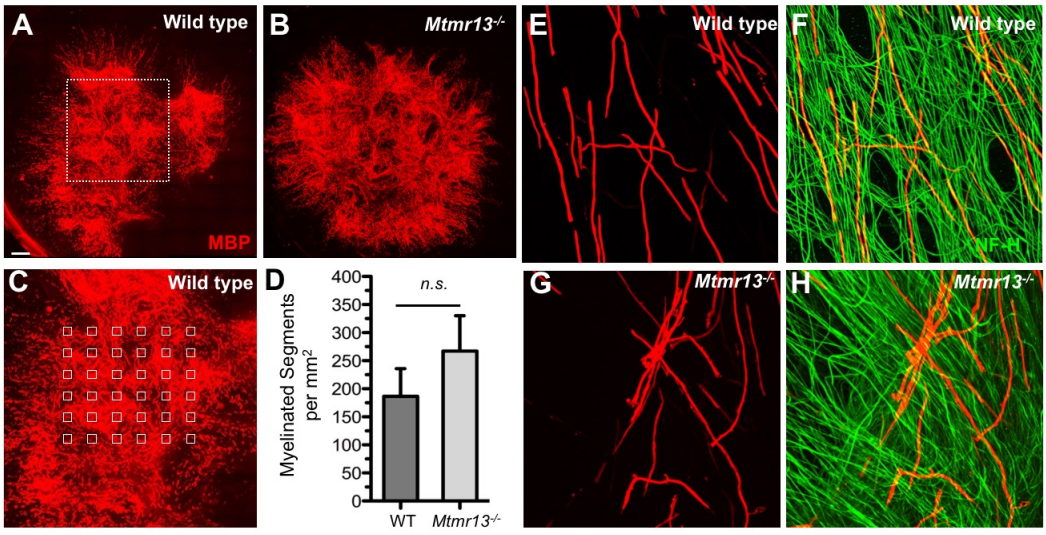

Figure 2.1 - Mtmr13$^{-/-}$ Schwann cell and neuron co-cultures myelinate robustly in vitro. (A, B) Representative images of whole SC DRG co-cultures immunostatined for MBP (red), scale bar = 2 mm. **(C)** Automated sampling wherein a grid of 36 images is centered on the myelinated region of the coverslip, scale bar = 3.5 mm. **(D)** Quantification of myelin segments per mm^2, displayed as mean and SEM. There is no significant difference between wild type and *Mtmr13*$^{-/-}$ SC DRG co-cultures, WT n = 6, *Mtmr13*$^{-/-}$ n = 7, Student's t- test p = 0.3273. **(E, F)** show representative images of wild type SC DRG co cultures stained for MPB (red) and NFH (green). **(G, H)** show a representative image of *Mtmr13*$^{-/-}$ SC DRG co-cultures. Scale bar in **E, F, G, H** = 133 μm.

Figure 2.2 — Mtmr13$^{-/-}$ Schwann cell and neuron co-cultures exhibit myelin outfoldings in vitro.

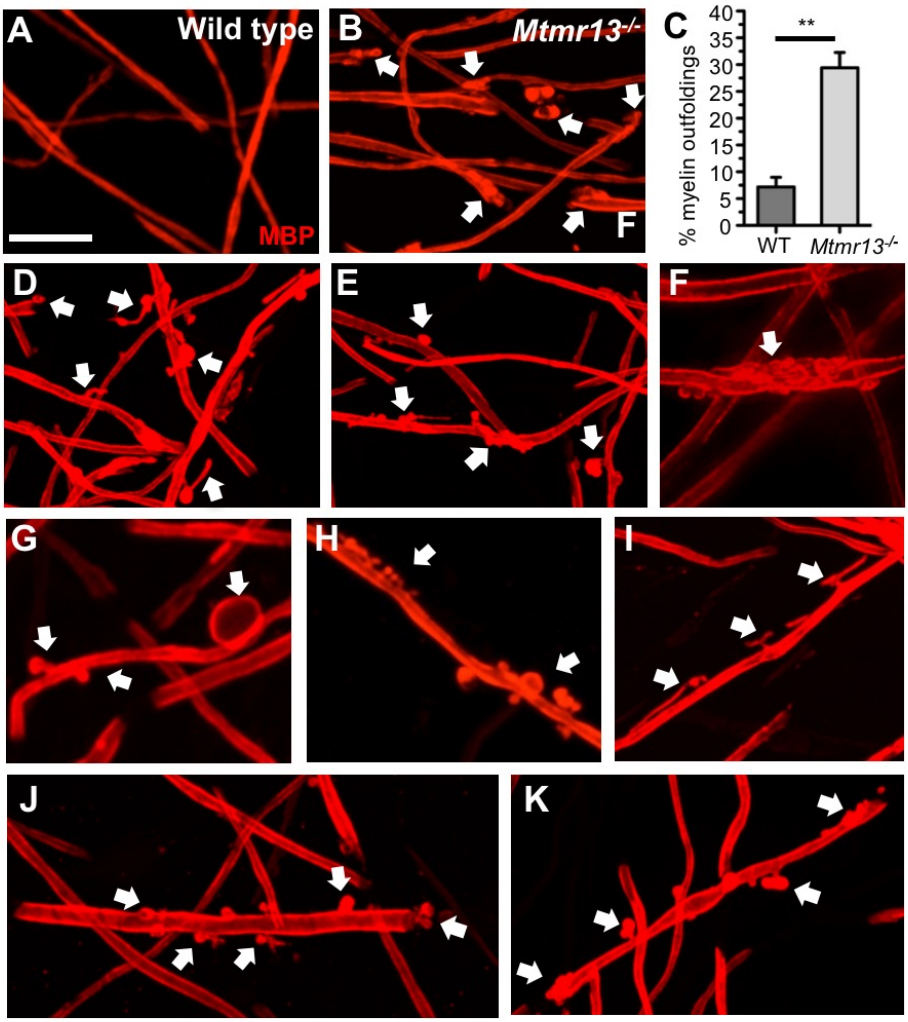

Figure 2.2 Mtmr13$^{-/-}$ Schwann cell and neuron co-cultures exhibit myelin outfoldings in vitro. (A, B) Images of myelin segments from wild type and Mtmr13$^{-/-}$ SC DRG co-cultures immunostatined for MBP (red), scale bar = 20 μm. **(C)** Quantification of the fraction of segments containing outfoldings for wild type and Mtmr13$^{-/-}$ SC DRG co-cultures. Data displayed as mean with SEM, WT n = 6, Mtmr13$^{-/-}$ n = 7, ** p = 0.0056 by Student's t test. **(D-K)** Myelin outfoldings observed in Mtmr13$^{-/-}$ SC DRG co-cultures. Outfoldings are marked with white arrows. Scale bar **(A-E)** = 20 μm, **(F)** = 15 μm, **(G, H)** = 24 μm, **(I-K)** = 26 μm.

Figure 2.3 — Electron microscopy of cultured SCs from Mtmr13$^{-/-}$ mice shows myelin outfolding phenotype similar to Mtmr13$^{-/-}$ sciatic nerve.

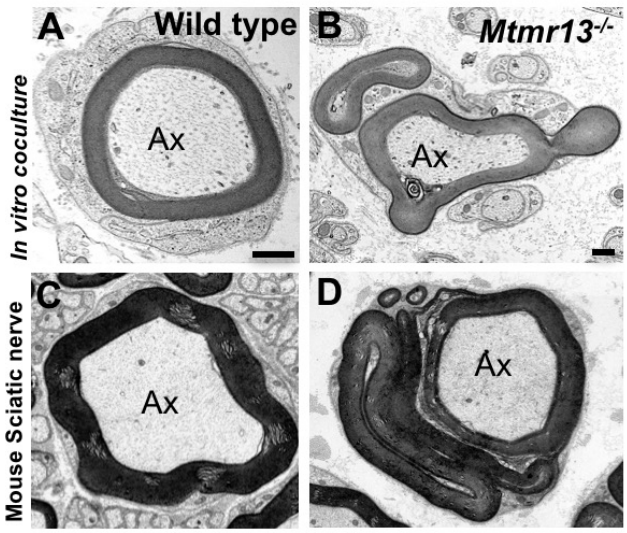

Figure 2.3 - Electron microscopy of cultured SCs from *Mtmr13*$^{-/-}$ mice show myelin outfolding phenotype similar to Mtmr13$^{-/-}$ sciatic nerve. (A, B) Transmission electron micrographs of myelin segment crossections from wild type **(A)** and *Mtmr13*$^{-/-}$ **(B)** SC DRG co-cultures. (**B)** Illustrates a *Mtmr13*$^{-/-}$ with a redundant loop of myelin and additional protrusion-like structures. **(C, D)** illustrate comparable mouse sciatic nerve from wildtype **(C)** and *Mtmr13*$^{-/-}$ **(D)** co-cultures. **D** Illustrates redundant myelin loop *in vivo* in the mouse sciatic nerve. Ax = axon. Scale bar **A, B** = 500 nm, **C, D** = (FLR). DCR prepared and imaged the *in vitro* samples shown in **(A,B)**, and FLR prepared and imaged the *in vivo* samples shown in **(C,D).**

Figure 2.4 — Robust expression of EGFP-MTMR2 in SC DRG Co-cultures.

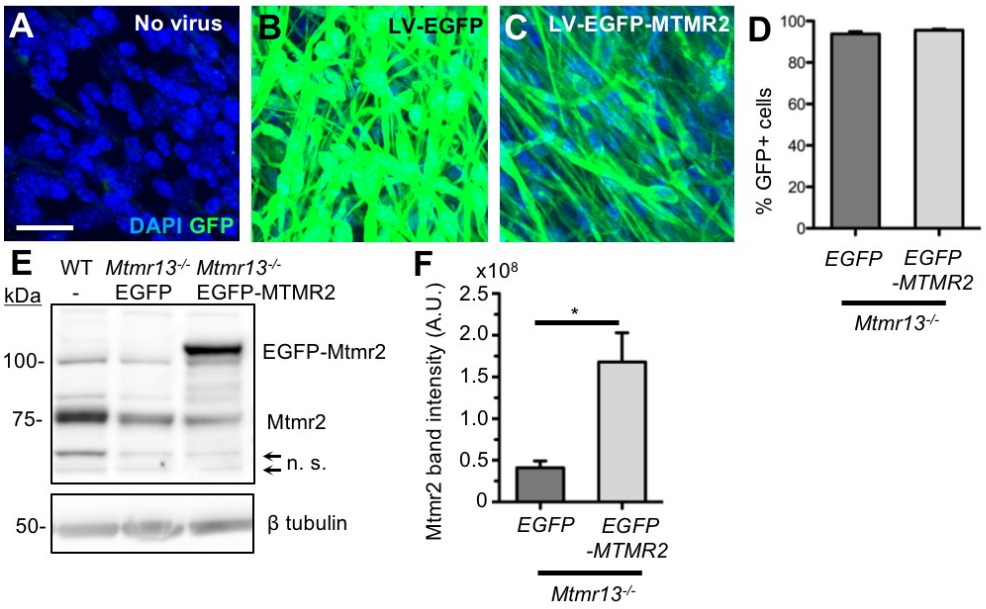

Figure 2.4: LV-EGFP-MTMR2 expresses robustly in SC DRG cocultures. **(A, B, C)** show representative 100 μm square images taken using the same laser power and microscope setting. **(A)** control SC DRG that did not receive virus, **(B)** received LV-EGFP at MOI = 15, **(C)** received LV-EGFP-MTMR2 at MOI =15. **(D)** Quantification of GFP-positive nuclei showed >90% transduction for LV-EGFP and LV-EGFP-MTMR2, n= 3 for each condition. **(E)** protein lysates were prepared from SC DRG co-cultures and examined by immunoblotting for Mtmr2. Endogenous Mtmr2 protein is visible in all lanes at 75 kDa. Exogenous EGFP-MTMR2 is visible just above the 100 kDa mark only in lane 3, *Mtmr13*$^{-/-}$ +EGFP-MTMR2. **(F)** Chemiluminescent quantification of Mtmr2 protein levels in immunoblots. The fraction of MTMR2 expressed over endogenous Mtmr2 in *Mtmr13*$^{-/-}$ is quantified, EGFP-MTMR2 introduces MTMR2 at levels significantly above those found in endogenous *Mtmr13*$^{-/-}$ co-cultures, data is displayed as mean and SEM, * p = 0.024 Student's t-test (raw data quantified in **(F)** shown in Figure S2.1, n=3 per condition. Scale bar **(A, B, C)** = 20 μm.

Figure 2.5 — Exogenous expression of the active phosphoinositide 3-phospahtase MTMR2 leads to a reduction in myelination.

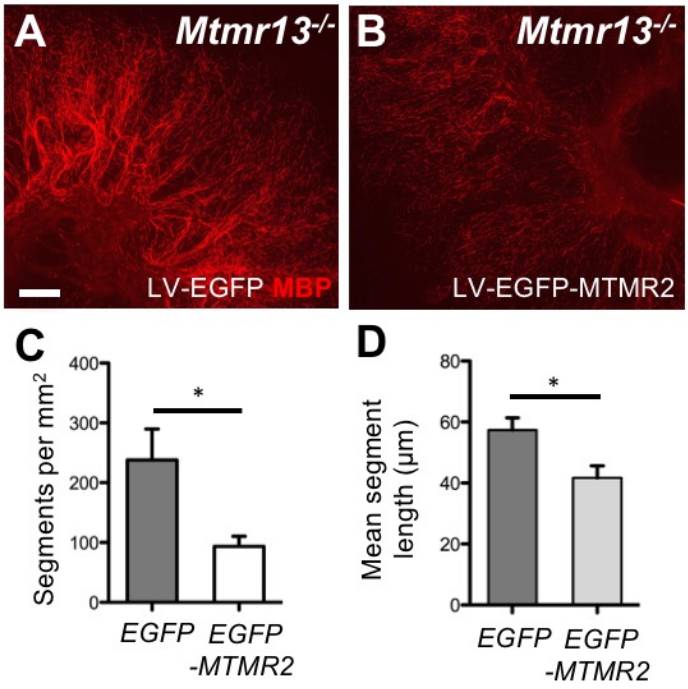

Figure 2.5: Exogenous expression of the active phosphoinositide 3-phospahtase MTMR2 leads to a reduction in myelination. (A) *Mtmr13*$^{-/-}$ SC DRG infected with control LV-EGFP stained for MBP. **(B)** *Mtmr13*$^{-/-}$ SC DRG infected with LV-EGFP-MTMR2 stained for MBP, illustrating a reduction my myelination. **(C)** LV-EGFP-MTMR2 coverslips show a reduction in segments per mm^2 *p = 0.016, n= 6 LV-EGFP, n= 7 LV-EGFP-MTMR2 **(D)** and a significant reduction in mean segment length *p = 0.03, Student's t-test. Data are displayed as mean and SEM. Scale bar = 1 mm.

Figure 2.6 — Exogenous expression of MTMR2 in Mtmr13$^{-/-}$ cultures reduces outfoldings.

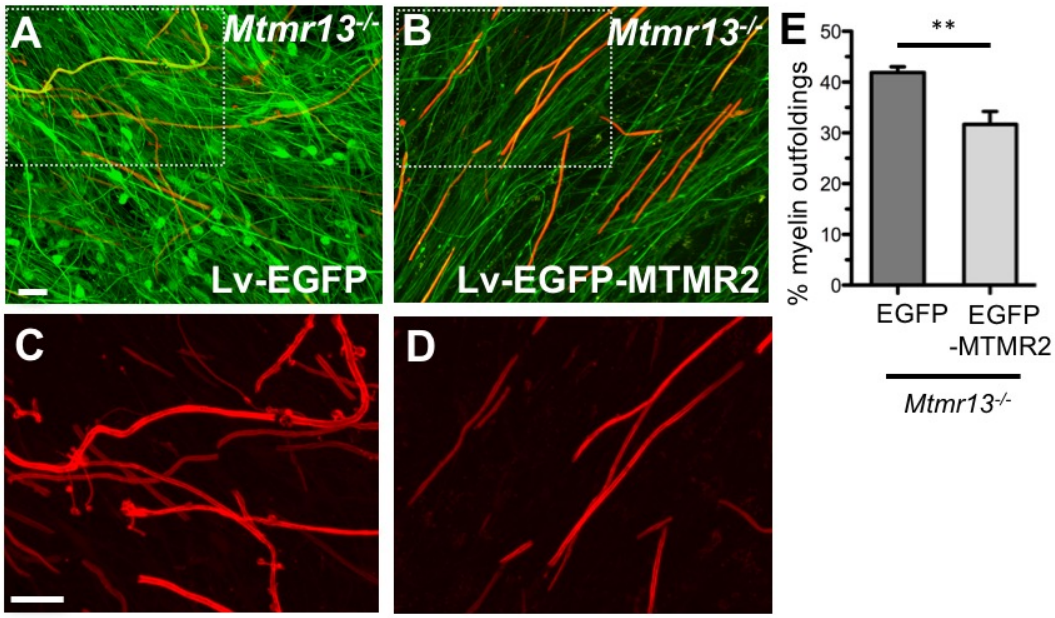

Figure 2.6 - Exogenous expression of MTMR2 in *Mtmr13*$^{-/-}$ cultures reduced the fraction of segments that contain outfoldings. (A) *Mtmr13*$^{-/-}$ SC DRG infected with control LV-EGFP stained for MBP. **(B)** *Mtmr13*$^{-/-}$ SC DRG infected with LV-EGFP-MTMR2 stained for MBP. **(C, D)** Details of **(A, B). (E)** Quantification of the fraction of segments containing outfoldings revealed a significant reduction in the fraction of segments containing outfoldings, ** p = 0.0056, n= 6 LV-EGFP, n= 7 LV-EGFP-MTMR2. Scale bar = 20 μm.

Figure S2.1 — Robust Expression of EGFP-MTMR2 in SC DRG Co-cultures, supplementary data

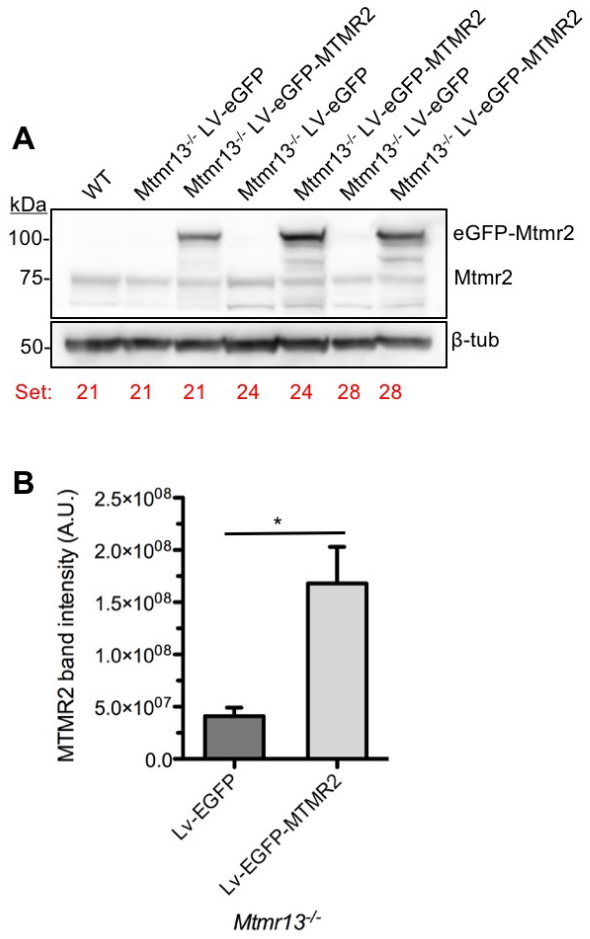

Figure S2.1 - Robust expression of eGFP-MTMR2 in myelinating co-cultures. (A) Immunoblot of MTMR2 expression in SC DRG coverslips from wild type (WT) or Mtmr13$^{-/-}$ infected with LV-EGFP or LV-EGFP-MTMR2 virus at an MOI of 15. **(B)** shows quantification of MTMR2 levels wild inMtmr13$^{-/-}$ infected with LV-EGFP or LV-EGFP-MTMR2. Data are displayed as mean and SEM, n = 3 coverslips in each condition. *p = 0.240 Student's t-test.

Figure S2.2 — Exogenous expression of MTMR2 in wild type cultures has no effect on myelin abnormalities.

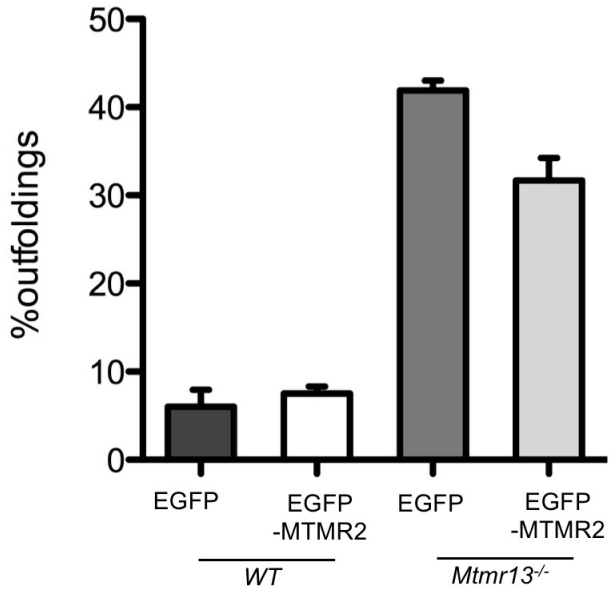

Figure S2.2 — MTMR2 does not impact the frequency of myelin outfoldings in wild type SC DRG co-cultures. WT +EGFP n = 3 coverslips, WT +EGFP-MTMR2 n = 3 coverslips. *Mtmr13*$^{-/-}$ +EGFP n = 6 coverslips *Mtmr13*$^{-/-}$ +EGFP-MTMR2, n = 7 coverslips. Data are displayed as mean with SEM.

Chapter 3. Mtmr13's DENN Domain: New Tools and Approaches to Clarify its Function in Schwann Cell Myelination

Forward

The LVPG-EGFP vector was originally created by Gregory A. Dissen and was given to FLR as a gift. FLR and AEM designed and created Rab21-Q67L, DCR made, concentrated and titred the lentivirus, as well as designed co-culture experiments using these viruses. DCR and FLR designed LVPG-EGFP-MTMR13-DENN-1-509 and LVPG-EGFP-MTMR13-DENN-1-509-2xFYVE, DCR created the plasmids, made the lentivirus, concentrated the viruses, and titred the viruses. Virus concentration was done with the use of the Cohen lab ultracentrifuge, based on a protocol kindly provided by Jeffrey Huang, PhD and Michael Cohen, PhD. Virus titring protocol is based on a protocol developed by Dr. Kim-Hien Dao, who also kindly provided training and access to the Guava Flow cytometer. DCR adapted these protocols, performed all experiments, collected, and analyzed the data in this chapter.

3.1 —Introduction

Myelin outfoldings are focally folded sheets of myelin characteristic of CMT4B2 (Previtali et al., 2007). However, however a direct link between these outfoldings and the function of Mtmr13 in Schwann cells has yet to be established (Robinson et al., 2008). The SC dysfunction caused by the loss of MTMR13 function that results in myelin outfoldings, and eventually the loss of distal axons, is currently untreatable (Reilly, 2016). A full understanding of the mechanisms behind CMT4B2 is the only way to develop therapeutic targets to help patients afflicted with this rare condition. A deeper mechanistic

understanding that could lead to reducing or rescuing this myelin phenotype in animal models remains a critical goal for the field. Chapter 2 explored MTMR13's relationship with the active phosphatase MTMR2. While there are loose ends to address, these data indicate that *Mtmr13*$^{-/-}$ myelin outfoldings can be impacted *in vitro* via lentivirus mediated gene transduction. In this chapter, I will discuss approaches that focus on the potential signaling role MTMR13's DENN domain.

In Chapter 2, I showed that exogenous expression of MTMR2 resulted in a partial rescue of the *Mtmr13*$^{-/-}$ myelin outfolding phenotype *in vitro*. One possible explanation for the incompleteness of the rescue of the *Mtmr13*$^{-/-}$ phenotype by MTMR2 *in vitro* is that other functions of MTMR13 are critical for normal myelination and myelin maintenance. We have shown that MTMR13 and MTMR2 also complex together and reciprocally boost protein levels (Ng et al., 2013). However, there is evidence that supports a role for MTMR13 beyond supporting MTMR2. If *Mtmr13*$^{-/-}$ outfoldings are not caused solely by the reduction in Mtmr2 PI phosphatase activity, the addition of exogenous MTMR2 could not be expected to completely rescue the outfolding phenotype.

A current theory in the field is that MTMR13's DENN domain may act as a Rab21 guanine exchange factor (GEF). Evidence for the role of DENN domains in Rab signaling has been emerging over the past ten years (Allaire et al., 2010; Jean et al., 2012; 2015) (Yoshimura et al., 2010). Yoshimura et al. characterized the Rab activation capabilities of multiple DENN domains, including MTMR13 which had the highest affinity for Rab28 in their study (Yoshimura et al., 2010). Recntly, Kiger's group used the MTMR13 *Drosophila* homolog Sbf to show direct evidence for DENN domain Rab GEF activity in certain cell types and conditions. In these reports, the Sbf DENN domain acts as GEF for Rab21, associating with GDP bound Rab21 and facilitating its exchange for GTP (Jean and Kiger,

2012). More recently, Kiger's group confirmed MTMR13— Rab21 GEF activity in human cell lines, and reported evidence (in specific cellular starvation conditions) for MTMR13 activated Rab21 to associate with VAMP8 (*Drosophila* Vamp7), which is required for autophagosome-lysosome fusion (Jean et al., 2015). A specific Rab activation function for MTMR13 at the early endosome would help explain why the loss of pseudophosphatases MTMR13 severely impairs SCs in CMT4B2. Although the work of Jean et al. showed Sbf Rab21 GEF activity, the cell lines used are not SCs and starvation conditions were necessary in some cases to see this interaction(Jean et al., 2015).

It is possible that Schwann cells enter a metabolically stressed state similar to starvation during myelin sheath formation, particularly in light of the ATG7-dependent cytoplasmic autophagy that is reported to be critical for normal SC development (Jang et al., 2015). Jang et al. reported that autohphagy, and specifically the fusion of the is critical during early stages of myelination (Jang et al., 2015). However, the $Atg7^{-/-}$ mice developed by Jang et al. have a very mild phenotype and another group saw no effect on SCs with the loss of ATG7 (Gomez-Sanchez et al., 2015). In light of this, it remains possible that SC myelination is dependent on autophagy and does involved a starvation-like state, wherein MTMR13 may act as a Rab GEF. The missing piece is direct evidence for MTMR13's Rab GEF activity in SCs. As SCs are the primary affected the cell type in CMT4B, and as SCs have unique structural, polarization, and trafficking needs, evidence of Rab GEF activity in this cell type is of great interest to the field.

To study the role of MTMR13's DENN domain I have used lentivirus to alter gene expression in SC-DRG co-cultures. This approach allowed specific exogenous expression of MTMR13 DENN domain and consitiutively active (CA) Rab21 in SCs, with the clinically relevant read-out of myelin outfoldings. This system will provide insight into the

pathomechanisms behind myelin dysfunction and outfoldings. *Mtmr13*$^{-/-}$ SC DRG co-culture demonstrates that the CMT4B2 phenotype is recapitulated *in vitro,* as described in Chapter 2. Partial rescue of the myelin outfolding phenotype in *Mtmr13*$^{-/-}$was attained through expression of EGFP-MTMR2. However, with this rescue came a loss of overall myelin segment number and a reduction in myelin segment length.

The DENN domain may hold the key to understanding the function of the enigmatic pseudophosphatase MTMR13. In this chapter, I will show experiments that tested the hypothesis that the DENN domain of Mtmr13 is sufficient to support normal myelination. In Chapter 2, I showed that altering the PI3P phosphatase/kinase balance by adding endogenous MTMR2 to Schwann cells *in vitro* affects the fraction of myelin segments that contain outfoldings. However, the field is lacking direct evidence for Mtmr13's role in other signaling pathways in Schwann cells. In Chapter 3, I will describe experiments designed to address the role of Mtmr13's DENN domain and its potential signaling partners in Schwann cells.

3.1 — Materials and Methods

3.1.1 — Development of a GFP-Tagged Mtmr13 DENN Domain

To express exogenous tagged proteins, cDNA was cloned into an LVPG vector with an EGFP reporter. The Robinson lab has a Myc-tagged human MTMR13, however critical regions of the mouse and human Mtmr13 proteins are differ significantly, so I worked with Fred Robinson to develop a mouse version of Mtmr13. The reference cDNA from mouse Mtmr13 was NM_177324.2, Protein NP_796298.2 (ncbi.nlm.nih.gov/nuccore/NM_ 177324). As no full length mouse Mtmr13 was commercially available, I worked with Fred Robinson to identify clean regions of sequence from the I.M.A.G.E. Consortium on listed

on GenBank. Two I.M.A.G.E. clones, BC048706.1 (I.M.A.G.E Clone ID: 6510503) and BC067204.1 (I.M.A.G.E Clone ID: 30138246), were identified and available from Dharmacon/GE. My goal was to create a mouse Mtmr13-DENN-only construct that would produce a stable protein when expressed via transfection or viral transduction *in vitro*. Previous unpublished work in our lab showed that truncating Mtmr13 right at the end of the DENN domain at amino acid 449 resulted in a poorly expressing protein (via transfection and immunoblot). I set out to include the entire DENN domain, and to truncate the protein at a place where it would still express well. Regions of low sequence homology and low hydrophobicity across species were identified using T-Coffee online multiple sequence alignment tool (tcoffee.org) (Notredame et al., 2000). The best places to truncate the protein were identified as amino acids 505-511 and region of amino acids 689-701. I then worked up a plasmid in an LVPG vector that contained the first 509 amino acids of Mtmr13 (Mtmr13-DENN-1-509) and another construct that contained the first 699 amino acids (Mtmr13-DENN-1-699). These constructs both omit the C-terminus, see Figure 3.1. By truncating the protein at amino acid 509 or 699, we limited the mutants ability to associate the membrane or other MTMRs. The inactive phosphatase domain, thought to associate with the PI3P rich endosomal membrane, was omitted. As was the coiled-coil domain, which is thought to link MTMR13 to myotubularins. Because the LV-EGFP-Mtmr13-DENN-1-509 and LV-EGFP-Mtmr13-DENN-1-699 do not contain inactive phosphatase or coiled-coil regions, I also made a third plasmid that included the DENN domain with two FYVE domains to ensure localization to PI3P-rich membranes, like the early endosome (Stahelin et al., 2014). This construct contained the first 509 amino acids of Mtmr13 followed by a short linking region and two PI3P-binding FYVE domains (LV-EGFP-Mtmr13-DENN-1-509-2xFYVE).

The LV-EGFP-Mtmr13-DENN-1-509 was selected because it allowed inclusion of the entire DENN domain and truncated the protein at a region of low sequence homology identified by multiple sequence alignment. To creatve LV-EGFP-Mtmr13-DENN-1-509, the the first 509 amino acids of the N-terminus end of mouse Mtmr13 were created from BC048706.1 (IMAGE Clone ID: 6510503) and BC067204.1 (IMAGE Clone ID: 30138246). PCR Primers DRO-011 and DRO-012 were used on BC048706.1. PCR Primers DRO-013 and DRO-015 were used on BC067204.1 (details on primer sequences in Appendix). These amplification reactions included 15 base pair overhangs and created components necessary for a double infusion reaction (In-Fusion HD CloneTec #011614). These components were made from BC048**706**.1 and BC067**204**.1, and are hereafter referred to as 706 and 204. Briefly, following PCR amplification of 706 and 204, PCR products were verified by staining with 6x DNA gel loading dye and run on a 0.8% Agarose TAE gel with SYBR safe DNA gel stain at 10 ul/100 ml (#S33102). DNA bands were visualized with UV, the bands were manually cut out, and DNA extracted with a gel extraction kit (Quiagen QIAquick Gel Extraction Kit # 28704). Resulting gel-purified DNA was eluted in purified water, DNA concentration was measured, and DNA was sequenced (Vollum Sequencing Core) to confirm successful addition of 15 base pair overhangs, linking regions, and stop codon. 706 contained a silent C to T mutation at base pair 15. LV-EGFP vector was linearized with restriction enzymes *BsrGI* and *SalI* (New England BioLabs) and gel purified. A double infusion reaction was set up with the 706 and 204 components with the linearized LV-EGFP, following a protocol adapted from the Clontec Infusion Cloning Manual (Protocol I: In-Fusion Cloning Procedure w/Spin-Column Purification).

To complete the infusion reaction, the linearized LV-EGFP was combined with 706 and 204 fragments, the HD-infusion enzyme, and deionized water. This mixture was

incubated for 15min at 50° C and then placed on ice. The infusion reaction was then transformed into competent cells and plated on ampicillin positive LB agar gel plates with at a volume of 40 μL, 150 μL and 250 μL, and 0 μL (negative control). These plates were incubated overnight at 30° C to avoid recombination in long terminal repeats. The following day, single colonies were picked and grown up in 4 mL of LB broth overnight in a closed floor shaker at 30° C in vent cap tubes. The resulting bacterial growth was harvested and prepped with a QIAprep Spin Miniprep Kit (#27104). The Miniprepped DNA was then sequenced to confirm successful infusion, and the successful preps were retransformed into bacteria and prepared via QIAGEN Plasmid Plus Maxi Kit (#12963).

LV-EGFP-Mtmr13-DENN-1-699 was prepared along with LV-EGFP-Mtmr13-DENN-1-509. I.M.A.G.E. clones BC048706.1 (I.M.A.G.E Clone ID: 6510503) and BC067204.1 (I.M.A.G.E Clone ID: 30138246) contained enough good sequence to enable the first 699 amino acids. Extending the sequence to 699 allows the inclusion of some of the SBF2 domain that follows the DENN domain. However, LV-EGFP-Mtmr13-DENN-1-699 expressed poorly at all points. The post-infusion bacterial plate yielded low number of colonies, low DNA yield at mini prep, and low protein expression after *in vitro* transfection. Because of this, LV-EGFP-Mtmr13-DENN-1-699 was abandoned. As LV-EGFP-Mtmr13-DENN-1-699 truncated the protein in the predicted-globular SBF domain globular, it is probable that Mtmr13-DENN-1-699 does not fold well. In order for a virally-mediated rescue of the myelin outfolding phenotype, near complete virally-mediated transduction must be achieved. Unfortunately, a low yield construct will produce a low titre virus that will not work well in the SC DRG co-culture system. This construct may be useful in other systems, however, where incomplete expression is acceptable.

LV-EGFP-Mtmr13-DENN-1-509 expressed well, and produced a virus of usable titre. However, because it does not contain the PH-GRAM, inactive phosphatase, or C-termial PH domains, it is possible that this protein would not localize properly. LV-EGFP-Mtmr13-DENN-1-509 was observed diffusely in the cell body, with no apparent preference for endomembrane structures. The inactive phosphatase and Ph-GRAM domains of Mtmr13 are thought to bind PI3P and localize to to the early endosome. While there is some evidence that DENN domains can associated with PI-rich membranes (Allaire et al., 2010), there was no way assurance that LV-EGFP-Mtmr13-DENN-1-509 would localize correctly and act with endogenous signaling partners in the cell.

To address localization, I added two FYVE domains to the C-terminus end of LV-EGFP-Mtmr13-DENN-1-509, see Figure 3.1. EGFP tagged 2x-FYVE (LV-EGFP-2xFYVE) expresses well via either transfection of the plasmid or lentivirus mediated transduction (see Figure 3.2 example fluorescence image and Figure S3.3 for western blot). LV-EGFP-2xFYVE localizes a GFP signal to the early endosome. As LV-EGFP-2xFYVE (See Figure S3.2) and LV-EGFP-Mtmr13-DENN-1-509 expressed well, I created a hybrid construct with added two FYVE (2x-FYVE) PI3P binding domains to the c-terminus of the 509 amino acid DENN domain fragment to ensure that Mtmr13-DENN-1-509 (LV-EGFP-Mtmr13-DENN-1-509-2xFYVE) would target to the correct location.

To create LV-EGFP-Mtmr13-DENN-1-509-2xFYVE, Mtmr13-DENN-1-509 was PCR'd off LV-EGFP-Mtmr13-DENN-1-509 with PCR primers PCR DRO-011 and DRO-016 (details on primer sequences in Appendix). The 2xFYVE was PCR'd off EGFP-2xFYVE (C2 vector) from Fred Robinson with PCR primers DRO-017, DRO-018. DNA was gel extracted as described above. A double infusion reaction with Mtmr13-DENN-1-

509, 2xFYVE, and linearized LVPG-EGFP (BsrG1 and Sal1) was carried out as described above.

As an alternate strategy, I also worked with a constitutively active Rab21 (CA-Rab21, Q67L), see Figure 3.1 and S3.3. This plasmid had been made in the Robinson lab (by Anna Mammel) and needed only to be packed for lentivirus mediated delivery. Based on unpublished work done in the Robinson lab and the work of Kiger's lab, Rab21 was the best candidate for interaction with MTMR13. If MTMR13's DENN domain acts as a Rab21 GEF, it is possible that exogenous expression of a constitutively active Rab21 could impact signaling downstream of MTMR13 and alter *Mtmr13*$^{-/-}$ myelin outfoldings.

3.2.2 – Protein Expression and Lentivirus Production

To validate and assess expression of the constructs and viruses described in this chapter, the following methods were used. New lentivirus vector plasmids were sequenced to confirm successful infusion. If sequencing revealed successful infusion, plasmids were transfected into HEK 293 cells to test protein expression relative to LV-EFP and LV-EGFP-MTMR2 via western blot, following the procedure outlined in Chapter. If the constructs transfected well, as assessed by western blot of GFP expression at the appropriate size for the tagged protein, they were then used to make virus. These virus' were then titred and protein expression was tested again via western blot in the DRG Schwann cell co-culture system, see Figure S3.3.

Lentivirus' for LV-EGFP, LV-EGFP-Mtmr13-DENN-1-509, LV-EGFP-Mtmr13-DENN-1-509-2xFYVE, LV-EGFP-2xFYVE, and LV-EGFP-CA-Rab21 were made as described in Chapter 2. Virus was applied to co-cultures, and cultures were imaged and analyzed as described in Chapter 2.

3.3 — Results

LV-EGFP-Mtmr13-DENN-1-509 and LV-EGFP-Mtmr13-DENN-1-509-2xFYVE were built to test the hypothesis that the DENN domain of Mtmr13 is sufficient for normal myelination. There is evidence to support SBF/MTMR13's DENN domain acting as a GEF for Rab-21 signaling. Is the DENN domain of MTMR13 critical to myelination? Will reintroduction of this domain into *Mtmr13*$^{-/-}$ cultures affect myelin outfoldings?

Exogenous GFP tagged Mtmr13-DENN-1-509 (LV-EGFP-Mtmr13-DENN-1-509) appeared to express well in DRG Schwann cell co-cultures. It expressed reasonably well when used at an MOI of 30, as assessed via western blot (see Figure 3.2). While levels of proteins expression via GFP western blot were less than that of LV-EGFP-MTMR2, a count of GFP-positive cell bodies revealed near complete transduction. The LV-EGFP-Mtmr13-DENN-1-509 localization was general and diffuse in Schwann cell bodies, it was excluded from the nucleus. It did, however, appeared dimmer (potentially less abundant) than EGFP-MTMR2 or EGFP. Quantification of myelin segments per unit area and fraction of segments containing myelin outfoldings was carried out as described in Chapter 2. However, no effect on myelin segments per unit area or fraction of segments containing outfoldings was observed.

LV-EGFP-Mtmr13-DENN-1-509 at an MOI of 30 in SC DRG co-cultures had no apparent effect on the number of myelin segments or the fraction of segments containing outfoldings. This points to the importance of the full length MTMR13 protein in normal myelination. However, I was unable to ensure PI3P-rich membrane localization as this mutant omitted all known PI3P associating domains. Unfortunately, LV-EGFP-Mtmr13-DENN-1-509-2xFYVE does not robustly infect cells at an MOI of 15. Because only 30-40% of SCs were infected, this virus was not efficient enough for use in SC DRG cultures.

However, the plasmid may be useful in another type of experiment, where incomplete protein expression is acceptable.

CA-Rab21, on the other hand, robustly infected cultures at an MOI of 15. Fluorescence microscopy confirmed near complete transduction, and immunoblotting indicated relatively high levels of protein expression. Quantification of myelin segments per unit area and fraction of segments containing myelin outfoldings was carried out as described in Chapter 2. No effect of LV-EGFP-CA-Rab21 was observed on segment density or segment length. However, interestingly, a small (20%) decrease in the fraction of segments containing outfoldings was observed.

3.3 — Discussion

This work presents evidence that Rab21 may play a role in SC myelination and that MTMR13's DENN domain is not sufficient to impact myelin outfoldings in *Mtmr13*$^{-/-}$. The most straightforward way to prevent or rescue the myelin outfoldings in CMT models where disease is caused by the loss of a protein is to reintroduce the missing protein. Reintroducing MTMR2 has been effective in the rodent model of CMT4B1, where exogenous MTMR2 reduced the frequency of segments containing outfoldings *in vitro* (Bolis et al., 2009). However, in my hands, robust expression of full length Mtmr13 proved elusive. Expression of full length Mtmr13 *in vitro* through viral transduction was attempted, however Mtmr13 repeatedly yielded a non-functional or low titre virus (despite reasonable efficacy when constructs were delivered via transfection), see Figure S3.1. To use myelin and myelin outfoldings in SC DRG co-cultures as a read-out, a high titre virus is required, i.e. over 90% of cells must be transduced. Without efficient transduction, it is impossible to assess the impact of genetic manipulation, as only a fraction of cells in SC DRG co-cultures produce

myelin sheaths. For this reason, I turned to truncated Mtmr13 mutants. As an alternative strategy, as MTMR13 has been proposed to act as a Rab GEF, Currently, the best candidate Rab for MTMR13 is Rab21, which was recently shown to interact with *Drosophila* MTMR13 homologue Sbf (Jean et al., 2012; 2015). I worked with a CA-Rab21, which expressed will in the SC DRG co-culture system

By focusing on the N-terminus end of Mtmr13, notably the DENN domain and its potential effectors, I hoped to address role of the DENN domain in Rab signaling in myelination. I was successful in creating a stable, EGFP tagged MTMR13 DENN domain that appeared to express well in culture. However, this construct failed to impact myelination or myelin outfoldings *in vitro*, see Figure 3.2. As the LV-EGFP-MTMR13-DENN-1-509 does not include the known membrane and myotubularin association domains present in full length MTMR13, I could not exclude the possibility that it would not localize appropriately. To address this caveat, I also made LV-EGFP-MTMR13-DENN-1-509-2xFYVE. This protein contained two PI3P binding FYVE domains at the C-terminus of the DENN domain chunk, which should localize the protein to the PI3P-rich membranes. Viral transduction of LV-EGFP-MTMR13-DENN-1-509-2xFYVE was successful, however not at high enough levels to be used in the SC DRG system.

While these two proteins failed to impact myelination, they may yet prove useful. For instance, LV-EGFP-MTMR13-DENN-1-509-2xFYVE may be useful in other systems where transfection, rather than lentivirus mediated transduction, is an appropriate mode of expression or where not every cell needs to express the protein. In addition, both of these DENN domain plasmids could be used to ask simpler questions. Though work in the lab is ongoing, we do not currently have strong evidence to support the idea that MTMR13's DENN domain is a Rab21 GEF in SCs. These DENN domain plasmids could be used in

cell lines as exogenous bait to test what Rabs the DENN domain associates with, whether the DENN domain association with Rabs depends on membrane targeting, or as part of a panel of MTMR13 pieces to identify possible interactors and effectors.

Identifying which parts of MTMR13 are sufficient to impact or even restore normal myelination *in vitro* remains a critical goal. MTMR13's domain's hint that it interacts with more than just MTMR2. To that end, Mtmr13-DENN-1-770 is the next logical place to truncate this protein. This variant would include the entire conserved SBF2 domain. While the function of this domain is unknown, there is some evidence that constructs including the SBF2 domain express well (Robinson and Dixon, 2005). Additionally, C-terminus fragments of MTMR13 have shown promising expression and should be tested in the SC DRG system (Robinson and Dixon, 2005; Ng et al., 2013). Specifically, a MTMR13 fragment including the inactive phosphatase, coiled-coil, and C-terminus PH domain may have the capability to restore and properly localize endogenous MTMR2 expression in the SC and impact myelination. These alternative strategies will be discussed in more detail in Chapter 4.

To test the hypothesis that Rab21 activity is sufficient to improve myelin outfoldings induced by the loss of Mtmr13, I transduced SC DRG co-cultures with a constitutively active Rab21 (CA-Rab21) in *Mtmr13*$^{-/-}$ SC DRG co-cultures. The addition of a constitutively active Rab21 to SCs could be expected to disrupt endosomal trafficking (Simpson et al., 2004). Indeed, as the lentivirus expression system infects all cell types *in vitro*, EGFP-positive (presumably endosomal) aggregations were observed in axons, see Figure 3.4. However, this did not seem to impair myelination or cause an increase in myelin outfoldings in wild type or *Mtmr13*$^{-/-}$ co-cultures, see Figure S3.4. In the context of *Mtmr13*$^{-/-}$, CA-Rab21 reduced the fraction of segments containing myelin outfoldings by 20% relative to EGFP controls

(Figure 3.4). CA-Rab21 had no impact on overall myelination, as assessed by both segments per unit area and myelin segment length.

These data imply that Rab21 may be downstream of MTMR13. A possible mechanism for this partial rescue is that MTMR13's DENN domain does indeed act as a Rab21 GEF. GTP-bound Rab21 at the early endosome is known to be critical for normal endosomal trafficking as well as integrin receptor trafficking and cytoskeletal actin dynamics (Simpson et al., 2004; Mai et al., 2011; Jean et al., 2012). The loss of MTMR13 in CMT4B2 may lead to both dysregulated PI hydrolysis via reduced expression of MTMR2 and dysregulated membrane endosomal/lysosomal trafficking that impacts cytoskeletal remodeling that may be critical for normal myelin sheath formation (Simpson et al., 2004; Mai et al., 2011; Jean et al., 2012; 2015). In this case, addition of a CA Rab21 would improve endosomal dynamics and normal autophagic processes in the *Mtmr13*$^{-/-}$ cells, leading to a partial remediation of the outfoldings. However essential data are missing from this mechanism, critically the interaction or activation of Rab21 by MTMR13 in SCs. Gathering evidence to support the interaction of MTMR13's DENN domain and Rab21 (and/or other Rabs, such as Rab11 and Rab28) a GEF role for MTMR13 in SCs will help to clarify its function and the disease mechanism of CMT4B2.

Figure 3.1 — Generation of MTMR13 and MTMR2 constructs developed for use in SC-DRG co-cultures

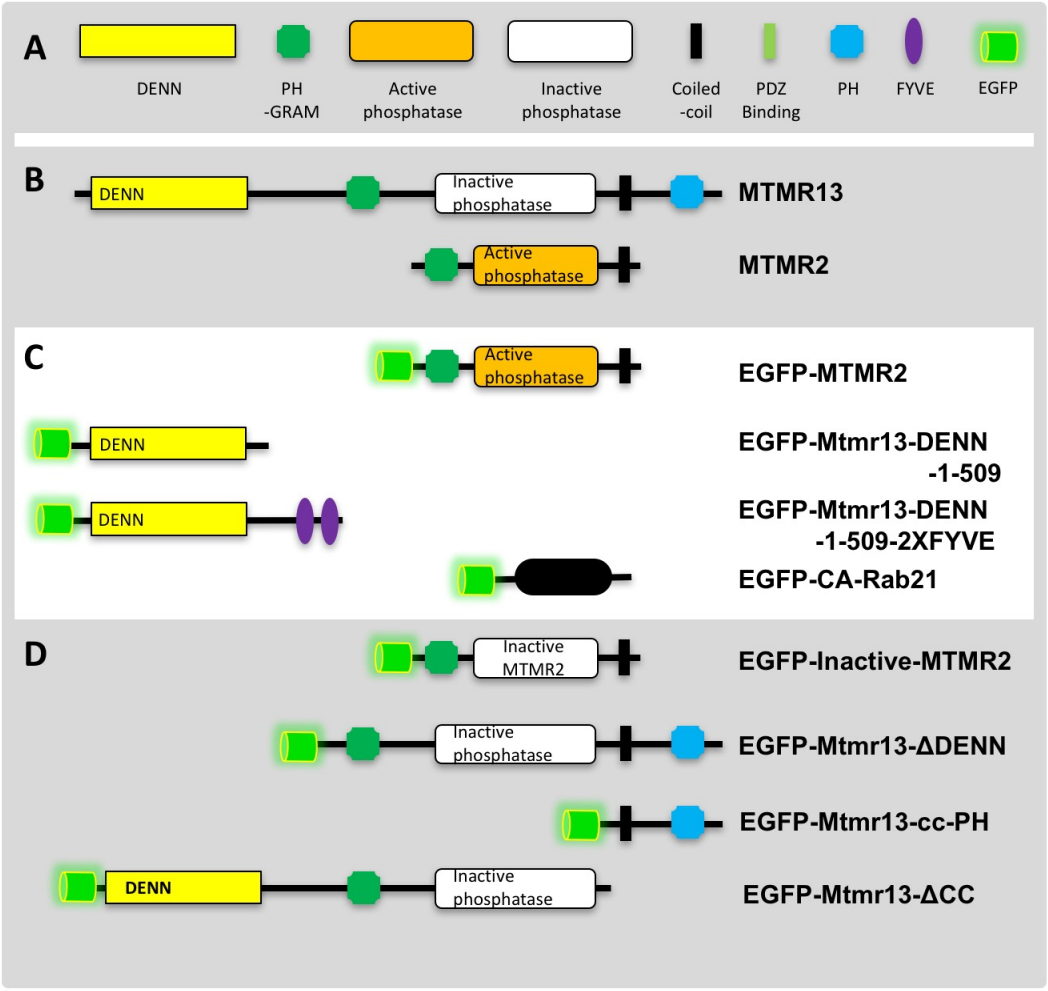

Figure 3.1. Generation of MTMR13 and MTMR2 constructs developed for use in SC-DRG co-cultures. (A) Key for relevant protein domains. **(B)** EGFP tagged MTMR2, MTMR13 truncated mutants, and constitutively active Rab21 prepared for lentivirus delivery in this work. Plasmids for EGFP-MTMR2 and EGFP-CA-Rab21 were developed by other members of the Robinson lab. **(D)** Illustrates four potential mutants. A catalytically inactivated MTMR2, a full length MTMR13 lacking the DENN domain (EGFP-Mtmr13-ΔDENN), a truncated MTMR13 containing only the PI membrane localization PH domain and coiled-coil domain, and a truncated MTMR13 mutant missing the coiled-coil and C-terminus PH domain.

Figure 3.2 — Exogenous expression of MTMR13-DENN does not impact myelin outfoldings

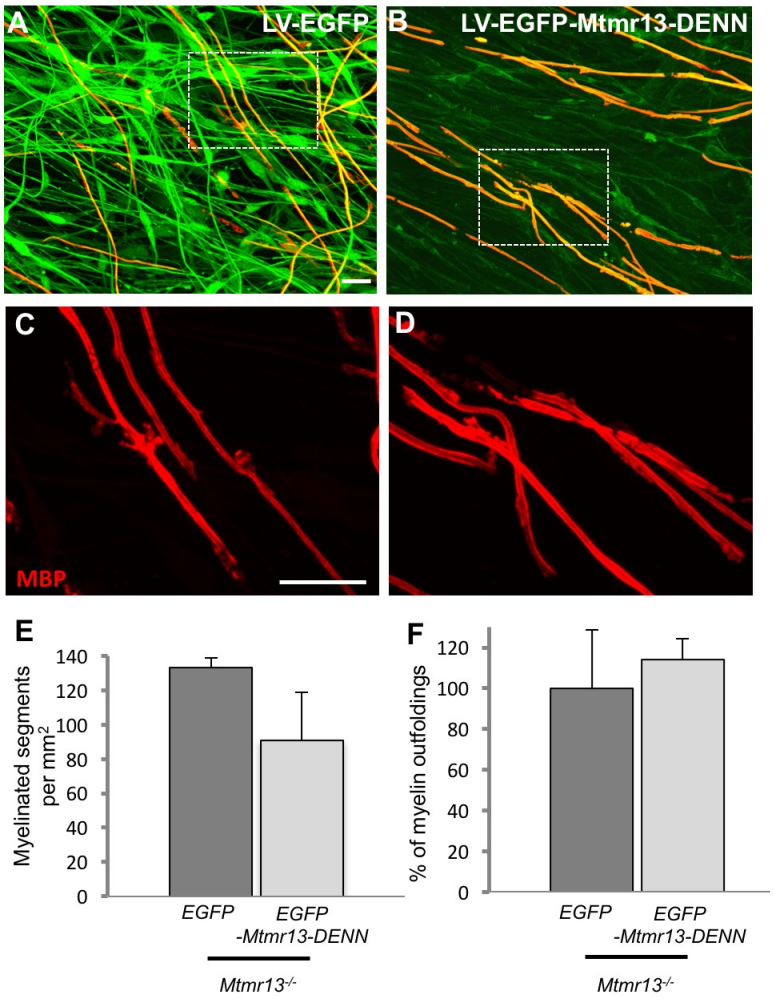

Figure 3.2 - Exogenous expression of MTMR13-DENN does not myelin outfoldings. SC DRG co-cultures were transduced with either LV-EGFP at an MOI of 15 or LV-EGFP-Mtmr13-DENN-1-509 at an MOI of 30. Despite low protein expression per cell, at an MOI of 30, >90% of cells were infected by LV-EGFP-Mtmr13-DENN-1-509 virus. After 21 DIV, coverslips were fixed and immunostained for MBP. **(A, B)** show representative fields of GFP and MBP in LV-EGFP **(A)** and LV-EGFP-MTMR13-DENN-1-509 **(B)** treated coverslips.

Figure 3.2 - Exogenous expression of MTMR13-DENN does not impact myelin outfoldings, continued. (C, D) are detail images from the MBP channel showing myelin outfoldings. **(E)** Quantifies the number of segments per mm^2 between EGFP and EGFP-Mtmr13-DENN-1-509, no significant change was observed ($p = 0.565$) **(F)** shows the quantification of the fraction of segments containing outfoldings, again no significant change was observed $p = 0.408$ between cultures that recieved EGFP and EGFP-Mtmr13-DENN-1-509. For **(E, F)** EGFP n = 2 coverslips, EGFP-Mtmr13-DENN-1-509 n=5 coverslips. Data presented as mean with SEM. Scale bar = 20 μm **(C, D).**

Figure 3.3 — Expression of Mtmr13 DENN domain plus two FYVE domains in SC DRG co-cultures

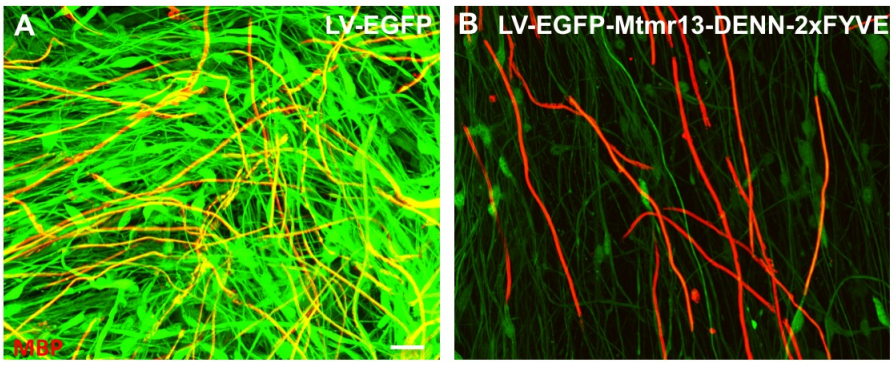

Figure 3.3 – Expression of Mtmr13 DENN domain plus two FYVE in SC DRG co-cultures. SC DRG co-cultures were transduced with either LV-EGFP at an MOI of 15 or LV-EGFP-Mtmr13-DENN-1-509-2xFYVE at an MOI of 15. The low titre of the virus made a attempting a higher MOI impractical, as it would result in concentrated virus as 20% of the cell culture media. **(A)** At an MOI of 15, >90% of EGFP infected cells exhibit GFP. **(B)** However, at an MOI of 15, only 30% of cells exhibited LV-EGFP-Mtmr13-DENN-2xFYVE. Scale bar = 20 μm.

Figure 3.4 — Expression of constitutively active Rab21 GTP-ase in Mtmr13$^{-/-}$ cultures reduces segments that contain outfoldings.

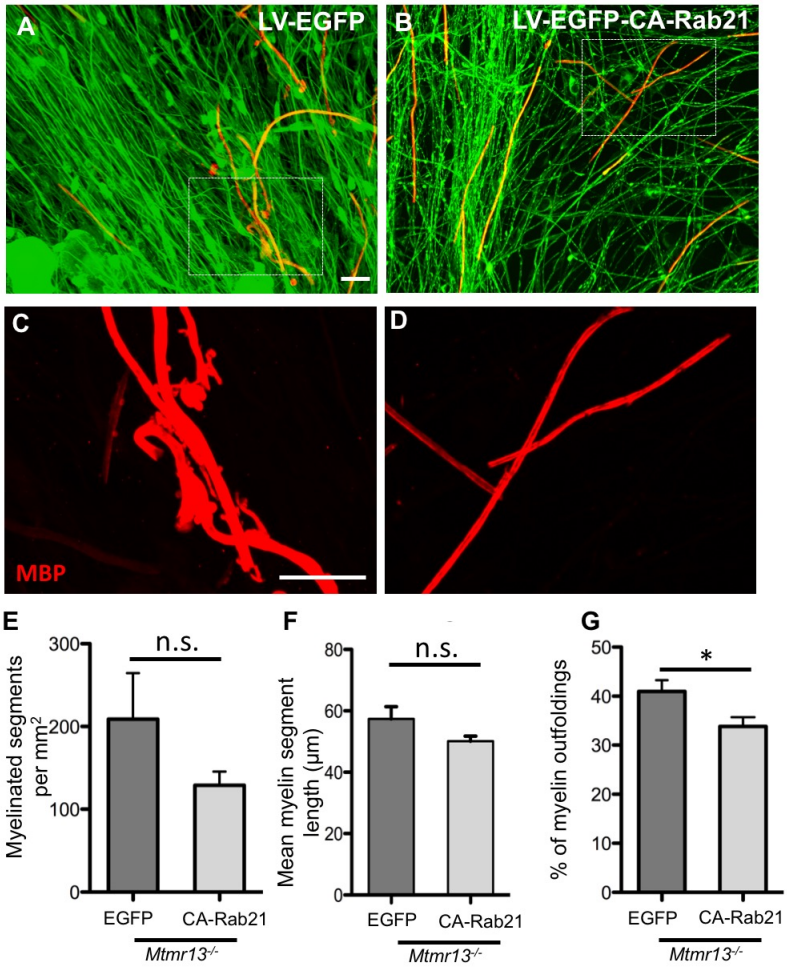

Figure 3.4 - **Expression of constitutively active Rab21 in *Mtmr13*$^{-/-}$ cultures reduces segments that contain outfoldings.**. SC DRG co-cultures were transduced with either LV-EGFP at an MOI of 15 or LV-EGFP-CA-Rab21 at an MOI of 15. >90% of cells were infected by both virus'. After 21 DIV, coverslips were fixed and immunostained for MBP. **(A, B)** show representative fields of GFP and MBP in LV-EGFP **(A)** and LV-EGFP-CA-Rab21 **(B)** treated coverslips. **(C, D)** are detail images from the MBP channel showing myelin segments.

Figure 3.4 - E**xpression of constitutively active Rab21 in *Mtmr13*$^{-/-}$ cultures reduces segments that contain outfoldings., continued. (E)** Quantifies the number of segments per mm^2 between EGFP and EGFP-CA-Rab21, no significant change was observed ($p = 0.208$) **(F)** shows quantification of segments lengths across four coverslips ($p = 0.136$) **(G)** shows the quantification of the fraction of segments containing outfoldings, a 20% reduction in the fraction of segments containing outfoldings was observed, ($^*p = 0.043$) cultures that recieved EGFP and EGFP-Mtmr13-DENN-1-509. For **(E, G)** EGFP n = 5 coverslips, EGFP-CA-Rab21 n=5 coverslips. Scale bar = 20 μm **(A-D).** All data shown as mean with SEM, comparisons were done using Student's t-test.

Figure S3.1 — Full length MTMR13 expresses via transfection but fails to express via lentivirus transduction

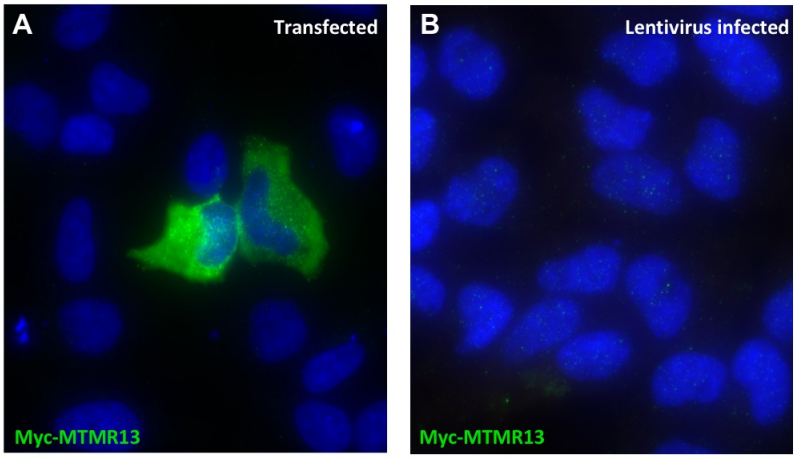

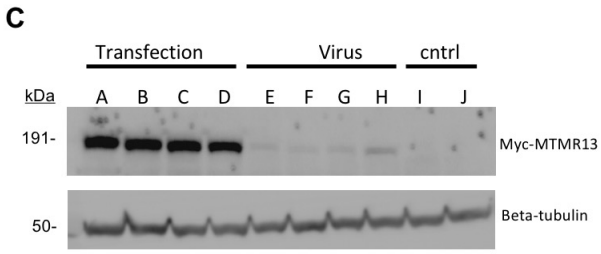

Figure S3.1: Full length MTMR13 expresses via transfection but fails to express via lentivirus transduction. 293-Dix cells were induced to express full length Myc-MTMR13, in and out of the LVPG vector, via XtremeGene transfection or viral infection with transduction boosters polybrene or PAS. Cells were fixed and immunostained for Myc or lysed and immunoblotted for Myc. **(A)** shows a representative image of Myc-MTMR13 where Myc+ cells are visible. **(B)** shows a representative image of lentivirus transduced Myc-MTMR13, no Myc+ cells were found. **(C)** Immunoblotting for Myc yielded robust bands where Myc-MTMR13 was transfected, regardless of the presence of absence of the LVPG vector. Low levels of Myc were detectable in the lentivirus transduced lanes. Lane identification: **A.** n-myc-R13 (xtremegene transfected) **B**. n-myc-R13 (xtremegene transfected) **C.** LVPG-myc-R13 (xtremegene transfected) **D.** LVPG-myc-R13 (xtremegene transfected) **E.** 25ul LVPG-myc-R13 virus +polybrene **F.** 25ul LVPG-myc-R13 virus +PAS **G.** 50ul LVPG-myc-R13 virus +polybrene **H.** 50ul LVPG-myc-R13 virus +PAS **I.** un-altered control

Figure S3.2 — EGFP-2xFYVE expresses robustly via lentivirus mediated transduction

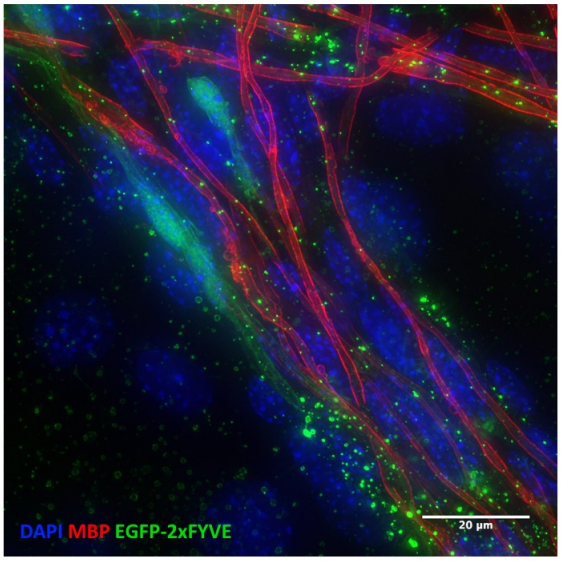

Figure S3.2 — EGFP-2xFYVE expresses robustly via lentivirus mediated transduction. SC DRG co-cultures infected with LV-EGFP-2xFYVE expressed GFP localized to cytoplasmic puncta and occasional diffuse cytoplasmic GFP was also observed. Importantly, no qualitative impact on myelination was observed.

Figure S3.3 - Virally mediated expression of GFP-tagged proteins in SC DRG co-culture.

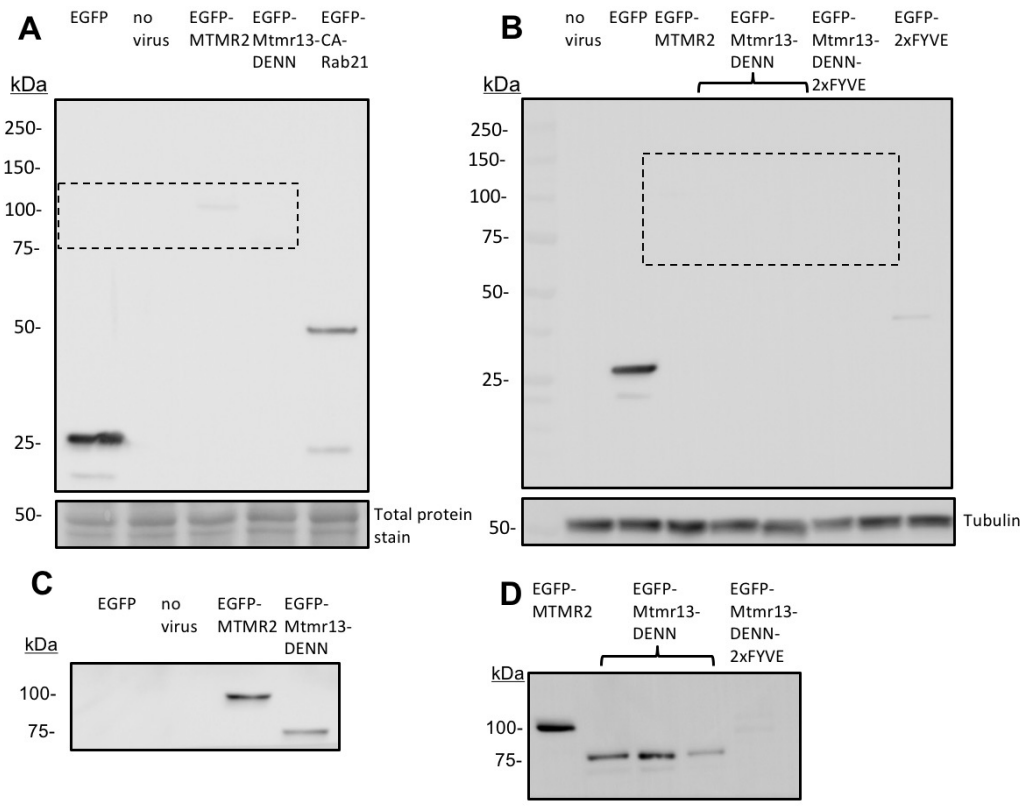

Figure S3.3 - Virally mediated expression of GFP-tagged proteins in co-culture. SC DRG co-cultures infected with various lentivirus'. All lanes are *Mtmr13*$^{-/-}$ immunoblotted for EGFP, **(A,B)** use the lower sensitivity "pico" **(C,D)** use high sensitivity "femto" to develop the blot. **(A)** shows a Memcode total protein loading control, while **(B)** was stripped and reblotted for tubulin. Relative expression of EGFP control to EGFP-MTMR2, CA-Rab21, and EGFP-Mtmr13-DENN1-509 are seen in **(A,C), (B,D)** show the poor expression of EGFP-Mtmr13-DENN-1-509-2xFYVE relative to several replicate samples of EGFP-MTMR13-DENN-1-509, EGFP-MTMR2, and EGFP-2xFYVE.

Figure S3.4 — Constitutively active Rab21 does not induce myelin abnormalities in wild type co-cultures

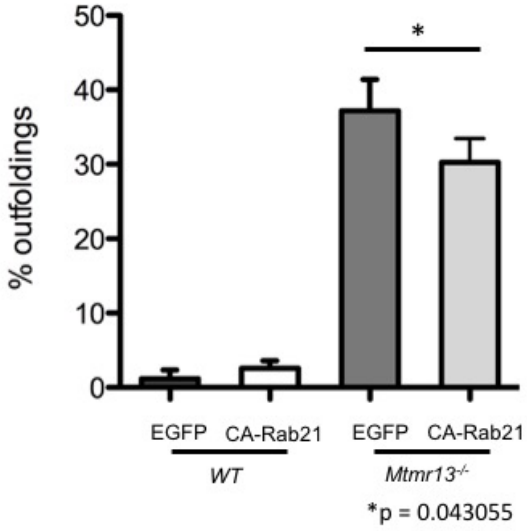

Figure S3.4 — Constitutively active Rab21 does not impact the frequency of myelin outfoldings in wild type SC DRG co-cultures. WT +EGFP n = 2 coverslips, WT +EGFP-CA-Rab21 n = 3 coverslips. *Mtmr13*$^{-/-}$ +EGFP n = 5 coverslips *Mtmr13*$^{-/-}$ +EGFP-CA-Rab21, n = 5 coverslips. Data shown as mean with SEM.

Chapter 4 — Discussion and Future Directions

4.1 — Summary and Discussion

Our understanding of the mechanisms behind inherited peripheral neuropathies has grown significantly in the last 15 years due to advances both next generation sequencing to enable identification of disease causing mutations in humans, and advances in genetic knockout strategies that facilitate *in vivo* and *in vitro* modeling of these conditions (Bolino et al., 2004; Robinson et al., 2008; Bolis et al., 2009; Timmerman et al., 2014; Vaccari et al., 2015). To date, however, therapies that have advanced to clinical trials have failed to make meaningful impacts on disease progression and patient quality of life (Gess et al., 2015). CMT4B2 is a rare from of CMT caused loss of function mutations impacting *MTMR13* gene. The Robinson lab has created a knockout mouse model (*Mtmr13*$^{-/-}$) of the disease that recapitulates the myelin dysfunction observed in patients, characterized by myelin outfoldings (Robinson et al., 2008). The Robinson lab used this mouse, along with *in vitro* experiments in cell lines, to produce a body of work that begins to explain the role of has informed the MTMR13 in SCs.

MTMR13 is found in cytosolic and membrane compartments where it complexes with the active phosphatase MTMR2 via coiled-coil interactions, and MTMR13's noncatalytic pesudophosphatase is involved in membrane association (Robinson and Dixon, 2005). In the sciatic nerve, levels of Mtmr13 and Mtmr2 are reduced when the other is knocked out, supporting the idea of reciprocal stabilization (Ng et al., 2013). Despite the clear cellular defects that result from knockout of Mtmr13, AKT and ERK1/2 levels remain normal. Early endosomal EEA1 and lysomal Lamp-1 immunostaining were also shown to be grossly normal in cultures cultures of nonmyelinating SCs (Ng et al., 2013). These studies have

clarified aspects of MTMR13's role in SCs, but also raise major questions about the disease mechanism of CMT4B2.

In order to approach the function of this enigmatic pseudophosphatase, I have worked to further develop an *in vitro* myelinating SC DRG co-culture system using cells from *Mtmr13*$^{-/-}$ mice. I have validated this model by showing no significant difference in myelin segment density between wild type and *Mtmr13*$^{-/-}$ SC DRG co-cultures, see Figure 2.1, and by showing that the myelin outfolding phenotype is replicated in *Mtmr13*$^{-/-}$ SC DRG co-cultures, see Figure 2.2. By manipulating gene expression in this system with lentivirus, I have partially rescued myelin outfoldings in the *Mtmr13*$^{-/-}$ SC DRG co-cultures with exogenous expression of EGFP-MTMR2 and EGFP-CA-Rab21. Neither of these rescues is a complete, but both point to aspects of MTMR13 function that bear further study.

Partial rescue of *Mtmr13*$^{-/-}$ outfoldings by MTMR2 implies that loss of endogenous Mtmr2 is a factor in the formation of *Mtmr13*$^{-/-}$ outfoldings. Reestablishing MTMR2 above wild type levels could affect myelin outfoldings either through altering PI3P levels or a noncatalytic mechanism. This ambiguity can be addressed by through two approaches. First, measuring the PI3P levels to confirm catalytic activity is key. To do this, further developing a lipid assay for the SC DRG co-culture system is required. Initial attempts to measure PI3P lipids at the conclusion of the experiment (21 days *in vitro*) were resulted in ambiguous data. Exogenous MTMR2 should act to deplete the PI3P in the cell. If this phosphatase activity is key to the reduction in outfoldings in *Mtmr13*$^{-/-}$cultures infected with LV-EGFP-MTMR2, then depleted PI3P should be measurable. Work to refine the lipid extraction protocol and identify the best time to read out the impact of MTMR2 will enable this approach. The second approach is to work with a catalytically dead version of MTMR2. If PI3P

phosphatase activity is the mechanism by which exogenous MTMR2 impacts *Mtmr13*$^{-/-}$ then a catlytically dead version of MTMR2 will have no impact on the *Mtmr13*$^{-/-}$ outfoldings. However, if MTMR2's physical association with DLG1, for example, is critical to myelination in *Mtmr13*$^{-/-}$, then adding exogenous cataytically dead MTMR2 to the system should result in a similar rescue of myelin outfoldings in *Mtmr13*$^{-/-}$ SC DRG co-cultures. These experiments will address loose ends and put the idea of partial rescue of *Mtmr13*$^{-/-}$ outfoldings by MTMR2 into a mechanistic context.

The reduction in myelin outfoldings initiated by exogenous MTMR2 reported in Chapter 2 underscores the importance of the full length MTMR13 in myelination. MTMR13 likely has a role beyond stabilizing or supporting levels of MTMR2. The partial rescue of *Mtmr13*$^{-/-}$ myelin outfoldings with the addition of exogenous CA-Rab21 implies a role for MTMR13 beyond membrane PI homeostasis. As the MTMR13 *Drosphila* homolog Sbf was recently shown to act as a Rab21 GEF with a role in both membrane remodeling and autophagy, it is possible that MTMR13 is also a GEF for Rab21 in SCa (Jean and Kiger, 2012; Jean et al., 2012; 2015). I tested CA-Rab21 in the SC DRG co-culture system and found that it reduced the fraction of segments containing outfoldings. This result is promising, however, key parts of the mechanism need to be clarified.

As we are lacking SC-specific evidence for MTMR13 GEF activity or Rab21, developing basic interaction and activational data is key to the next phase of this project. The work of Kiger's group shows that SbF associates with and activates Rab21, however complex conditions (starvation) and specialized cell types (macrophages, fly larval fat bodies) are used in parts of this work (Jean et al., 2012; 2015). Specifically, in 2012 Jean et al. found that Sbf acted as a GEF for Rab21 as well as recruited and stabilized the fly MTMR2 homolog Mtm

to the endosome. They found that Sbf regulates both class II PI 3-kinase activity and active Mtm PI hydrolysis at the early endosome, and knockdown of Rab21 or Sbf yielded a reduction in actin-positive macrophage protrusions, indicating involvement in membrane remodeling (Jean et al., 2012). Sbf's Rab21 activation regulation of PI membrane identity and drives membrane exit from the endosome and pushes membrane towards recycling via Rab11 to the plasma membrane. Finally, Jean et al. posit that this drives structural actin remodeling at the membrane (Jean and Kiger, 2012; Jean et al., 2012). In 2015, Jean et al. described that starvation conditions promoted the MTMR13/Sbf and Rab21 interaction in human cell lines (and fly larval fat bodies). This work was partially done in human cell lines, where they found MTMR13 acted as a GEF for Rab21 in specific starvation conditions, linking a specialized metabolic state and autophagic processes to endosomal regulation of membrane by MTMR13 (Jean et al., 2015). They found that starvation stimulated Rab21 activation and association with VAMP8 (critical for autophagosome-lysosome fusion), and that this pathway was dependent on MTMR13. It is unclear whether this mechanism is generalizable to SCs. It is possible that SCs enter a stressed, starvation-like state during myelination. Jang et al. reported that knocking down Atg7 in SCs yields an autophagy defect that manifests as abnormally large cytoplasm, linking cytoplasmic autophagy to normal SC development (Jang et al., 2015). An important line of inquiry in the future will be to assess whether MTMR13 acts as a Rab21 GEF in SCs, and whether there is a timepoint in myelination where this activity is critical for myelin sheath formation.

Full length MTMR13 was not usable in this system due to low lentivirus titre, so I attempted to address the function of MTMR13's DENN domain with EGFP tagged DENN domain constructs, with and without PI3P binding 2xFYVE additions to ensure localization. While MTMR13's DENN domain may indeed act as a GEF, in my hands, I saw no evidence

that exogenous expression of DENN constructs impacted myelination in SC DRG co-cultures. Though Lv-MTMR13-DENN-1-509 did not appear to impact myelin outfoldings or myelination, this plasmid may be useful for future experiments designed to assess the role of the DENN domain. Although MTMR13-DENN-1-509-2xFYVE was not usable in this system, it may also be useful in the future. If the DENN domain is shown to have GEF activity, MTMR13-DENN-1-509-2xFYVE could be used to assess whether this activity increased when localized to PI3P-rich membranes. As discussed in Chapter 3, several other version of truncated MTMR13 are good candidates for expression in the SC DRG co-culture system.

4.1.3 — Future Directions for Investigation

This work raises questions about the cellular mechanisms behind the formation of myelin outfoldings in *Mtmr13*$^{-/-}$ mice. In some ways, it is more straightforward when SCs suffer a mutation causing a loss of function and, for example, fail to differentiate or fail to myelinate. In the case of CMT4B2, however, the loss of function mutation results in a rather elaborate morphological phenotype, suggesting that a stop signal is inactivated somewhere. The SC DRG co-culture system represents one avenue of approach to understand this disease phenotype. The use of biochemical approaches to clarify critical associations at the protein level will inform the future use of the SC DRG system. In particular, experiments to investigate the potential GEF activity and Rab association of MTMR13's DENN domain are a priority.

If the work of Kiger's group translates to SCs, identifying the time in development at which myelinating SCs enter a starvation-like state will be critical to observing MTMR13 DENN Rab21 GEF activity and/or the interaction between the DENN domain and Rab21.

There may also be other Rabs in play. Yoshimura et al. characterized the Rab GEF activity of multiple DENN domain containing proteins. Via GDP release assay, Yoshimura et al. and found a strong specificity of MTMR13 and MTMR5 for Rab28 (Yoshimura et al., 2010). Jean et al.'s work showed Rab28 knockdown in human cells did impact the number of LC3/Atg8-positive autophagosomes. But while Rab21 and MTMR13 knockdown increased the number of LC3/Atg8-positive autophagosomes, Rab28 or VARP (a Rab21 GEF) knockdown decreased them (Zhang et al., 2006; Jean et al., 2015). These results support the idea that Rab21 and MTMR13 play a role in autophagy, but do not exclude Rab28 from enodsomal activation by MTMR13.

Myelin outfoldings are redundant loops of compact myelin. Their elaborate morphology, see Figure 2.2 and 2.3, implies that proteins critical to myelin compaction mechanisms and are not majorly disrupted by the loss of MTMR13. However, the volume of membrane and/or the initial outlay of membrane that is later wrapped and compacted may be dysregulated, or regions of cytoplasm and membrane normally disposed of via autophagy are left behind. At an essential level, this does not conflict with mechanisms developed by Kiger's group. If myelinating SCs enter a critical state during development where membrane and cytoplasm are remodeled via MTMR13 and Rab21 dependent autophagic processes, then dysregulation via loss of MTMR13 could be linked directly to altered membrane structure.

Indeed, cytoskeletal regulation has long been regarded as critical for SC myelination as SCs need to initiate major cell shape changes to wrap axons (Fernandez-Valle et al., 1997; Pereira et al., 2012). Actin polymerization is critical to normal radial sorting and myelination (Montani et al., 2014). Upregulation of actin cytoskeletal regulator N-WASp at the initiation of myelination has been observed, along with myelin defects in with N-WASp knockouts

animals (Jin et al., 2011). Actin polymerization and depolymerization have both been shown to be critical in myelination. Nawaz et al. recently showed that oligodendrocyte myelination is driven by the ADF/cofilin initiated depolymerization of filamentous actin (f-actin) at the inner tongue (Nawaz et al., 2015). While the work of Zuchero et al., which showed that myelin initiation - but not myelin wrapping - depends on actin polymerization regulator Arp2/3 (Zuchero et al., 2015). The activity and localization of actin regulator Arp2/3 has been shown to respond to PI availability in *Drosphila* myoblasts (Bothe et al., 2014). Impaired Arp2/3 regulation of f-actin polymerization can also lead to myelin abnormalities, including myelin outfoldings. Conditional knockdown of Arp2/3 in SCs lead to the formation of oligodendrocyte myelin sheath outfoldings, though at relatively low frequency (Zuchero et al., 2015). This deeper understanding of actin regulation extends the model put forth by Snaidero et al. wherein myelination proceeds via the inner tongue and is dependent on actin regulation and PI levels (specifically, $PI(3,4,5P)_3$ in oligodendrocytes) (Snaidero et al., 2014b). What role myotubularins may play in regulating actin networks in SCs is an open area of study.

4.1.4 — Concluding Remarks

The work presented in this dissertation laws the groundwork for future studies using the SC DRG co-culture system to dissect the function of MTMR13. I have established a robust method to culture, manipulate genes via viral transduction, and collect data from SC DRG co-cultures. I have determined that both exogenous MTMR2 and constitutively active Rab21 impact the frequency *Mtmr13*$^{-/-}$ myelin outfoldings. These results will inform the direction of future work in the lab. I have also determined that MTMR13's DENN domain does not impact myelination, but the tools created for these experiment may be repurposed in the lab

for future study of MTMR13's DENN domain. The work presented here adds to the understanding of the molecular basis of CMT, and puts forth a new *in vitro* model with which to study CMT4B2.

Appendix

I. Detailed protocol: Myelinating explant cultures from dorsal root ganglia

Wild type (C57BL/6) or *Mtmr13*$^{-/-}$ female mice (N8 on C57BL/6) were bred to males of their same genotype, respectively. At 13.5 days of gestation, pregnant females were deeply anesthetized with isoflurane and quickly euthanized by cervical dislocation. Embryonic day 13.5 (E13.5) embryos were removed and placed in Dulbecco's phosphate buffered saline (DPBS; Life Technologies 14040-133) on ice. Each litter of embryos was held in DPBS on ice while awaiting dissection. To isolate E13.5 dorsal root ganglia (DRG), embryos were removed from DPBS and placed for gross dissection in 37°C Leibovitz's L-15 medium (Life Technologies 11415-064) containing 10% fetal bovine serum (FBS) and 0.5% penicillin-streptomycin (P-S; 50 units/mL of penicillin; 50 μg/mL of streptomycin) (L-15+FBS+P-S). Once the trunk of the embryo was isolated, it was transferred to a new dish, containing fresh 37°C L-15+FBS+P-S, for final spinal cord isolation.

The spinal cord with attached DRG was dissected from the vertebral column in 37°C L-15 media (10% FBS and 0.5% P-S). The spinal cord was transferred to fresh 37°C L-15 medium (L-15+FBS+P-S), in a Sylgard-184®-lined Petri dish and DRG were individually plucked off with Dumont #5 forceps (Fine Science Tools, Biology Tips/Straight/Inox/11 cm; catalog #11254-20). Great care was taken to collect only the DRG and avoid any contaminating spinal cord tissue.

DRG were then removed from the dissection dish and transferred, using a 200 μL micropipette tip, to a 14 mL conical tube containing 7 mL of L-15+FBS+P-S. This conical tube was held in a 37°C water bath in between dissection of embryos. All of the DRG dissected from the embryos of a given pregnant female were pooled in a single conical tube. Embryos from different females of the same genotype were kept separate.

When the dissections were complete, the volume was adjusted to 14 mL with L-15+FBS+P-S in a biological safety cabinet. DRG were allowed to settle in the conical tube for 10-20 minutes in a 37°C in water bath. All subsequent procedures were carried out in a biological safety cabinet with all media warmed to 37°C. The media was carefully removed and DRG were washed with 14 mL of L-15 medium lacking serum and P-S. DRG were again allowed to settle for 10 minutes in a 37°C water bath.

The L15 medium was replaced with 5 mL of Trypsin-EDTA (0.25%; Invitrogen; 25200-056) and the DRG were incubated in a 37°C water bath for 45 minutes. Five mL of L-15+FBS+P-S was added and DRG were pelleted by centrifugation for 30 seconds at 1000 rpm (170 x *g* in Model 236 rotor). The trypsin-containing medium was removed and the DRG were washed with 10 mL of 37°C L-15+FBS+P-S. DRG were centrifuged at 170 x *g* for 10 min. The L-15 media was removed and replaced with 2-3 mL of pre-warmed (37°C) M1 medium (Modified Eagles Medium [MEM]; Life Technologies 11095-080; 4.3 g/L D-glucose; 10% FBS) containing mouse nerve growth factor (NGF 2.5S Native Mouse Protein; Life Technologies 13257-019) at 10 ng/mL.

DRG were triturated by aggressively pipetting up and down about 10 times using a 200 μL micropipette. Triturated isolates were centrifuged for 5 minutes at 170 x *g* and subsequently resuspended in 1 mL of M1-NGF medium. Cells were counted using a hemocytometer. Dissociated DRG were plated at density of 130,000 total cells per well by

placing a 160 μL drop of the cell suspension in the center of a 25 mm circular coverslip (thickness #1.5 [0.16 to 0.19 mm]; Fisher catalog # 25CIR1.5D600) that had been coated with a solution of rat tail collagen (0.5 mg/mL). Using a fine pipette tip on a 20 μL micropipette, 3 bubbles were introduced at the center of the drop of suspended cells (to encourage the cells to adhere in the center of the coverslip). Cultures were incubated overnight at 37°C in 5% CO_2.

Culturing of DRG explants, days 1-21

The day on which embryos were dissected was designated as Day 0.

Day 1: 1 mL of M1-NGF medium (pre-warmed to 37°C) was added to each well of explant culture.

Day 3: Explants all received media changes with 2 mL of M1-NGF medium (pre-warmed to 37°C). M1 media was changed every other day until day 8 for explants that did not receive virus. On day 3, clusters of neurons should be visible in the center of each culture explant.

Day 5: The media was changed again 2 mL of M1-NGF medium (pre-warmed to 37°C). If virus is added, it is added to the M1-NGF medium on this day.

Day 6: No change if virus was not added on day 5. If virus was added, after a 24-hour incubation with virus, virus-containing media was removed, cells were gently washed 2X with C medium (10 ng/mL NGF; no AA), then 2 mL of C-medium (10 ng/mL NGF; no AA) was added to each well. The SC DRG co-cultures were left alone until day 8, when the media was exchanged for 2 mL of C-medium with ascorbic acid (10 ng/mL NGF; 50μg/mL Ascorbic Acid). Media was then changed every two days and cultures were fixed on day 21.

Day 7: If virus was not added on Day 5, the media was changed again 2 mL of M1-NGF medium (pre-warmed to 37°C).

Day 8: The medium was removed and replaced with pre-warmed C-medium containing 50 μg/mL ascorbic acid (Sigma 255564-5G; protect from light at RT) to promote myelination. Ascorbic acid was freshly dissolved for each media change in distilled deionized water at 100 mg/mL and sterilized by passing though a sterile 22 μm filter (Millipore, SLGP033RB), prior its addition to C-media.

Day 8-21: The culture medium was replaced with fresh C-medium (with NGF and ascorbic acid) every two days.

Day 21: Fix cells on day 21 (total of 14 days in C-media+AA+NGF).

On day 21, DRG cultures were fixed in 4% paraformaldehyde (PFA) in PBS (pH 7.4) for 15 min at room temperature on a rocking platform. Fixed cultures were washed three times with 1x PBS and subsequently permeabilized in ice-cold methanol for exactly 5 min on ice. After washing once with 1x PBS, cultures were blocked for 1 hour in 1x PBS containing 10% normal goat serum (NGS). Fixed cells were covered with a solution of PBS with 0.1% Tween-20 (PBST), which contained 2% NGS and appropriately diluted primary antibodies, and subsequently incubated overnight at 4°C on a rocking platform. For MPB staining, Rat anti-MBP was used at 1:250 (MBP Antibody Rat, Millipore, MAB386) and Chicken anti-NFH was used at 1:10,000 (NF-H Neurofilament Chicken Abcam AB4680). After overnight incubation, cultures were washed three times with 1x PBST (10 min each).

Fluorescent secondary antibodies (Jackson ImmunoResearch) were diluted 1:500 in 1X PBST containing 2% NGS and applied to cultures. Cultures were then incubated for 1

hour at room temperature (protected from light) on a rocking platform. For typical myelin basic protein (MBP) staining, Cy3 anti-Rat was used at 1:1000 to stain MBP (Cy3 Goat anti-Rat H+L Jackson IR 112-165-143, stock solution at 1.4mg/mL). Alexa Fluor 647-Goat Anti-Chicken IgY (Jackson IR 103-605-155, stock solution at 1.5mg/mL) secondary antibody was typically used to detect anti-neurofilament heavy chain (NF-H) chicken IgY antibodies. This strategy reserved the green (488/GFP) channel for green fluorescent protein (GFP) or a myc or FLAG tag with an organic dye secondary with excitation at 488 nm.

After incubation with secondary antibodies, the cultures were washed three times with 1x PBST (10 min per wash) at room temperature on the rocker. Cell nuclei were labeled with 4',6-diamidino-2-phenylindole (DAPI), via a one minute room temperature incubation in 0.36 μM final DAPI (Molecular Probes D-21490; 14.3 mM stock in deionized water (dH2O) diluted 1:40,000 in PBST).

Cultures were next washed twice for 5 minutes with 1x PBST. During this time, 1 mL aliquots of Elvanol were defrosted and heated to 65°C. To mount on slides ColorFrost Plus microscope slides (Thermo, 9951APLUS-006), a coverslip was carefully removed from the 6 well plate, rinsed once by dipping in distilled deionized water, and carefully blotted at the edge with a Kimwipe to remove excess water. Fifty μL of Elvanol was placed on the slide, the left edge of the coverslip was landed in the Elvanol drop and the right edge was slowly lowered down. Slides mounted in Elvanol were stored at 4°C and were allowed to set overnight at 4°C before imaging.

II. Infusion cloning primer sequences

DRO-011	ATGGACGAGCTGTACAAGCAAGGACAAGGATCTATGGCCCGGCTGGCtGAC
DRO-012	GGGGATATACGGGTAACTGTACTTCAGAGG
DRO-013	TACCCGTATATCCCCATTCTTCCGG
DRO-015	GAGGTTGATTGTCGACTCAAAGATTTTCCTGTATTAGTTCTTGAACCCG
DRO-016	CTGAGTCCGGCCGGAAAGATTTTCCTGTATTAGTTCTTGAACCCGGGC
DRO-017	ATACAGGAAAATCTTTCCGGCCGGACTCAGATC
DRO-018	ATCCAGAGGTTGATTGTCGACGGTACCGTCGACTTATGC

Table 1. Automated sample processing for Electron Microscopy

The following table lists the microwave settings used to postfix, dehydrate, and embed samples in resin to prepare them for ultrathin sectioning. This protocol was developed by Bob Kayton PhD and Lisa Veccarelli and is included so that this work can be reproduced.

STEP#	Description	Time (min:sec)	Power (W)	Temp (°C)	Vacuum
1	CACODYLATE RINSE	00:40	150	60	ON
2	CACODYLATE RINSE	00:40	150	60	ON
3	OSMIUM (Wattage ON)	03:00	100	60	ON
4	OSMIUM (Wattage OFF)	02:00	0	60	ON
5	OSMIUM (Wattage ON)	03:00	100	60	ON
6	OSMIUM (Wattage OFF)	02:00	0	60	ON
7	OSMIUM (Wattage ON)	03:00	100	60	ON
8	dH20 RINSE	00:40	150	60	ON
9	dH20 RINSE	00:40	150	60	ON
10	UA	02:00	100	60	ON
11	UA	02:00	0	60	ON
12	UA	02:00	100	60	ON
13	50% ETOH	00:40	150	60	OFF
14	75% ETOH	00:40	150	60	OFF
15	95% ETOH	00:40	150	60	OFF
16	100% ETOH	00:40	150	60	OFF
17	100% ETOH	00:40	150	60	OFF
18	PROPYLENE OXIDE (PO)	00:40	150	60	ON
19	1:1 PO/RESIN	03:00	150	60	ON
20	100% RESIN	03:00	150	60	ON
21	100% RESIN	03:00	150	60	ON
22	100% RESIN	03:00	150	60	ON
23	100% RESIN	03:00	350	60	ON

References

Aggarwal S, Snaidero N, Pähler G, Frey S, Sánchez P, Zweckstetter M, Janshoff A, Schneider A, Weil M-T, Schaap IAT, Görlich D, Simons M. 2013. Myelin membrane assembly is driven by a phase transition of myelin basic proteins into a cohesive protein meshwork. PLoS Biol 11:e1001577.

Aggarwal S, Yurlova L, Snaidero N, Reetz C, Frey S, Zimmermann J, Pähler G, Janshoff A, Friedrichs J, Müller DJ, Goebel C, Simons M. 2011. A Size Barrier Limits Protein Diffusion at the Cell Surface to Generate Lipid-Rich Myelin-Membrane Sheets. Developmental Cell 21:445–456.

Agrawal PB, Joshi M, Marinakis NS, Schmitz-Abe K, Ciarlini PDSC, Sargent JC, Markianos K, De Girolami U, Chad DA, Beggs AH. 2014. Expanding the phenotype associated with the NEFL mutation: neuromuscular disease in a family with overlapping myopathic and neurogenic findings. JAMA Neurol 71:1413–1420.

Allaire PD, Marat AL, Dall'Armi C, Di Paolo G, McPherson PS, Ritter B. 2010. The Connecdenn DENN domain: a GEF for Rab35 mediating cargo-specific exit from early endosomes. Mol Cell 37:370–382.

Amici SA, Dunn WA, Murphy AJ, Adams NC, Gale NW, Valenzuela DM, Yancopoulos GD, Notterpek L. 2006. Peripheral myelin protein 22 is in complex with alpha6beta4 integrin, and its absence alters the Schwann cell basal lamina. Journal of Neuroscience 26:1179–1189.

Amoasii L, Hnia K, Laporte J. 2012. Myotubularin phosphoinositide phosphatases in human diseases. Curr Top Microbiol Immunol 362:209–233.

Arnaud E, Zenker J, de Preux Charles A-S, Stendel C, Roos A, Médard J-J, Tricaud N, Kleine H, Luscher B, Weis J, Suter U, Senderek J, Chrast R. 2009. SH3TC2/KIAA1985 protein is required for proper myelination and the integrity of the node of Ranvier in the peripheral nervous system. Proc Natl Acad Sci USA 106:17528–17533.

Ashwell KWS, Waite PME. 2012. Development of the Peripheral Nervous System. In: The Human Nervous System. Elsevier. p 14–30.

Attarian S, Vallat J-M, Magy L, Funalot B, Gonnaud P-M, Lacour A, Péréon Y, Dubourg O, Pouget J, Micallef J, Franques J, Lefebvre M-N, Ghorab K, Al-Moussawi M, Tiffreau V, Preudhomme M, Magot A, Leclair-Visonneau L, Stojkovic T, Bossi L, Lehert P, Gilbert W, Bertrand V, Mandel J, Milet A, Hajj R, Boudiaf L, Scart-Grès C, Nabirotchkin S, Guedj M, Chumakov I, Cohen D. 2014. An exploratory randomised double-blind and placebo-controlled phase 2 study of a combination of baclofen, naltrexone and sorbitol (PXT3003) in patients with Charcot-Marie-Tooth disease type 1A. Orphanet J Rare Dis 9:199.

Attarian S, Vallat J-M, Magy L, Funalot B, Gonnaud P-M, Lacour A, Péréon Y, Dubourg O, Pouget J, Micallef J, Franques J, Lefebvre M-N, Ghorab K, Al-Moussawi M, Tiffreau V, Preudhomme M, Magot A, Leclair-Visonneau L, Stojkovic T, Bossi L, Lehert P, Gilbert W, Bertrand V, Mandel J, Milet A, Hajj R, Boudiaf L, Scart-Grès C, Nabirotchkin S, Guedj M, Chumakov I, Cohen D. 2016. Erratum to: An exploratory randomised double-blind and placebo-controlled phase 2 study of a combination of baclofen, naltrexone and sorbitol (PXT3003) in patients with Charcot-Marie-Tooth disease type 1A. Orphanet J Rare Dis 11:92.

Awwad HO, Iyer V, Rosenfeld JL, Millman EE, Foster E, Moore RH, Knoll BJ. 2007. Inhibitors of

phosphoinositide 3-kinase cause defects in the postendocytic sorting of beta2-adrenergic receptors. Exp Cell Res 313:2586–2596.

Azzedine H, Bolino A, Taieb T, Birouk N, Di Duca M, Bouhouche A, Benamou S, Mrabet A, Hammadouche T, Chkili T, Gouider R, Ravazzolo R, Brice A, Laporte J, LeGuern E. 2003. Mutations in MTMR13, a New Pseudophosphatase Homologue of MTMR2 and Sbf1, in Two Families with an Autosomal Recessive Demyelinating Form of Charcot-Marie-Tooth Disease Associated with Early-Onset Glaucoma. The American Journal of Human Genetics 72:1141–1153.

Bakhti M, Aggarwal S, Simons M. 2014. Myelin architecture: zippering membranes tightly together. Cell Mol Life Sci 71:1265–1277.

Balla T. 2013. Phosphoinositides: tiny lipids with giant impact on cell regulation. Physiological Reviews 93:1019–1137.

Baumann N, Pham-Dinh D. 2001. Biology of Oligodendrocyte and Myelin in the Mammalian Central Nervous System. Physiological Reviews 81:871–927.

Beirowski B, Babetto E, Golden JP, Chen Y-J, Yang K, Gross RW, Patti GJ, Milbrandt J. 2014. Metabolic regulator LKB1 is crucial for Schwann cell–mediated axon maintenance. Nature Neuroscience 17:1351–1361.

Bensoussan L, Jouvion A, Kerzoncuf M, Delarque A, Theodoridou E, Milhe de Bovis V, Thefenne L, Attarian S, Viton J-M. 2016. Orthopaedic shoes along with physical therapy was effective in Charcot-Marie-Tooth patient over 10 years. Prosthet Orthot Int 40:636–642.

Berciano J, Sevilla T, Casasnovas C, Sivera R, Vílchez JJ, Infante J, Ramón C, Pelayo-Negro AL, Illa I. 2012. Guidelines for molecular diagnosis of Charcot-Marie-Tooth disease. Neurología (English Edition) 27:169–178.

Berger P, Niemann A, Suter U. 2006. Schwann cells and the pathogenesis of inherited motor and sensory neuropathies (Charcot-Marie-Tooth disease). Glia 54:243–257.

Berger P, Schaffitzel C, Berger I. 2003. Membrane association of myotubularin-related protein 2 is mediated by a pleckstrin homology-GRAM domain and a coiled-coil dimerization module.

Bitoun M, Durieux A-C, Prudhon B, Bevilacqua JA, Herledan A, Sakanyan V, Urtizberea A, Cartier L, Romero NB, Guicheney P. 2009. Dynamin 2 mutations associated with human diseases impair clathrin-mediated receptor endocytosis. Hum Mutat 30:1419–1427.

Blondeau F, Laporte J, Bodin S, Superti-Furga G, Payrastre B, Mandel JL. 2000. Myotubularin, a phosphatase deficient in myotubular myopathy, acts on phosphatidylinositol 3-kinase and phosphatidylinositol 3-phosphate pathway. Hum Mol Genet 9:2223–2229.

Blümer J, Rey J, Dehmelt L, Mazel T, Wu Y-W, Bastiaens P, Goody RS, Itzen A. 2013. RabGEFs are a major determinant for specific Rab membrane targeting. J Cell Biol 200:287–300.

Boggs JM. 2006. Myelin basic protein: a multifunctional protein. Cell Mol Life Sci 63:1945–1961.

Bolino A, Bolis A, Previtali SC, Dina G, Bussini S, Dati G, Amadio S, Del Carro U, Mruk DD, Feltri ML, Cheng CY, Quattrini A, Wrabetz L. 2004. Disruption of Mtmr2 produces CMT4B1-like

neuropathy with myelin outfolding and impaired spermatogenesis. Journal of Cell Biology 167:711–721.

Bolino A, Muglia M, Conforti FL, LeGuern E, Salih MA, Georgiou DM, Christodoulou K, Hausmanowa-Petrusewicz I, Mandich P, Schenone A, Gambardella A, Bono F, Quattrone A, Devoto M, Monaco AP. 2000. Charcot-Marie-Tooth type 4B is caused by mutations in the gene encoding myotubularin-related protein-2. Nature Genetics 25:17–19.

Bolis A, Coviello S, Bussini S, Dina G, Pardini C, Previtali SC, Malaguti M, Morana P, Del Carro U, Feltri ML, Quattrini A, Wrabetz L, Bolino A. 2005. Loss of Mtmr2 phosphatase in Schwann cells but not in motor neurons causes Charcot-Marie-Tooth type 4B1 neuropathy with myelin outfoldings. Journal of Neuroscience 25:8567–8577.

Bolis A, Coviello S, Visigalli I, Taveggia C, Bachi A, Chishti AH, Hanada T, Quattrini A, Previtali SC, Biffi A, Bolino A. 2009. Dlg1, Sec8, and Mtmr2 regulate membrane homeostasis in Schwann cell myelination. Journal of Neuroscience 29:8858–8870.

Bonifacino JS, Rojas R. 2006. Retrograde transport from endosomes to the : trans: -Golgi network : Abstract : Nature Reviews Molecular Cell Biology. Nat Rev Mol Cell Biol.

Bothe I, Deng S, Baylies M. 2014. PI(4,5)P2 regulates myoblast fusion through Arp2/3 regulator localization at the fusion site. Development 141:2289–2301.

Boullerne AI. 2016. The history of myelin. Exp Neurol 283:431–445.

Brady ST, Witt AS, Kirkpatrick LL, de Waegh SM, Readhead C, Tu PH, Lee VM. 1999. Formation of compact myelin is required for maturation of the axonal cytoskeleton. Journal of Neuroscience 19:7278–7288.

Bridges D, Ma J-T, Park S, Inoki K, Weisman LS, Saltiel AR. 2012. Phosphatidylinositol 3,5-bisphosphate plays a role in the activation and subcellular localization of mechanistic target of rapamycin 1. Mol Biol Cell 23:2955–2962.

Britsch S, Goerich DE, Riethmacher D, Peirano RI, Rossner M, Nave KA, Birchmeier C, Wegner M. 2001. The transcription factor Sox10 is a key regulator of peripheral glial development. Genes Dev 15:66–78.

Brooks AP, Emery AE. 1982. A family study of Charcot-Marie-Tooth disease. J Med Genet 19:88–93.

Buj-Bello A, Biancalana V, Moutou C, Laporte J, Mandel JL. 1999. Identification of novel mutations in the MTM1 gene causing severe and mild forms of X-linked myotubular myopathy. Hum Mutat 14:320–325.

BUNGE RP, BUNGE MB, Bates M. 1989. Movements of the Schwann cell nucleus implicate progression of the inner (axon-related) Schwann cell process during myelination. Journal of Cell Biology 109:273–284.

Buyse GM, Voit T, Schara U, Straathof CSM, D'Angelo MG, Bernert G, Cuisset J-M, Finkel RS, Goemans N, McDonald CM, Rummey C, Meier T, DELOS Study Group. 2015. Efficacy of idebenone on respiratory function in patients with Duchenne muscular dystrophy not using glucocorticoids (DELOS): a double-blind randomised placebo-controlled phase 3 trial. Lancet

385:1748–1757.

Cantley LC. 2002. The phosphoinositide 3-kinase pathway. Science 296:1655–1657.

Chen M, Wu J, Liang N, Tang L, Chen Y, Chen H, Wei W, Wei T, Huang H, Yi X, Qi M. 2014. Identification of a novel SBF2 frameshift mutation in charcot-marie-tooth disease type 4B2 using whole-exome sequencing. Genomics Proteomics Bioinformatics 12:221–227.

Ching W, Zanazzi G, Levinson SR, Salzer JL. 1999. Clustering of neuronal sodium channels requires contact with myelinating Schwann cells. J Neurocytol 28:295–301.

Chow CY, Zhang Y, Dowling JJ, Jin N, Adamska M, Shiga K, Szigeti K, Shy ME, Li J, Zhang X, Lupski JR, Weisman LS, Meisler MH. 2007. Mutation of FIG4 causes neurodegeneration in the pale tremor mouse and patients with CMT4J. Nature 448:68–72.

Chumakov I, Milet A, Cholet N, Primas G, Boucard A, Pereira Y, Graudens E, Mandel J, Laffaire J, Foucquier J, Glibert F, Bertrand V, Nave K-A, Sereda MW, Vial E, Guedj M, Hajj R, Nabirotchkin S, Cohen D. 2014. Polytherapy with a combination of three repurposed drugs (PXT3003) down-regulates Pmp22 over-expression and improves myelination, axonal and functional parameters in models of CMT1A neuropathy. Orphanet J Rare Dis 9:201.

Claramunt R, Pedrola L, Sevilla T, de Munain AL, Berciano J, Cuesta A, Sanchez-Navarro B, Millan JM, Saifi GM, Lupski JR, Vílchez JJ, Espinós C, Palau F. 2005. Genetics of Charcot-Marie-Tooth disease type 4A: mutations, inheritance, phenotypic variability, and founder effect.

Compston A, Coles A. 2002. Multiple sclerosis. Lancet 359:1221–1231.

Conforti FL, Muglia M, Mazzei R, Patitucci A, Valentino P, Magariello A, Sprovieri T, Bono F, Bergmann C, Gabriele AL, Peluso G, Nisticò R, Senderek J, Quattrone A. 2004a. A new SBF2 mutation in a family with recessive demyelinating Charcot-Marie-Tooth (CMT4B2). Neurology 63:1327–1328.

Conforti FL, Muglia M, Mazzei R, Patitucci A, Valentino P, Magariello A, Sprovieri T, Bono F, Bergmann C, Gabriele AL, Peluso G, Nisticò R, Senderek J, Quattrone A. 2004b. A new SBF2 mutation in a family with recessive demyelinating Charcot-Marie-Tooth (CMT4B2). Neurology 63:1327–1328.

Cornett KMD, Menezes MP, Bray P, Halaki M, Shy RR, Yum SW, Estilow T, Moroni I, Foscan M, Pagliano E, Pareyson D, Laurá M, Bhandari T, Muntoni F, Reilly MM, Finkel RS, Sowden J, Eichinger KJ, Herrmann DN, Shy ME, Burns J, Inherited Neuropathies Consortium. 2016. Phenotypic Variability of Childhood Charcot-Marie-Tooth Disease. JAMA Neurol 73:645–651.

Corrado L, Magri S, Bagarotti A, Carecchio M, Piscosquito G, Pareyson D, Varrasi C, Vecchio D, Zonta A, Cantello R, Taroni F, D'Alfonso S. 2016. A novel synonymous mutation in the MPZ gene causing an aberrant splicing pattern and Charcot-Marie-Tooth disease type 1b. Neuromuscul Disord 26:516–520.

Cotter L, Ozçelik M, Jacob C, Pereira JA, Locher V, Baumann R, Relvas JB, Suter U, Tricaud N. 2010. Dlg1-PTEN interaction regulates myelin thickness to prevent damaging peripheral nerve overmyelination. Science 328:1415–1418.

Court FA, Wrabetz L, Feltri ML. 2006. Basal lamina: Schwann cells wrap to the rhythm of space-

time. Curr Opin Neurobiol 16:501–507.

Dang H, Li Z, Skolnik EY, Fares H. 2004. Disease-related myotubularins function in endocytic traffic in Caenorhabditis elegans. Mol Biol Cell 15:189–196.

de Jonghe P, Timmerman V, Ceuterick C, Nelis E, De Vriendt E, Löfgren A, Vercruyssen A, Verellen C, Van Maldergem L, Martin JJ, Van Broeckhoven C. 1999. The Thr124Met mutation in the peripheral myelin protein zero (MPZ) gene is associated with a clinically distinct Charcot–Marie–Tooth phenotype. Brain 122:281–290.

de Waegh SM, Lee VM, Brady ST. 1992. Local modulation of neurofilament phosphorylation, axonal caliber, and slow axonal transport by myelinating Schwann cells. Cell 68:451–463.

DeBruin LS, Haines JD, Wellhauser LA, Radeva G, Schonmann V, Bienzle D, Harauz G. 2005. Developmental partitioning of myelin basic protein into membrane microdomains. J Neurosci Res 80:211–225.

Denu JM, Dixon JE. 1998. Protein tyrosine phosphatases: mechanisms of catalysis and regulation. Current Opinion in Chemical Biology 2:633–641.

Denu JM, Zhou G, Wu L, Zhao R, Yuvaniyama J, Saper MA, Dixon JE. 1995. The purification and characterization of a human dual-specific protein tyrosine phosphatase. J Biol Chem 270:3796–3803.

Di Paolo G, De Camilli P. 2006. Phosphoinositides in cell regulation and membrane dynamics. Nature 443:651–657.

Duex JE, Tang F, Weisman LS. 2006. The Vac14p-Fig4p complex acts independently of Vac7p and couples PI3,5P2 synthesis and turnover. Journal of Cell Biology 172:693–704.

Elmer LW, Black JA, Waxman SG, Angelides KJ. 1990. The voltage-dependent sodium channel in mammalian CNS and PNS: antibody characterization and immunocytochemical localization. Brain Research 532:222–231.

Falkenburger BH, Jensen JB, Dickson EJ, Suh B-C, Hille B. 2010. Phosphoinositides: lipid regulators of membrane proteins. The Journal of Physiology 588:3179–3185.

Faroni A, Castelnovo LF, Procacci P, Caffino L, Fumagalli F, Melfi S, Gambarotta G, Bettler B, Wrabetz L, Magnaghi V. 2014. Deletion of GABA-B receptor in Schwann cells regulates remak bundles and small nociceptive C-fibers. Glia 62:548–565.

Feely SME, Laura M, Siskind CE, Sottile S, Davis M, Gibbons VS, Reilly MM, Shy ME. 2011. MFN2 mutations cause severe phenotypes in most patients with CMT2A. Neurology 76:1690–1696.

Feltri ML, Poitelon Y, Previtali SC. 2016. How Schwann Cells Sort Axons: New Concepts. The Neuroscientist 22:252–265.

Feltri ML, Wrabetz L. 2005. Laminins and their receptors in Schwann cells and hereditary neuropathies. J Peripher Nerv Syst 10:128–143.

Ferguson CJ, Lenk GM, Meisler MH. 2009. Defective autophagy in neurons and astrocytes from mice deficient in PI(3,5)P2. Hum Mol Genet 18:4868–4878.

Fernandez-Valle C, Gorman D, Gomez AM, BUNGE MB. 1997. Actin plays a role in both changes in cell shape and gene-expression associated with Schwann cell myelination. J Neurosci 17:241–250.

Fields RD. 2014. Myelin Formation and Remodeling. Cell 156:15–17.

Filbin M, Tennekoon G. 1993. Homophilic adhesion of the myelin P0 protein requires glycosylation of both molecules in the homophilic pair. Journal of Cell Biology 122:451.

Firestein R, Nagy PL, Daly M, Huie P, Conti M, Cleary ML. 2002. Male infertility, impaired spermatogenesis, and azoospermia in mice deficient for the pseudophosphatase Sbf1. J Clin Invest 109:1165–1172.

Fridman V, Bundy B, Reilly MM, Pareyson D, Bacon C, Burns J, Day J, Feely S, Finkel RS, Grider T, Kirk CA, Herrmann DN, Laura M, Li J, Lloyd T, Sumner CJ, Muntoni F, Piscosquito G, Ramchandren S, Shy R, Siskind CE, Yum SW, Moroni I, Pagliano E, Zuchner S, Scherer SS, Shy ME, Inherited Neuropathies Consortium. 2015. CMT subtypes and disease burden in patients enrolled in the Inherited Neuropathies Consortium natural history study: a cross-sectional analysis. J Neurol Neurosurg Psychiatr 86:873–878.

Gajofatto A, Bongianni M, Zanusso G, Bianchi MR, Turatti M, Benedetti MD, Monaco S. 2013. Clinical and biomarker assessment of demyelinating events suggesting multiple sclerosis. Acta Neurol Scand 128:336–344.

Garratt AN, Voiculescu O, Topilko P, Charnay P, Birchmeier C. 2000. A dual role of erbB2 in myelination and in expansion of the schwann cell precursor pool. Journal of Cell Biology 148:1035–1046.

Gess B, Baets J, De Jonghe P, Reilly MM, Pareyson D, Young P. 2015. Ascorbic acid for the treatment of Charcot-Marie-Tooth disease. Cochrane Database Syst Rev:CD011952.

Gillespie CS, Sherman DL, Fleetwood-Walker SM, Cottrell DF, Tait S, Garry EM, Wallace VC, Ure J, Griffiths IR, Smith A, Brophy PJ. 2000. Peripheral demyelination and neuropathic pain behavior in periaxin-deficient mice. Neuron 26:523–531.

Giovannetti AM, Brambilla L, Torri Clerici V, Antozzi C, Mantegazza R, Černiauskaitė M, Confalonieri P. 2017. Difficulties in adjustment to multiple sclerosis: vulnerability and unpredictability of illness in the foreground. Disabil Rehabil 39:897–903.

Girault J-A, Peles E. 2002. Development of nodes of Ranvier. Curr Opin Neurobiol 12:476–485.

Gomez-Sanchez JA, Carty L, Iruarrizaga-Lejarreta M, Palomo-Irigoyen M, Varela-Rey M, Griffith M, Hantke J, Macias-Camara N, Azkargorta M, Aurrekoetxea I, De Juan VG, Jefferies HBJ, Aspichueta P, Elortza F, Aransay AM, Martínez-Chantar ML, Baas F, Mato JM, Mirsky R, Woodhoo A, Jessen KR. 2015. Schwann cell autophagy, myelinophagy, initiates myelin clearance from injured nerves. J Cell Biol 210:153–168.

Gould RM, Mattingly G. 1990. Regional localization of RNA and protein metabolism in Schwann cellsin vivo. J Neurocytol 19:285–301.

Greenfield S, Brostoff S, Eylar EH, Morell P. 1973. Protein composition of myelin of the peripheral nervous system. Journal of Neurochemistry 20:1207–1216.

Guan KL, Dixon JE. 1991. Evidence for protein-tyrosine-phosphatase catalysis proceeding via a cysteine-phosphate intermediate. J Biol Chem 266:17026–17030.

Guimarães-Costa R, Latour P, Ferrer X, Solé G, Husson I, Lacour A, Dubourg O, Leonard-Louis S, Stojkovic T. 2015. Charcot–Marie–Tooth type 4B1 (MTMR2 gene): Confounding clinical presentation and report of 5 original mutations. Neuromuscular Disorders 25:S285.

Hayasaka K, Himoro M, Wang Y, Takata M, Minoshima S, Shimizu N, Miura M, Uyemura K, Takada G. 1993. Structure and chromosomal localization of the gene encoding the human myelin protein zero (MPZ). Genomics 17:755–758.

Heller BA, Ghidinelli M, Voelkl J, Einheber S, Smith R, Grund E, Morahan G, Chandler D, Kalaydjieva L, Giancotti F, King RH, Fejes-Toth AN, Fejes-Toth G, Feltri ML, Lang F, Salzer JL. 2014. Functionally distinct PI 3-kinase pathways regulate myelination in the peripheral nervous system. J Cell Biol 204:1219–1236.

Hildebrand C, Bowe CM, Remahl IN. 1994. Myelination and myelin sheath remodelling in normal and pathological PNS nerve fibres. Prog Neurobiol 43:85–141.

Hirano R, Takashima H, Umehara F, Arimura H, Michizono K, Okamoto Y, Nakagawa M, Boerkoel CF, Lupski JR, Osame M, Arimura K. 2004. SET binding factor 2 (SBF2) mutation causes CMT4B with juvenile onset glaucoma. Neurology 63:577–580.

Hnia K, Vaccari I, Bolino A, Laporte J. 2012. Myotubularin phosphoinositide phosphatases: cellular functions and disease pathophysiology. Trends Mol Med 18:317–327.

Horn M, Baumann R, Pereira JA, Sidiropoulos PNM, Somandin C, Welzl H, Stendel C, Lühmann T, Wessig C, Toyka KV, Relvas JB, Senderek J, Suter U. 2012. Myelin is dependent on the Charcot-Marie-Tooth Type 4H disease culprit protein FRABIN/FGD4 in Schwann cells. Brain 135:3567–3583.

Houlden H, King RHM, Wood NW, Thomas PK, Reilly MM. 2001. Mutations in the 5' region of the myotubularin-related protein 2 (MTMR2) gene in autosomal recessive hereditary neuropathy with focally folded myelin. Brain 124:907–915.

Huxley AF, Stämpeli R. 1949. Evidence for saltatory conduction in peripheral myelinated nerve fibres. The Journal of Physiology 108:315–339.

Ikonomov OC, Sbrissa D, Shisheva A. 2001. Mammalian cell morphology and endocytic membrane homeostasis require enzymatically active phosphoinositide 5-kinase PIKfyve. J Biol Chem 276:26141–26147.

Ino D, Iino M. 2016. Schwann cell mitochondria as key regulators in the development and maintenance of peripheral nerve axons. Cell Mol Life Sci.

Jagalur NB, Ghazvini M, Mandemakers W, Driegen S, Maas A, Jones EA, Jaegle M, Grosveld F, Svaren J, Meijer D. 2011. Functional dissection of the Oct6 Schwann cell enhancer reveals an essential role for dimeric Sox10 binding. Journal of Neuroscience 31:8585–8594.

Jang SY, Shin YK, Park SY, Park JY, Rha S-H, Kim JK, Lee HJ, Park HT. 2015. Autophagy Is Involved in the Reduction of Myelinating Schwann Cell Cytoplasm during Myelin Maturation of the Peripheral Nerve. PLoS ONE 10:e0116624.

Jean S, Cox S, Nassari S, Kiger AA. 2015. Starvation-induced MTMR13 and RAB21 activity regulates VAMP8 to promote autophagosome-lysosome fusion. Nature Publishing Group 16:297–311.

Jean S, Cox S, Schmidt EJ, Robinson FL, Kiger A. 2012. Sbf/MTMR13 coordinates PI(3)P and Rab21 regulation in endocytic control of cellular remodeling. Mol Biol Cell 23:2723–2740.

Jean S, Kiger AA. 2012. Coordination between RAB GTPase and phosphoinositide regulation and functions. Nat Rev Mol Cell Biol 13:463–470.

Jean S, Kiger AA. 2014. Classes of phosphoinositide 3-kinases at a glance. Journal of Cell Science 127:923–928.

Jessen KR, Mirsky R. 2005. The origin and development of glial cells in peripheral nerves. Nat Rev Neurosci 6:671–682.

Jessen KR, Mirsky R. 2010. Control of Schwann cell myelination. F1000 Biol Rep 2.

Jessen KR, Mirsky R. 2016. The repair Schwann cell and its function in regenerating nerves. The Journal of Physiology 594:3521–3531.

Jessen KR. 2004. Glial cells. The International Journal of Biochemistry & Cell Biology 36:1861–1867.

Jin F, Dong B, Georgiou J, Jiang Q, Zhang J, Bharioke A, Qiu F, Lommel S, Feltri ML, Wrabetz L, Roder JC, Eyer J, Chen X, Peterson AC, Siminovitch KA. 2011. N-WASp is required for Schwann cell cytoskeletal dynamics, normal myelin gene expression and peripheral nerve myelination. Development 138:1329–1337.

Jordanova A, de Jonghe P, Boerkoel CF, Takashima H, De Vriendt E, Ceuterick C, Martin JJ, Butler IJ, Mancias P, Papasozomenos SC, Terespolsky D, Potocki L, Brown CW, Shy M, Rita DA, Tournev I, Kremensky I, Lupski JR, Timmerman V. 2003. Mutations in the neurofilament light chain gene (NEFL) cause early onset severe Charcot-Marie-Tooth disease. Brain 126:590–597.

Kachhap SK, Faith D, Qian DZ, Shabbeer S, Galloway NL, Pili R, Denmeade SR, DeMarzo AM, Carducci MA. 2007. The N-Myc down regulated Gene1 (NDRG1) Is a Rab4a effector involved in vesicular recycling of E-cadherin. PLoS ONE 2:e844.

Kagiava A, Sargiannidou I, Theophilidis G, Karaiskos C, Richter J, Bashiardes S, Schiza N, Nearchou M, Christodoulou C, Scherer SS, Kleopa KA. 2016. Intrathecal gene therapy rescues a model of demyelinating peripheral neuropathy. Proceedings of the National Academy of Sciences 113:E2421–9.

Kaplan S, Odaci E, Unal B, Sahin B. 2009. Chapter 2 Development of the Peripheral Nerve. International review of ….

Kaya F, Belin S, Bourgeois P, Micaleff J, Blin O, Fontés M. 2007. Ascorbic acid inhibits PMP22 expression by reducing cAMP levels. Neuromuscul Disord 17:248–253.

Ketel K, Krauss M, Nicot A-S, Puchkov D, Wieffer M, Müller R, Subramanian D, Schultz C, Laporte J, Haucke V. 2016. A phosphoinositide conversion mechanism for exit from endosomes. Nature 529:408–412.

Kidd GJ, Ohno N, Trapp BD. 2013. Biology of Schwann cells. Handb Clin Neurol 115:55–79.

Kim S-A, Vacratsis PO, Firestein R, Cleary ML, Dixon JE. 2003. Regulation of myotubularin-related (MTMR)2 phosphatidylinositol phosphatase by MTMR5, a catalytically inactive phosphatase. Proceedings of the National Academy of Sciences 100:4492–4497.

Klein CJ, Duan X, Shy ME. 2013. Inherited neuropathies: Clinical overview and update. Muscle Nerve:n/a–n/a.

Klugmann M, Schwab MH, Pühlhofer A, Schneider A, Zimmermann F, Griffiths IR, Nave KA. 1997. Assembly of CNS myelin in the absence of proteolipid protein. Neuron 18:59–70.

Kutateladze TG. 2010. translation of the phosphoinositide code by pI effectors. Nat Methods 6:507–513.

Laporte J, Blondeau F, Buj-Bello A, Tentler D, Kretz C, Dahl N, Mandel JL. 1998. Characterization of the myotubularin dual specificity phosphatase gene family from yeast to human. Hum Mol Genet 7:1703–1712.

Laporte J, Hu LJ, Kretz C, Mandel JL, Kioschis P, Coy JF, Klauck SM, Poustka A, Dahl N. 1996. A gene mutated in X-linked myotubular myopathy defines a new putative tyrosine phosphatase family conserved in yeast. Nature Genetics 13:175–182.

Laurá M, Hutton EJ, Blake J, Lunn MP, Fox Z, Pareyson D, Solari A, Radice D, Koltzenburg M, Reilly MM. 2014. Pain and small fiber function in Charcot-Marie-Tooth disease type 1A. Muscle Nerve 50:366–371.

Lee SM, Chin L-S, Li L. 2016. Dysregulation of ErbB Receptor Trafficking and Signaling in Demyelinating Charcot-Marie-Tooth Disease. Mol Neurobiol.

Lemmon MA. 2008. Membrane recognition by phospholipid-binding domains. Nat Rev Mol Cell Biol 9:99–111.

Leonard TA, Hurley JH. 2011. Regulation of protein kinases by lipids. Current Opinion in Structural Biology 21:785–791.

Lewis RA, McDermott MP, Herrmann DN, Hoke A, Clawson LL, Siskind C, Feely SME, Miller LJ, Barohn RJ, Smith P, Luebbe E, Wu X, Shy ME, Muscle Study Group. 2013. High-dosage ascorbic acid treatment in Charcot-Marie-Tooth disease type 1A: results of a randomized, double-masked, controlled trial. JAMA Neurol 70:981–987.

Li H, Yang H, Liu Y, Huan W, Zhang S, Wu G, Lu Q, Wang Q, Wang Y. 2011. The cyclin-dependent kinase inhibitor p27(Kip1) is a positive regulator of Schwann cell differentiation in vitro. J Mol Neurosci 45:277–283.

Li L-X, Zhao S-Y, Liu Z-J, Ni W, Li H-F, Xiao B-G, Wu Z-Y. 2016. Improving molecular diagnosis of Chinese patients with Charcot-Marie-Tooth by targeted next-generation sequencing and functional analysis. Oncotarget 7:27655–27664.

Lillie RS. 1925. FACTORS AFFECTING TRANSMISSION AND RECOVERY IN THE PASSIVE IRON NERVE MODEL. The Journal of General Physiology 7:473–507.

Liu BP, Fournier A, GrandPré T, Strittmatter SM. 2002. Myelin-associated glycoprotein as a functional ligand for the Nogo-66 receptor. Science 297:1190–1193.

Liu Z, Wang Y, Yedidi RS, Brunzelle JS, Kovari IA, Sohi J, Kamholz J, Kovari LC. 2012. Crystal structure of the extracellular domain of human myelin protein zero. Proteins 80:307–313.

Lupski JR, Reid JG, Gonzaga-Jauregui C, Rio Deiros D, Chen DCY, Nazareth L, Bainbridge M, Dinh H, Jing C, Wheeler DA, McGuire AL, Zhang F, Stankiewicz P, Halperin JJ, Yang C, Gehman C, Guo D, Irikat RK, Tom W, Fantin NJ, Muzny DM, Gibbs RA. 2010. Whole-Genome Sequencing in a Patient with Charcot–Marie–Tooth Neuropathy. The New England journal of medicine 362:1181–1191.

Lutz D, Loers G, Kleene R, Oezen I, Kataria H, Katagihallimath N, Braren I, Harauz G, Schachner M. 2014. Myelin basic protein cleaves cell adhesion molecule L1 and promotes neuritogenesis and cell survival. Journal of Biological Chemistry 289:13503–13518.

Luzio JP, Gray SR, Bright NA. 2010. Endosome–lysosome fusion: Figure 1. Biochm Soc Trans 38:1413–1416.

Maffucci T. 2012. An introduction to phosphoinositides. Curr Top Microbiol Immunol 362:1–42.

Mai A, Veltel S, Pellinen T, Padzik A, Coffey E, Marjomaki V, Ivaska J. 2011. Competitive binding of Rab21 and p120RasGAP to integrins regulates receptor traffic and migration. J Cell Biol 194:291–306.

Mannil M, Solari A, Leha A, Pelayo-Negro AL, Berciano J, Schlotter-Weigel B, Walter MC, Rautenstrauss B, Schnizer TJ, Schenone A, Seeman P, Kadian C, Schreiber O, Angarita NG, Fabrizi GM, Gemignani F, Padua L, Santoro L, Quattrone A, Vita G, Calabrese D, CMT-TRIAAL/CMT-TRAUK Group, Young P, Laurá M, Haberlová J, Mazanec R, Paulus W, Beissbarth T, Shy ME, Reilly MM, Pareyson D, Sereda MW. 2014. Selected items from the Charcot-Marie-Tooth (CMT) Neuropathy Score and secondary clinical outcome measures serve as sensitive clinical markers of disease severity in CMT1A patients. Neuromuscul Disord 24:1003–1017.

Marko Jovic MSJRSC. 2010. The early endosome: a busy sorting station for proteins at the crossroads. Histology and histopathology 25:99.

Marrosu MG, Vaccargiu S, Marrosu G, Vannelli A, Cianchetti C, Muntoni F. 1998. Charcot-Marie-Tooth disease type 2 associated with mutation of the myelin protein zero gene. Neurology 50:1397–1401.

Masaki T. 2012. Polarization and myelination in myelinating glia. ISRN Neurol 2012:769412.

Mathis S, Goizet C, Tazir M, Magdelaine C, Lia A-S, Magy L, Vallat J-M. 2015. Charcot-Marie-Tooth diseases: an update and some new proposals for the classification. J Med Genet 52:681–690.

Mellman I, Nelson WJ. 2008. Coordinated protein sorting, targeting and distribution in polarized cells. Nat Rev Mol Cell Biol 9:833–845.

Monk KR, Feltri ML, Taveggia C. 2015. New insights on schwann cell development. Glia.

Montani L, Buerki-Thurnherr T, de Faria JP, Pereira JA, Dias NG, Fernandes R, Gonçalves AF, Braun A, Benninger Y, Böttcher RT, Costell M, Nave K-A, Franklin RJM, Meijer D, Suter U, Relvas JB. 2014. Profilin 1 is required for peripheral nervous system myelination. Development 141:1553–1561.

Murakami T, Kutoku Y, Nishimura H, Hayashi M, Abe A, Hayasaka K, Sunada Y. 2013. Mild phenotype of Charcot-Marie-Tooth disease type 4B1. Journal of the Neurological Sciences 334:176–179.

Murphy P, Topilko P, Schneider-Maunoury S, Seitanidou T, Evercooren AB-V, Charnay P. 1996. The regulation of Krox-20 expression reveals important steps in the control of peripheral glial cell development. Development 122:2847–2857.

Myllykoski M, Raasakka A, Lehtimäki M, Han H, Kursula I, Kursula P. 2013. Crystallographic analysis of the reaction cycle of 2',3'-cyclic nucleotide 3'-phosphodiesterase, a unique member of the 2H phosphoesterase family. Journal of Molecular Biology 425:4307–4322.

Myllykoski M, Seidel L, Muruganandam G, Raasakka A, Torda AE, Kursula P. 2016. Structural and functional evolution of 2',3'-cyclic nucleotide 3'-phosphodiesterase. Brain Research 1641:64–78.

Nakhro K, Park J-M, Hong YB, Park JH, Nam SH, Yoon BR, Yoo JH, Koo H, Jung S-C, Kim H-L, Kim JY, Choi K-G, Choi B-O, Chung KW. 2013. SET binding factor 1 (SBF1) mutation causes Charcot-Marie-Tooth disease type 4B3. Neurology 81:165–173.

Nave K-A, Sereda MW, Ehrenreich H. 2007. Mechanisms of Disease: inherited demyelinating neuropathies—from basic to clinical research. Nat Clin Pract Neurol 3:453–464.

Nave K-A. 2010a. Myelination and the trophic support of long axons. Nat Rev Neurosci 11:275–283.

Nave K-A. 2010b. Myelination and support of axonal integrity by glia. Nature [Internet] 468:244–252. Available from: http://www.nature.com/nature/journal/v468/n7321/abs/nature09614.html

Nave KA, Salzer JL. 2006. Axonal regulation of myelination by neuregulin 1. Curr Opin Neurobiol.

Nawaz S, Sánchez P, Schmitt S, Snaidero N, Mitkovski M, Velte C, Brückner BR, Alexopoulos I, Czopka T, Jung SY, Rhee JS, Janshoff A, Witke W, Schaap IAT, Lyons DA, Simons M. 2015. Actin filament turnover drives leading edge growth during myelin sheath formation in the central nervous system. Developmental Cell 34:139–151.

Negrão L, Almendra L, Ribeiro J, Matos A, Geraldo A, Pinto-Basto J. 2014. Charcot-Marie-Tooth 4B2 caused by a novel mutation in the MTMR13/SBF2 gene in two related Portuguese families. Acta Myol 33:144–148.

Nelis E, Van Broeckhoven C, de Jonghe P, Löfgren A, Vandenberghe A, Latour P, Le Guern E, Brice A, Mostacciuolo ML, Schiavon F, Palau F, Bort S, Upadhyaya M, Rocchi M, Archidiacono N, Mandich P, Bellone E, Silander K, Savontaus ML, Navon R, Goldberg-Stern H, Estivill X, Volpini V, Friedl W, Gal A. 1996. Estimation of the mutation frequencies in Charcot-Marie-Tooth disease type 1 and hereditary neuropathy with liability to pressure palsies: a European collaborative study. Eur J Hum Genet 4:25–33.

Ng AA, Logan AM, Schmidt EJ, Robinson FL. 2013. The CMT4B disease-causing phosphatases Mtmr2 and Mtmr13 localize to the Schwann cell cytoplasm and endomembrane compartments, where they depend upon each other to achieve wild-type levels of protein expression. Hum Mol Genet 22:1493–1506.

Nolano M, Manganelli F, Provitera V, Pisciotta C, Stancanelli A, Caporaso G, Iodice R, Shy ME,

Santoro L. 2015. Small nerve fiber involvement in CMT1A. Neurology 84:407–414.

Notredame C, Higgins DG, Heringa J. 2000. T-coffee: a novel method for fast and accurate multiple sequence alignment. Journal of Molecular Biology 302:205–217.

Occhi S, Zambroni D, Del Carro U, Amadio S, Sirkowski EE, Scherer SS, Campbell KP, Moore SA, Chen Z-L, Strickland S, Di Muzio A, Uncini A, Wrabetz L, Feltri ML. 2005. Both laminin and Schwann cell dystroglycan are necessary for proper clustering of sodium channels at nodes of Ranvier. Journal of Neuroscience 25:9418–9427.

Ozçelik M, Cotter L, Jacob C, Pereira JA, Relvas JB, Suter U, Tricaud N. 2010. Pals1 is a major regulator of the epithelial-like polarization and the extension of the myelin sheath in peripheral nerves. Journal of Neuroscience 30:4120–4131.

Padua L, Aprile I, Caliandro P, Pazzaglia C, Commodari I, Tonali P. 2006. Reliability and validity of the CMT neuropathy score as a measure of disability. Neurology 66:614–5– author reply 614–5.

Pagliano E, Moroni I, Baranello G, Magro A, Marchi A, Bulgheroni S, Ferrarin M, Pareyson D. 2011. Outcome measures for Charcot-Marie-Tooth disease: clinical and neurofunctional assessment in children. J Peripher Nerv Syst 16:237–242.

Parkinson DB, Bhaskaran A, Droggiti A, Dickinson S, D'Antonio M, Mirsky R, Jessen KR. 2004. Krox-20 inhibits Jun-NH 2-terminal kinase/c-Jun to control Schwann cell proliferation and death. Journal of Cell Biology 164:385–394.

Parkinson Study Group QE3 Investigators, Beal MF, Oakes D, Shoulson I, Henchcliffe C, Galpern WR, Haas R, Juncos JL, Nutt JG, Voss TS, Ravina B, Shults CM, Helles K, Snively V, Lew MF, Griebner B, Watts A, Gao S, Pourcher E, Bond L, Kompoliti K, Agarwal P, Sia C, Jog M, Cole L, Sultana M, Kurlan R, Richard I, Deeley C, Waters CH, Figueroa A, Arkun A, Brodsky M, Ondo WG, Hunter CB, Jimenez-Shahed J, Palao A, Miyasaki JM, So J, Tetrud J, Reys L, Smith K, Singer C, Blenke A, Russell DS, Cotto C, Friedman JH, Lannon M, Zhang L, Drasby E, Kumar R, Subramanian T, Ford DS, Grimes DA, Cote D, Conway J, Siderowf AD, Evatt ML, Sommerfeld B, Lieberman AN, Okun MS, Rodriguez RL, Merritt S, Swartz CL, Martin WRW, King P, Stover N, Guthrie S, Watts RL, Ahmed A, Fernandez HH, Winters A, Mari Z, Dawson TM, Dunlop B, Feigin AS, Shannon B, Nirenberg MJ, Ogg M, Ellias SA, Thomas C-A, Frei K, Bodis-Wollner I, Glazman S, Mayer T, Hauser RA, Pahwa R, Langhammer A, Ranawaya R, Derwent L, Sethi KD, Farrow B, Prakash R, Litvan I, Robinson A, Sahay A, Gartner M, Hinson VK, et al. 2014. A randomized clinical trial of high-dosage coenzyme Q10 in early Parkinson disease: no evidence of benefit. JAMA Neurol 71:543–552.

Pellegatta M, De Arcangelis A, D'Urso A, Nodari A, Zambroni D, Ghidinelli M, Matafora V, Williamson C, Georges-Labouesse E, Kreidberg J, Mayer U, McKee KK, Yurchenco PD, Quattrini A, Wrabetz L, Feltri ML. 2013. α6β1 and α7β1 integrins are required in Schwann cells to sort axons. Journal of Neuroscience 33:17995–18007.

Pereira JA, Lebrun-Julien F, Suter U. 2012. Molecular mechanisms regulating myelination in the peripheral nervous system. Trends in Neurosciences.

Petersen SC, Luo R, Liebscher I, Giera S, Jeong S-J, Mogha A, Ghidinelli M, Feltri ML, Schöneberg T, Piao X, Monk KR. 2015. The Adhesion GPCR GPR126 Has Distinct, Domain- Dependent Functions in Schwann Cell Development Mediated by Interaction with Laminin-211. Neuron 85:755–769.

Poliak S, Matlis S, Ullmer C, Scherer SS, Peles E. 2002. Distinct claudins and associated PDZ proteins form different autotypic tight junctions in myelinating Schwann cells. Journal of Cell Biology 159:361–372.

Porrello E, Rivellini C, Dina G, Triolo D, Del Carro U, Ungaro D, Panattoni M, Feltri ML, Wrabetz L, Pardi R, Quattrini A, Previtali SC. 2014. Jab1 regulates Schwann cell proliferation and axonal sorting through p27. Journal of Experimental Medicine 211:29–43.

Presas-Rodríguez S, Grau-López L, Hervás-García JV, Massuet-Vilamajó A, Ramo-Tello C. 2016. Myelitis: Differences between multiple sclerosis and other aetiologies. Neurologia 31:71–75.

Previtali SC, Quattrini A, Bolino A. 2007. Charcot-Marie-Tooth type 4B demyelinating neuropathy: deciphering the role of MTMR phosphatases. Expert Rev Mol Med 9:1–16.

Procacci P, Ballabio M, Castelnovo LF, Mantovani C, Magnaghi V. 2013. GABA-B receptors in the PNS have a role in Schwann cells differentiation? Front Cell Neurosci 6.

Puelles L. 2013. Plan of the Developing Vertebrate Nervous System. In: Patterning and Cell Type Specification in the Developing CNS and PNS. Elsevier. p 187–209.

Qin W, Wunderley L, Barrett AL, High S, Woodman PG. 2016. The Charcot Marie Tooth disease protein LITAF is a zinc-binding monotopic membrane protein. Biochem J 473:3965–3978.

Quarles RH. 2007. Myelin-associated glycoprotein (MAG): past, present and beyond. Journal of Neurochemistry 100:1431–1448.

Raess MA, Friant S, Cowling BS, Laporte J. 2016. WANTED - Dead or alive: Myotubularins, a large disease-associated protein family. Adv Biol Regul.

Ramdharry GM, Pollard A, Anderson C, Laurá M, Murphy SM, Dudziec M, Dewar EL, Hutton E, Grant R, Reilly MM. 2014. A pilot study of proximal strength training in Charcot-Marie-Tooth disease. J Peripher Nerv Syst 19:328–332.

Ramdharry GM, Pollard AJ, Grant R, Dewar EL, Laurá M, Moore SA, Hallsworth K, Ploetz T, Trenell MI, Reilly MM. 2016. A study of physical activity comparing people with Charcot-Marie-Tooth disease to normal control subjects. Disabil Rehabil:1–6.

Reilly MM. 2016. Untreatable genetic disorders: to test or not to test. Pract Neurol 16:174–175.

Robinson FL, Dixon JE. 2005. The phosphoinositide-3-phosphatase MTMR2 associates with MTMR13, a membrane-associated pseudophosphatase also mutated in type 4B Charcot-Marie-Tooth disease. J Biol Chem 280:31699–31707.

Robinson FL, Dixon JE. 2006. Myotubularin phosphatases: policing 3-phosphoinositides. Trends in Cell Biology 16:403–412.

Robinson FL, Niesman IR, Beiswenger KK, Dixon JE. 2008. Loss of the inactive myotubularin-related phosphatase Mtmr13 leads to a Charcot-Marie-Tooth 4B2-like peripheral neuropathy in mice. Proc Natl Acad Sci USA 105:4916–4921.

Rosenbluth J. 1999. A brief history of myelinated nerve fibers: one hundred and fifty years of controversy. J Neurocytol 28:251–262.

Rossor AM, Tomaselli PJ, Reilly MM. 2016. Recent advances in the genetic neuropathies. Curr Opin Neurol 29:537–548.

Rudnik-Schöneborn S, Tölle D, Senderek J, Eggermann K, Elbracht M, Kornak U, Hagen von der M, Kirschner J, Leube B, Müller-Felber W, Schara U, Au von K, Wieczorek D, Bußmann C, Zerres K. 2016. Diagnostic algorithms in Charcot-Marie-Tooth neuropathies: experiences from a German genetic laboratory on the basis of 1206 index patients. Clin Genet 89:34–43.

Salim K, Bottomley MJ, Querfurth E, Zvelebil MJ, Gout I, Scaife R, Margolis RL, Gigg R, Smith CI, Driscoll PC, Waterfield MD, Panayotou G. 1996. Distinct specificity in the recognition of phosphoinositides by the pleckstrin homology domains of dynamin and Bruton's tyrosine kinase. EMBO J 15:6241–6250.

Salzer JL. 2003. Polarized Domains of Myelinated Axons. Neuron 40:297–318.

Salzer JL. 2015. Schwann cell myelination. Cold Spring Harbor Perspectives in Biology 7:a020529.

Sanmaneechai O, Feely S, Scherer SS, Herrmann DN, Burns J, Muntoni F, Li J, Siskind CE, Day JW, Laurá M, Sumner CJ, Lloyd TE, Ramchandren S, Shy RR, Grider T, Bacon C, Finkel RS, Yum SW, Moroni I, Piscosquito G, Pareyson D, Reilly MM, Shy ME, Inherited Neuropathies Consortium - Rare Disease Clinical Research Consortium (INC-RDCRC). 2015. Genotype-phenotype characteristics and baseline natural history of heritable neuropathies caused by mutations in the MPZ gene. Brain 138:3180–3192.

Saporta MA, Shy ME. 2013. Inherited Peripheral Neuropathies. Neurologic clinics.

Scherer SS, Wrabetz L. 2008. Molecular mechanisms of inherited demyelinating neuropathies. Glia [Internet] 56:1578–1589. Available from: http://onlinelibrary.wiley.com.liboff.ohsu.edu/doi/10.1002/glia.20751/full

Scherer SS. 2011. CMT2A: The name doesn't tell the whole story. Neurology 76:1686–1687.

Schindelin J, Arganda-Carreras I, Frise E, Kaynig V, Longair M, Pietzsch T, Preibisch S, Rueden C, Saalfeld S, Schmid B, Tinevez J-Y, White DJ, Hartenstein V, Eliceiri K, Tomancak P, Cardona A. 2012. Fiji: an open-source platform for biological-image analysis. Nat Methods 9:676–682.

Senderek J, Bergmann C, Weber S, Ketelsen U-P, Schorle H, Rudnik-Schöneborn S, Büttner R, Buchheim E, Zerres K. 2003. Mutation of the SBF2 gene, encoding a novel member of the myotubularin family, in Charcot–Marie–Tooth neuropathy type 4B2/11p15. Hum Mol Genet 12:349–356.

Sheean ME, McShane E, Cheret C, Walcher J, Müller T, Wulf-Goldenberg A, Hoelper S, Garratt AN, Krüger M, Rajewsky K, Meijer D, Birchmeier W, Lewin GR, Selbach M, Birchmeier C. 2014. Activation of MAPK overrides the termination of myelin growth and replaces Nrg1/ErbB3 signals during Schwann cell development and myelination. Genes Dev 28:290–303.

Shen Y-AA, Chen Y, Dao DQ, Mayoral SR, Wu L, Meijer D, Ullian EM, Chan JR, Lu QR. 2014. Phosphorylation of LKB1/Par-4 establishes Schwann cell polarity to initiate and control myelin extent. Nature Communications 5:4991.

Sherman DL, Brophy PJ. 2005. Mechanisms of axon ensheathment and myelin growth. Nat Rev

Neurosci [Internet] 6:683–690. Available from: http://www.nature.com.liboff.ohsu.edu/nrn/journal/v6/n9/full/nrn1743.html

Shibata S, Kawanai T, Hara T, Yamamoto A, Chaya T, Tokuhara Y, Tsuji C, Sakai M, Tachibana T, Inagaki S. 2016. ARHGEF10 directs the localization of Rab8 to Rab6-positive executive vesicles. Journal of Cell Science 129:3620–3634.

Shubin RA, Weiner LP. 1989. Viruses And Demyelination. In: Myelination and Demyelination. Boston, MA: Springer US. p 129–143.

Shy ME, Blake J, Krajewski K, Fuerst DR, Laura M, Hahn AF, Li J, Lewis RA, Reilly M. 2005. Reliability and validity of the CMT neuropathy score as a measure of disability. Neurology 64:1209–1214.

Simons M, Snaidero N, Aggarwal S. 2012. Cell polarity in myelinating glia: from membrane flow to diffusion barriers. … Acta (BBA)-Molecular and Cell ….

Simons M, Trotter J. 2007. Wrapping it up: the cell biology of myelination. Curr Opin Neurobiol 17:533–540.

Simpson JC, Griffiths G, Wessling-Resnick M. 2004. A role for the small GTPase Rab21 in the early endocytic pathway. Journal of Cell Science 117:6297–6311.

Snaidero N, Möbius W, Czopka T, Hekking LHP, Mathisen C, Verkleij D, Goebbels S, Edgar J, Merkler D, Lyons DA, Nave K-A, Simons M. 2014a. Myelin Membrane Wrapping of CNS Axons by PI(3,4,5)P3-Dependent Polarized Growth at the Inner Tongue. Cell 156:277–290.

Snaidero N, Möbius W, Czopka T, Hekking LHP, Mathisen C, Verkleij D, Goebbels S, Edgar J, Merkler D, Lyons DA, Nave K-A, Simons M. 2014b. Myelin Membrane Wrapping of CNS Axons by PI(3,4,5)P3-Dependent Polarized Growth at the Inner Tongue. Cell [Internet] 156:277–290. Available from: http://www.sciencedirect.com/science/article/pii/S0092867413015304

Snaidero N, Simons M. 2014. Myelination at a glance. Journal of Cell Science 127:2999–3004.

Sobottka B, Ziegler U, Kaech A, Becher B, Goebels N. 2011. CNS live imaging reveals a new mechanism of myelination: the liquid croissant model. Glia 59:1841–1849.

Sönnichsen B, De Renzis S, Nielsen E, Rietdorf J, Zerial M. 2000. Distinct membrane domains on endosomes in the recycling pathway visualized by multicolor imaging of Rab4, Rab5, and Rab11. Journal of Cell Biology 149:901–914.

Stahelin RV, Scott JL, Frick CT. 2014. Cellular and molecular interactions of phosphoinositides and peripheral proteins. Chem Phys Lipids 182:3–18.

Stenmark H. 2009. Rab GTPases as coordinators of vesicle traffic. Nat Rev Mol Cell Biol 10:513–525.

Steshenko O, Andrade DM, Honigmann A, Mueller V, Schneider F, Sezgin E, Hell SW, Simons M, Eggeling C. 2016. Reorganization of Lipid Diffusion by Myelin Basic Protein as Revealed by STED Nanoscopy. Biophys J 110:2441–2450.

Stolt CC, Wegner M. 2016. Schwann cells and their transcriptional network: Evolution of key regulators of peripheral myelination. Brain Research 1641:101–110.

Suresh S, Wang C, Nanekar R, Kursula P, Edwardson JM. 2010. Myelin Basic Protein and Myelin Protein 2 Act Synergistically to Cause Stacking of Lipid Bilayers. Biochemistry.

Suter U, Scherer SS. 2003. Disease mechanisms in inherited neuropathies. Nat Rev Neurosci 4:714–726.

Svaren J, Meijer D. 2008. The molecular machinery of myelin gene transcription in Schwann cells. Glia 56:1541–1551.

Sylvester J, Kumar K, Mulligan S, Ng K. 2014. 17. Multifocal central nervous system demyelination with Lhermitte's phenomenon secondary to chemotherapy. Clinical Neurophysiology 125:e6.

Szigeti K, Garcia CA, Lupski JR. 2006. Genetics in Medicine - Abstract of article: Charcot-Marie-Tooth disease and related hereditary polyneuropathies: Molecular diagnostics determine aspects of medical management. Genetics in Medicine.

Tasaki I. 1939. Electric stimulation and the excitatory process in the nerve fiber. Amer J Physiol.

Taveggia C. 2016. Schwann cells-axon interaction in myelination. Curr Opin Neurobiol 39:24–29.

Taylor CM, Coetzee T, Pfeiffer SE. 2002. Detergent-insoluble glycosphingolipid/cholesterol microdomains of the myelin membrane. Journal of Neurochemistry 81:993–1004.

Taylor GS, Maehama T, Dixon JE. 2000. Myotubularin, a protein tyrosine phosphatase mutated in myotubular myopathy, dephosphorylates the lipid second messenger, phosphatidylinositol 3-phosphate. Proceedings of the National Academy of Sciences 97:8910–8915.

Thumm M, Simons M. 2015. Myelinophagy: Schwann cells dine in. J Cell Biol 210:9–10.

Timmerman V, Strickland AV, Züchner S. 2014. Genetics of Charcot-Marie-Tooth (CMT) Disease within the Frame of the Human Genome Project Success. Genes (Basel) 5:13–32.

Trapp BD, Kidd GJ, Hauer P, Mulrenin E, Haney CA, Andrews SB. 1995. Polarization of myelinating Schwann cell surface membranes: role of microtubules and the trans-Golgi network. Journal of Neuroscience 15:1797–1807.

Uchida Y, Rutaganira FU, Jullie D, Shokat KM, Zastrow von M. 2016. Endosomal phosphatidylinositol 3-kinase is essential for canonical GPCR signaling. Mol Pharmacol.

Vaccari I, Carbone A, Previtali SC, Mironova YA, Alberizzi V, Noseda R, Rivellini C, Bianchi F, Del Carro U, D'Antonio M, Lenk GM, Wrabetz L, Giger RJ, Meisler MH, Bolino A. 2015. Loss of Fig4 in both Schwann cells and motor neurons contributes to CMT4J neuropathy. Hum Mol Genet 24:383–396.

Vaccari I, Dina G, Tronchère H, Kaufman E, Chicanne G, Cerri F, Wrabetz L, Payrastre B, Quattrini A, Weisman LS, Meisler MH, Bolino A. 2011. Genetic interaction between MTMR2 and FIG4 phospholipid phosphatases involved in Charcot-Marie-Tooth neuropathies. PLoS Genet 7:e1002319.

van Paassen BW, van der Kooi AJ, van Spaendonck-Zwarts KY, Verhamme C, Baas F, de Visser M. 2014. PMP22 related neuropathies: Charcot-Marie-Tooth disease type 1A and Hereditary Neuropathy with liability to Pressure Palsies. Orphanet J Rare Dis 9:38.

Vanhaesebroeck B, Stephens L, Hawkins P. 2012. PI3K signalling: the path to discovery and understanding. Nat Rev Mol Cell Biol 13:195–203.

Verhoeven K, De Jonghe P, Coen K, Verpoorten N, Auer-Grumbach M, Kwon JM, FitzPatrick D, Schmedding E, De Vriendt E, Jacobs A, Van Gerwen V, Wagner K, Hartung H-P, Timmerman V. 2003. Mutations in the small GTP-ase late endosomal protein RAB7 cause Charcot-Marie-Tooth type 2B neuropathy. Am J Hum Genet 72:722–727.

Viader A, Sasaki Y, Kim S, Strickland A, Workman CS, Yang K, Gross RW, Milbrandt J. 2013. Aberrant Schwann cell lipid metabolism linked to mitochondrial deficits leads to axon degeneration and neuropathy. Neuron 77:886–898.

Vijay S, Chiu M, Dacks JB, Roberts RC. 2016. Exclusive expression of the Rab11 effector SH3TC2 in Schwann cells links integrin-α6 and myelin maintenance to Charcot-Marie-Tooth disease type 4C. Biochim Biophys Acta 1862:1279–1290.

Voas MG, Glenn TD, Raphael AR, Talbot WS. 2009. Schwann Cells Inhibit Ectopic Clustering of Axonal Sodium Channels. J Neurosci 29:14408–14414.

Waldman AT, Banwell BL. 2011. Acquiring new insights: Incidence of acquired demyelination and MS in US children. Neurology 77:1112–1113.

Waxman SG. 1980. Determinants of conduction velocity in myelinated nerve fibers. Muscle Nerve 3:141–150.

Woodhoo A, Sommer L. 2008. Development of the Schwann cell lineage: From the neural crest to the myelinated nerve. Glia 56:1481–1490.

Yang D, Bierman J, Tarumi YS, Zhong Y-P, Rangwala R, Proctor TM, Miyagoe-Suzuki Y, Takeda S, Miner JH, Sherman LS, Gold BG, Patton BL. 2005. Coordinate control of axon defasciculation and myelination by laminin-2 and -8. Journal of Cell Biology 168:655–666.

Yin X, Crawford TO, Griffin JW, Tu PH, Lee VM, Li C, Roder J, Trapp BD. 1998. Myelin-associated glycoprotein is a myelin signal that modulates the caliber of myelinated axons. J Neurosci 18:1953–1962.

Yoshimura S-I, Gerondopoulos A, Linford A, Rigden DJ, Barr FA. 2010. Family-wide characterization of the DENN domain Rab GDP-GTP exchange factors. J Cell Biol 191:367–381.

Zenker J, Stettner M, Ruskamo S, Domènech-Estévez E, Baloui H, Médard J-J, Verheijen MHG, Brouwers JF, Kursula P, Kieseier BC, Chrast R. 2014. A role of peripheral myelin protein 2 in lipid homeostasis of myelinating Schwann cells. Glia 62:1502–1512.

Zhang X, He X, Fu X-Y, Chang Z. 2006. Varp is a Rab21 guanine nucleotide exchange factor and regulates endosome dynamics. Journal of Cell Science 119:1053–1062.

Zhao C, Takita J, Tanaka Y, Setou M, Nakagawa T, Takeda S, Yang HW, Terada S, Nakata T, Takei

Y, Saito M, Tsuji S, Hayashi Y, Hirokawa N. 2001. Charcot-Marie-Tooth Disease Type 2A Caused by Mutation in a Microtubule Motor KIF1Bβ. Cell 105:587–597.

Zollinger DR, Chang K-J, Baalman K, Kim S, Rasband MN. 2015. The Polarity Protein Pals1 Regulates Radial Sorting of Axons. Journal of Neuroscience 35:10474–10484.

Zoncu R, Perera RM, Balkin DM, Pirruccello M, Toomre D, De Camilli P. 2009. A phosphoinositide switch controls the maturation and signaling properties of APPL endosomes. Cell 136:1110–1121.

Zou J, Chang S-C, Marjanovic J, Majerus PW. 2009. MTMR9 increases MTMR6 enzyme activity, stability, and role in apoptosis. J Biol Chem 284:2064–2071.

Zou J, Zhang C, Marjanovic J, Kisseleva MV, Majerus PW, Wilson MP. 2012. Myotubularin-related protein (MTMR) 9 determines the enzymatic activity, substrate specificity, and role in autophagy of MTMR8. Proc Natl Acad Sci USA 109:9539–9544.

Zuchero JB, Barres BA. 2011. Between the sheets: a molecular sieve makes myelin membranes. Developmental Cell 21:385–386.

Zuchero JB, Fu M-M, Sloan SA, Ibrahim A, Olson A, Zaremba A, Dugas JC, Wienbar S, Caprariello AV, Kantor C, Leonoudakis D, Leonoudakus D, Lariosa-Willingham K, Kronenberg G, Gertz K, Soderling SH, Miller RH, Barres BA. 2015. CNS myelin wrapping is driven by actin disassembly. Developmental Cell 34:152–167.